# „Design of Al Diffusion Coatings for Fe-based and Ni-based Alloys“

Von der Fakultät für Georessourcen und Materialtechnik
der Rheinisch-Westfälischen Technischen Hochschule Aachen

zur Erlangung des akademischen Grades eines

Doktors der Naturwissenschaften

genehmigte Dissertation
vorgelegt von **Dipl.-Phys.**

**Ammar Naji**

aus Frankfurt am Main

**Berichter:** Prof. Dr.-Ing. Michael Schütze
Univ.-Prof. Dr.-Ing. Wolfgang Beck

Tag der mündlichen Prüfung: 15.06.2018

# Abstract

Components, which consist of metallic materials and operate at high temperatures, can degrade due to high temperature corrosion attack. The most frequently occurring phenomenon is oxidation. When metallic materials are exposed to an oxidizing atmosphere, it is desired that elements, which are called protective oxide forming elements, diffuse from the material interior to the material surface and form a dense and slow-growing oxide scale, which acts as a diffusion barrier and decelerates further oxidation. Since for several reasons most high temperature alloys contain only a limited amount of protective oxide forming elements, coatings are applied with higher amount of these elements. The concept of the diffusion coatings is to enrich the substrate surface with one or more protective oxide forming elements (e.g. Al). Aluminization of Fe- and Ni-based alloys leads to Al diffusion coatings, which can consist of one phase or several stacked phases, depending on the Al activity within the intermetallic phase, according to the Fe-Al and Ni-Al phase diagrams. In this work, the aim was to develop a predictive design procedure for the manufacturing of pack cementation Al coatings on austenitic steels and Ni-based alloys. The pack cementation process is a CVD (chemical vapour deposition) process, where the substrate to be coated is embedded in a powder mixture, consisting of the deposition element (e.g. Al), an activator (e.g. $NH_4Cl$) and a filler (e.g. $Al_2O_3$) and is heated in a tube furnace for several hours in an Ar/5%$H_2$ inert atmosphere. The coating design is based on thermodynamic and kinetic considerations of the pack cementation process. Thermodynamic considerations were conducted by calculations with the thermodynamic software FactSage®, to determine the Al activity (total partial pressure of Al carrying halides) within the pack powder as a function of process temperature and powder composition. Furthermore, the determination of the full range of the binary phase diagram of the Fe-Al and Ni-Al systems and the Al activities of these systems were calculated as a function of temperature and mole fraction. Kinetic values, as the diffusion coefficient, which affect the resulting coating thickness, have been determined via a limited amount of experiments for each alloy system, followed by Matano analysis. It was shown that based on the model considerations and the collection of the thermodynamic and kinetics data for a material/deposition element couple, the coating design approach developed enables a quantitative prediction and adjustment of the resulting coating properties (intermetallic phases and coating thickness) for a wide range of process

parameters. Coating experiments on austenitic steels (AISI 321, AISI 314 and Alloy 800) and a Ni-based alloy (Alloy 601) have shown that low pack process temperatures (up to 900°C) promote the formation of HA coatings. This observation is in agreement with the thermodynamic calculations, but also kinetic considerations show that a high process temperature promotes the interdiffusion of Al from the coating to the interior of the material during the coating process, which promotes the formation of LA coatings. The coating design postulates that it is possible to determine the entire kinetic values (the pre-factor $D_0$, the activation energy $E_A$ and the constant $q$) for a deposition element/substrate couple by means of three "calibration" pack experiments at three different temperatures. The determined diffusion coefficients for the coating procedure on AISI 321, AISI 314, Alloy 800 and Alloy 601 at 800, 900 and 1000°C showed good agreement with literature values. The collection of the entire thermodynamic and kinetic information made it possible to predict the coating microstructure for these four materials and to compare the predicted and experimentally formed coating properties, which showed good agreement. On the other side, the coating design contains limitations. For example, an extensive activator amount in the pack, which would theoretically cause a higher Al activity in the pack, leads to an attack of the substrate by the hydrogen halides. The co-deposition of another element to the main deposition element Al reduces the Al activity within the pack, since the activator is consumed by both deposition elements. Experiments have shown that Si and Hf can be co-deposited to an Al coating. The coating thickness is reduced in comparison to a mono-element Al coating, which is not only caused by the Al activity reduction due to co-deposition. Diffusion coefficient determinations of Al and the co-deposition elements (Si and Hf) have shown that also the diffusion coefficient of Al was reduced, because the co-deposition element occupies Al lattice sites. Cyclic oxidation experiments in an oxidizing and reducing atmosphere at 1000°C have shown that Si co-deposited Al coatings enhance the high temperature corrosion resistance, since the Al activity within this two-element coating is lower in comparison with the mono-element Al coating. Thus, the Al interdiffusion to the interior substrate and the coating brittleness is reduced. Also, Hf co-deposited Al coatings have shown an enhancement compared to the mono-element Al coating in a way that oxide scale thickness is lower, which indicates a slower oxide scale growth rate. The design concept has successfully been applied to a combustion chamber in a reformer system and is available for further use in coating technology.

# Kurzfassung

Bauteile, die aus metallischen Werkstoffen bestehen und bei hohen Temperaturen arbeiten, können durch Hochtemperaturkorrosion beschädigt werden. Das am häufigsten vorkommende Phänomen ist die Oxidation. Wenn metallische Werkstoffe einer oxidierenden Atmosphäre ausgesetzt werden, ist es erwünscht, dass Elemente - Oxidbildner genannt - vom Werkstoffinneren zur Werkstoffoberfläche diffundieren und eine dichte und langsam wachsende Oxidschicht bilden, die als Diffusionsbarriere dient. Somit wird weitere Oxidation verlangsamt. Da die meisten Legierungen nur eine begrenzte Menge an Oxidbildner enthalten können, werden sie beschichtet, so dass die Schicht als Reservoir für die Oxidbildner dient. Bei Diffusionsbeschichtungen wird die Substratoberfläche mit einen oder mehreren Oxidbildnern (z. B. Al) angereichert. Die Aluminisierung von Legierungen auf Fe- und Ni-Basis führt zu Al-Diffusionsschichten, die aus einer Phase oder mehreren gestapelten Phasen gemäß den Fe-Al- und Ni-Al-Phasendiagrammen bestehen können. Ziel dieser Arbeit war es, im Pulverpackverfahren entwickelte Al-Diffusionsschichten auf austenitische Stähle und Ni-Basislegierungen zu designen und ihre resultierende Mikrostruktur zu steuern. Das Pulverpackverfahren ist ein CVD-Verfahren (Chemical Vapour Deposition), bei dem das zu beschichtende Substrat in eine Pulvermischung eingebettet wird. Die Pulvermischung besteht aus dem Diffusionselement (z. B. Al), einem Aktivator (z. B. $NH_4Cl$) und einem Füllstoff (z. B. $Al_2O_3$). Das eingebettete Substrat wird mit dem Pulvergemisch in einem Rohrofen für mehrere Stunden in einer inerten Ar/5%$H_2$ Atmosphäre geheizt. Das Schichtdesign basiert auf thermodynamischen und kinetischen Betrachtungen des Pulverpackverfahrens. Thermodynamische Berechnungen mit der Software FactSage® wurden durchgeführt, um die Al-Aktivität (Gesamtpartialdruck aller Al-Halogenide) innerhalb des Packpulvers als eine Funktion der Prozesstemperatur und der Pulverzusammensetzung zu bestimmen. Darüber hinaus wurden die binären Phasendiagramme der Fe-Al- und Ni-Al-Systeme samt den Al-Aktivitäten dieser Systeme als Funktion der Temperatur und des Al-Molenbruchs berechnet. Bei der kinetischen Betrachtung wurde z.B. der Diffusionskoeffizient eines Schichtelement/Substrat-Paares über eine begrenzte Anzahl von Experimenten und einer Matano-Analyse bestimmt. Es wurde gezeigt, dass das erarbeitete Schichtdesign eine quantitative Vorhersage der resultierenden Schichtstruktur (intermetallische Phasen und Schichtdicke) für eine große Bandbreite von Prozessparametern

(Prozesszeit, Prozesstemperatur, Pulvergemisch, Werkstoff etc.) ermöglicht. Beschichtungsversuche an austenitischen Stählen (AISI 321, AISI 314 und Alloy 800) und einer Ni-Basis-Legierung (Alloy 601) haben gezeigt, dass niedrige Prozesstemperaturen im Pulverpack (bis zu 900°C) die Bildung von aluminiumreichen Diffusionsschichten fördern. Diese Beobachtung stimmt mit den thermodynamischen Berechnungen überein. Kinetische Berechnungen zeigten, dass eine hohe Prozesstemperatur die Interdiffusion von Al aus der Beschichtung in das Innere des Werkstoffs während des Beschichtungsprozesses fördert, was die Bildung von aluminiumärmeren Schichten begünstigt. Die berechneten thermodynamischen und kinetischen Werte ermöglichten es, die Schichtstruktur bei diesen vier Werkstoffen vorherzusagen. Die gleichzeitige Beschichtung eines anderen Elements neben dem Hauptbeschichtungselement Al verringert die Al-Aktivität innerhalb des Packs, da der Aktivator von beiden Beschichtungselementen verbraucht wird. Unsere Experimente haben gezeigt, dass es möglich ist Si und Hf gleichzeitig mit Al zu beschichten. Die Schichtdicke ist im Vergleich zu einer Monoelement-Al-Beschichtung reduziert. Dies wird nicht nur durch die Al-Aktivitätsverringerung aufgrund der gemeinsamen Abscheidung verursacht wird. Unsere kinetischen Berechnungen haben gezeigt, dass der Diffusionskoeffizient von Al reduziert wird, da das zweite Beschichtungselement Al-Gitterplätze besetzt. Dabei zeigten die vorhergesagten und experimentell gebildeten Schichtstrukturen gute Übereinstimmungen. Das erarbeitete Schichtdesign hat auch Grenzen. Zum Beispiel führt eine übermäßige Aktivatormenge im Pack, die theoretisch eine höhere Al-Aktivität zur Folge hätte, zu einer Beschädigung des Substrats durch Halogenwasserstoffe. Zyklische Auslagerungsversuche in einer oxidierenden und reduzierenden Atmosphäre bei 1000°C haben gezeigt, dass Al-Si-Beschichtungen die Hochtemperaturkorrosionsbeständigkeit verbessern, da die Al-Aktivität innerhalb dieser Zweielementbeschichtung im Vergleich zu der Monoelement-Al-Beschichtung geringer ist. Somit ist die Al-Diffusion in das innere Substrat und die Sprödigkeit der Diffusionsschicht verringert. Auch Al-Hf Diffusionsschichten zeigten eine Verbesserung der Hochtemperatur-korrosionsbeständigkeit im Vergleich zu der Monoelement-Al-Beschichtung. Dabei war die Oxidschichtdicke geringer, was auf eine langsamer wachsende Oxidschicht hinweist. Das Design-Konzept wurde erfolgreich in einer Brennkammer eines Reformersystems angewendet und steht für die weitere Verwendung in der Beschichtungstechnologie zur Verfügung.

# Danksagung

Diese Arbeit entstand im Rahmen meiner Tätigkeit am DECHEMA-Forschungsinstitut in der Arbeitsgruppe Hochtemperaturwerkstoffe.

Ich bedanke mich beim Bundesministerium für Wirtschaft und Energie (BMWi), das meine IGF-Projekte über die Arbeitsgemeinschaft industrieller Forschungs-vereinigungen (AiF) finanziell gefördert hat.

Herr Prof. Dr. Michael Schütze, zu dieser Zeit Arbeitsgruppenleiter und gleichzeitig Leiter des DECHEMA-Forschungsinstituts, betreute diese Arbeit. Ich danke Ihnen mir die Möglichkeit gegeben zu haben Teil Ihrer Arbeitsgruppe zu sein. Ich erinnere mich noch an den Tag, an dem wir das erste Mal die Ansätze des Schicht-Designs diskutierten und Sie mir entscheidende Ratschläge gaben. Ich danke Ihnen für Ihre aufmunternde E-Mail einige Tage vor der Prüfung, das hat mich gestärkt und glücklich gemacht.

Herr Univ.-Prof. Dr.-Ing. Wolfgang Beck, Leiter des Lehrstuhls für Eisenhüttenkunde, war zweiter Gutachter meiner Dissertation und zweiter Prüfer am Tag der mündlichen Prüfung. Ich danke Ihnen für Ihre Arbeit als Gutachter und Prüfer.

Herr Univ.-Prof. Dr.-Ing. Gerhard Hirt war Vorsitzender am Tag der mündlichen Prüfung. Ich danke Ihnen für Ihre Zeit.

Während meiner Zeit im DECHEMA-Forschungsinstitut habe ich mich nicht nur fachlich, sondern auch menschlich weiterentwickelt. Dafür möchte ich mich bei meinen Kolleginnen und Kollegen der Arbeitsgruppe Hochtemperaturwerkstoffe bedanken. Es war eine unvergessliche Zeit, auf die ich gerne zurückblicke.

Mathias Galetz, zu dieser Zeit zweiter Arbeitsgruppenleiter, unterstütze mich in allen fachlichen Fragestellungen und half mir bei der Erstellung meiner Arbeit. Dafür danke ich Dir. Ich danke Dir für deinen respektvollen und offenen Umgang, so dass ich mich bei dir gut aufgehoben fühlte.

Ellen, Daniela und Susann, verantwortliche der Abteilung Metallografie, halfen mir meine Proben zu präparieren und metallografische Bilder anzufertigen. Wenn es brenzlig wurde, übernahmen sie die komplette Arbeit. Ich danke Euch für Eure tatkräftige und fachliche Unterstützung in allen metallografischen Angelegenheiten.

Gerald und Melanie, verantwortlich für die Elektronenstrahlmikrosonde, machten Scans an den Proben-Querschliffen, so dass ich wissen konnte, ob meinen Schichten auch die Elemente enthalten, die sie sollen. Ich danke Euch für Eure Unterstützung.

Mathias Röhrig unterstützte mich beim Aufbau der Versuchsstände und hatte auch für kniffelige Angelegenheiten Lösungen parat. Ich danke Dir für deine Geduld und deine Unterstützung.
Ich möchte mich auch bei meinen restlichen Kolleginnen und Kollegen aus der Arbeitsgruppe für eine schöne Zeit bedanken, die ich mit Euch haben durfte.

Mein herzlicher Dank gilt meinen Freunden und meiner Familie. Ich möchte mich bei Ümit, Kerim, Erkan, Faruk, Aysar, Haydar, Abel und Jerome für die jahrzehntelange Freundschaft bedanken. Ihr seid längst Teil meiner Familie. Meinem Schwager Mohammed danke ich für die moralische Unterstützung und meinem Schwager Fadi für das Korrekturlesen meiner Arbeit. Ich danke meinen Geschwistern Fatima, Alladin, Abdullah, Mariam, Yazan, Haya und Malek für den familiären Zusammenhalt und für die Liebe, die Ihr mir gegeben habt. Ich bin froh und stolz Euer Bruder zu sein.
Mein tiefster und herzlichster Dank geht an meine Mutter Sana und meine Frau Rahmeh. Eure unendliche Liebe machen mich zu einem glücklichen Menschen. Ihr habt mich auch dann bedingungslos geliebt und unterstützt, wenn ich durch schwere Zeiten ging und unerträglich war. Danke für all das und danke dafür, dass es Euch gibt. Diese Arbeit widme ich Euch und meinem ungeborenen Kind.

**Table of Contents**

## Abbreviations

| | |
|---|---|
| AE | Active elements |
| at.% | Atomic percent |
| CTE | Coefficient of thermal expansion |
| CVD | Chemical vapour deposition |
| EDS | Energy Dispersive X-ray Spectroscopy |
| EPMA | Electron micro probe analysis |
| HA | High activity |
| LA | Low activity |
| SEM | Scanning electron microscope |
| WDS | Wavelength Dispersive X-ray Spectroscopy |
| wt.% | Weight percent |

# 1. Introduction

The latest surveys on the worldwide annual costs of corrosion show values between 1.3 and 1.4 trillion €. In industrial nations these costs correspond to about 3.1 to 3.5% of the gross domestic product. Corrosion experts have found that a net of 20 to 25% of the above annual costs can be saved by applying currently available corrosion control technologies [1]. These technologies include process optimization and selection of suitable materials for component manufacturing. However, it is well known that the efficiency of a process increases with increasing the temperature. Furthermore, aggressive process environments are unavoidable for several processes in industry. The combination of high temperature and aggressive medium accelerates the material damage and thus, decreases the components and systems lifetime. At high temperature, the corrosive media can be solid, gaseous or molten. In such environments, metallic materials form corrosion products such as *oxides*, sulphides, nitrides, carbides, etc.. Some elements (Al, Cr, Si etc.) react preferentially with components of the atmosphere, e.g. oxygen, and form a closed and *protective oxide scale* in the ideal case. This protective oxide scale can act as a diffusion barrier between the exposed material and the atmosphere, for which often a parabolic oxide scale growth is observed under isothermal exposure [2]. However, components are affected by alternating operation conditions. For example, temperature gradients induced by operation temperature changes can cause mechanical stresses, which lead to spallation of the oxide scale. Oxide forming elements then re-diffuse from the material interior to the surface in order to heal the damaged area by forming a new oxide scale. The healing process is protective until a *depleted zone* below the oxide scale is formed. This means that not enough *oxide forming elements* can then diffuse to the materials surface for further oxide scale formation, which often equals the end of the materials life-time [3]. To overcome this limitation, higher alloyed materials can be used.

However, the alloying degree should be carefully controlled in order to not affect the other material properties such as the weldability and mechanical properties. Furthermore, these materials are known to be expensive, which is a limitation for their use at a large scale. In recent years, diffusion coatings have emerged to be an economic and more effective technique for lifetime extension of components. These can be achieved by enrichment of the surface of components with an oxide forming element. Diffusion coatings act as a reservoir for elements underneath the surface forming protective oxide scales. They can be manufactured at a comparatively low cost and only 50 to 200 µm of the material is influenced due to the coating process. Thus, coatings have to fulfil three different requirements simultaneously: improvement of corrosion resistance, maintenance of material properties and economization.

In this work, Al diffusion coatings were developed, optimized and applied on a combustion chamber of a reformer system for hydrogen reforming. This reformer system yields hydrogen and carbon monoxide from methane gas and water vapour. The main component of the reformer system is the combustion chamber, which contains an atmosphere with a combination of oxygen and water vapour at its inner side, and has a temperature of 1000°C. At its outer side the gas is enriched with hydrogen gas and water vapour, where the reforming process takes place. Since this reformer system is considered to work, among other applications in households, the reformer system undergoes several turn on and off cycles a day. High temperatures, aggressive atmospheres and cyclic operating conditions promote material degradation. Fatally, if the combustion chamber is damaged the entire reformer system will fail. Austenitic alloy such as Alloy 800 (X10CrNiAlTi 32-20) is chosen for the combustion chamber, since the application of Ni-based super alloys is not economic. Diffusion coatings are an efficient way to increase the components life time and are simultaneously economic. Diffusion coatings can be applied by several methods. The most often used method is pack cementation. In this process the component to be coated is embedded in a powder mixture, consisting of the deposition element, an activator and inert filler. Heat treatment in a reducing ($Ar/H_2$ atmosphere) or inert (Ar) atmosphere promotes the interdiffusion between the deposition element, in this case Al, and elements of the component (mostly Fe). As a result, a coating, consisting of an intermetallic aluminide phase is formed as a metal subsurface zone. The coating properties, such as the type of intermetallic phases and the coating thickness, depend on the pack cementation process parameters (process temperature, process time, and

powder pack mixture). Under cyclic operating conditions the occurrence of cracks within the coating is very critical. Thus, the parameters coating thickness, brittleness of the intermetallic phase and differences in the CTE (coefficient of thermal expansion) between the intermetallic phase of the coating and the material are crucial for the success of the coating. Therefore, the pack cementation process parameters have to be chosen in such a way that the resulting diffusion coating consists of the intermetallic phase with suitable properties.

# 2. Motivation

The goal of this work is to optimise Al diffusion coatings on Fe- and Ni-based alloys by coating design. This coating design is based on thermodynamic and kinetic considerations of the pack cementation process and correlates the pack cementation process parameters with the resulting coating properties. The thermodynamic considerations examine the intermetallic phases of which the resulting Al coating consists and the correlated Al activity in the pack. The kinetic considerations describe the diffusion properties of Al in the material to be coated. The pack cementation process reveals a couple of effects, which complicate the modelling. Will a high amount of activator (e.g. $NH_4Cl$) in the pack lead to a high Al concentration within the coating, as it is predicted by the thermodynamic calculations? Must the Al activity in the pack not be considered as 1, since Al is used as pure element in the pack powder? How is it possible to calculate the thickness of the surface layer of intermetallic phases, if interdiffusion occurs during the pack cementation process, which changes the Al amount in the intermetallic phases and their thicknesses?

In this work, the coating design will be discussed with its corresponding thermodynamic and kinetic considerations, the comparison with experimental results and challenges of the coating design. Finally, a coating design procedure is presented that is capable to describe the coating procedure well. The peculiarity of the coating design of this work is that the entire thermodynamic and kinetic values are determined by a thermodynamic calculation program or experimentally in a way, that the coating design model becomes a self-sufficient system that does not depend on literature values beyond those present in the common thermodynamic databases, e.g. of the thermodynamic calculation program FactSage®.

# 3. State of the Art

## 3.1. High Temperature Corrosion

High temperature corrosion occurs, if a material is chemically reacting with its surrounding gas, liquid or solid medium at elevated temperatures. High temperature corrosion differs from aqueous corrosion because of the medium and the temperature range. Basic types of high temperature corrosion are oxidation, carburization, nitration, chlorination and sulfidation [4]. In this work, mainly high temperature oxidation was investigated and will be described in the following chapters. Since high temperature oxidation phenomena as such cannot be prevented, they have to be influenced in such a way that the resulting corrosion product (metal oxide) serves as a diffusion barrier and protects the material as a surface layer from the surrounding atmosphere. Ideally, the metal reacts with the oxygen in the atmosphere, and forms a slowly growing protective metal oxide scale as a corrosion product, which covers the metal surface:

$$xM + \frac{y}{2}O_2 \rightleftharpoons M_xO_y \quad (1)$$

where $M$, $O$ and $M_xO_y$ are the metal, oxygen and metal oxide, respectively, whereas $x$ and $y$ are stoichiometric factors. The Ellingham diagrams illustrate how stable metals are in the presence of gases by plotting the Gibbs free energy $\Delta G^0$ of the corrosion products (e.g. oxides) over the temperature (Figure 1). The right axis indicates the oxygen partial pressure. If a certain $O_2$ partial pressure is connected by a line to the absolute zero point (-273.15°C), the oxides whose $\Delta G^0$values are below this line are thermodynamically stable. During oxidation, the formation of a thermodynamically stable metal oxide that is slow growing and, thus, protective at the given conditions is preferred, because slow growing oxides are those with a low lattice disorder and, thus,

low (self)diffusion rates, i.e. good diffusion barriers. Such oxides are $Al_2O_3$, $Cr_2O_3$, $SiO_2$, as well as some of their spinels. Fe- oxides can serve as protective oxides below about 570°C. Besides the thermodynamic stability of the oxides formed, their growth rates determine their protective behaviour. Titanium oxides for example, are thermodynamically more stable than chromium oxides at high temperatures, but are not protective because of their high growth rates (high lattice disorder), which can lead to spallation of the oxide scales. Aluminium, chromium and silicon are commonly alloyed to steels and Ni base alloys as protective oxide forming elements.

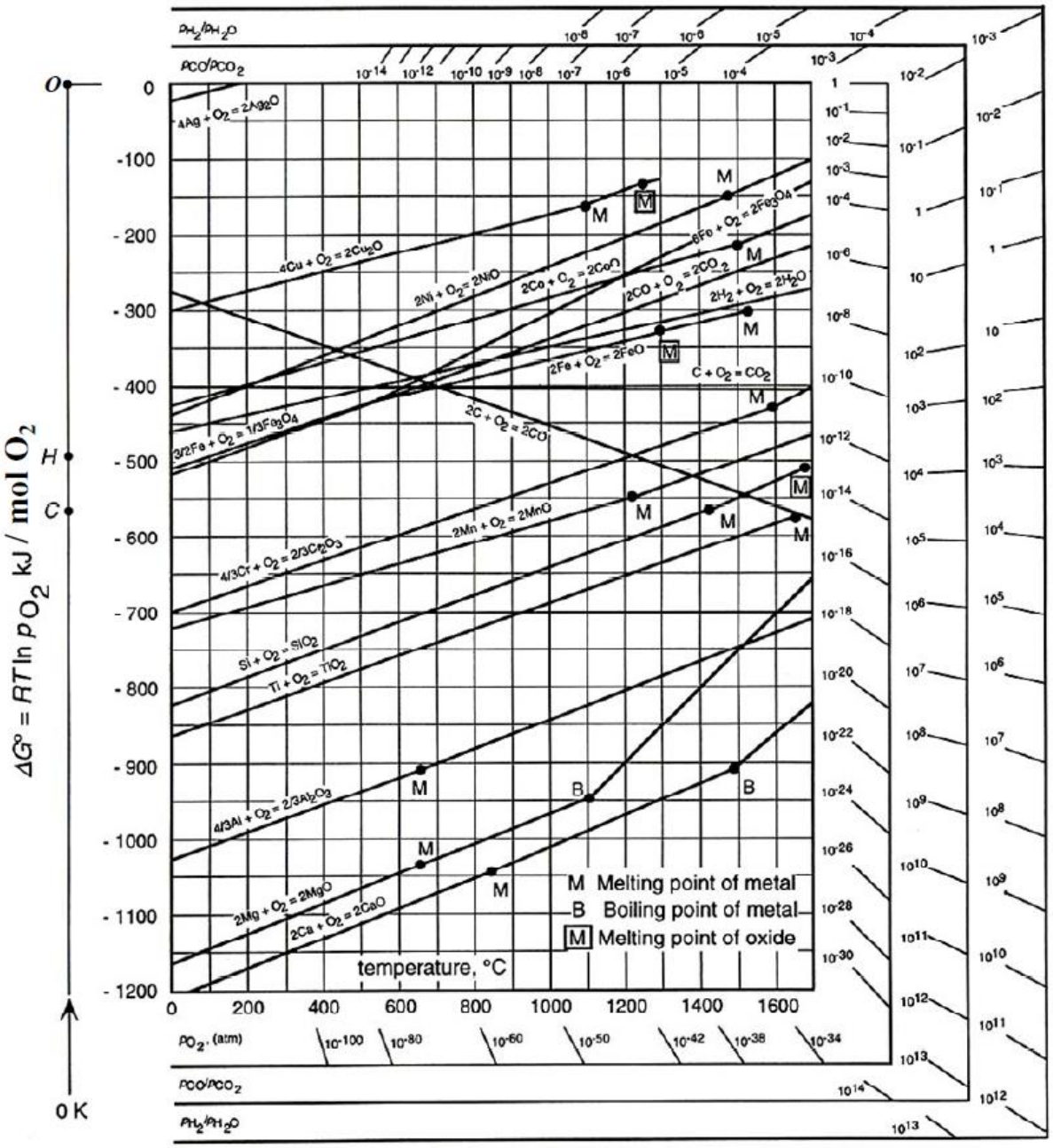


**Figure 1: Ellingham diagram showing the standard free energy as a function of temperature for selected oxides [5].**

The maximum content of oxide forming elements in alloyed materials is limited, because other material properties (e.g. mechanical properties) may be adversely affected (e.g. increasing of the brittleness [6]). To overcome this limitation, it is recommended to enrich the surface of the material with oxide forming elements by a coating procedure. There are various coating methods and different types of coatings existing, which have to be selected and optimized according to the working conditions of the component to be coated.

## 3.2. Pack Cementation Coatings as a cost-efficient Coating Procedure

Basically, coatings are divided into two types, the overlay and diffusion coatings [7]. For the overlay coatings, e.g. thermal spray coatings, the coating element is applied on the top of the component, without significant chemical bonding between the coating elements and the elements of the substrate. However, for diffusion coatings, the coating element and the substrate elements dissolve among each other and can undergo a chemical reaction to form an intermetallic phase. In any case, the coating consists of the substrate and the coating elements that act as a reservoir for the oxide forming elements.

Aluminium is the most common element used for diffusion coatings. Several methods exist to form aluminide diffusion coatings, of which the pack cementation process is the most common. It is a cost efficient, reliable method, by which uniform diffusion coatings can be manufactured even on relatively large components with complex geometries [8], which makes it widely used in the coatings industry [9, 10]. The first public description of pack aluminization was reported in 1911 by Van Aller in a U.S. patent [11]. The first industrial use of the pack cementation procedure was performed in 1957 [12, 13], when aircraft turbines consisting of Ni-based super alloys were coated [14, 15]. Nowadays, aluminization is a widely used technique to enhance the oxidation and corrosion resistance of alloys at high temperature.

Pack Cementation is a CVD (**C**hemical **V**apour **D**eposition) process [4], in which all metallic materials from low alloy steels, refractory metals up to Ni-based super alloys can be coated [16]. In Pack Cementation, the component to be coated is embedded in a powder mixture that is composed of the deposition element (Al, Cr, Si etc.), an activator ($NH_4Cl$, $AlF_3$ etc.) for activating the coating process, and a filler ($Al_2O_3$) for the prevention of sintering. All halides, i.e. chlorides, fluorides, bromides and iodides, can be used depending on the choice of the deposition element.

In Figure 2, the pack cementation process is shown schematically. Generally, the coating process is divided into a number of steps, which affect the pack process and, thus, the coating structure, respectively:

1. Formation of metal halides by reaction of the deposition element (or alloy) with the activator.
2. Metal halide transport to the substrate surface via gas phase diffusion.
3. Dissociation of the metal halide and deposition of the deposition element at the substrate surface.

4. Diffusion of the deposition element into the substrate via solid state diffusion.
5. Transport of the residual reaction products back to the pack.

While step 1 and 3 are thermodynamically important, step 2 and 4 are kinetically crucial. The formation of a metal halide (step 1), which is the basis of deposition, has a negative Gibbs free energy of formation.

It is believed that steps 1, 3 and 5 are fast, so that the pack process kinetics are controlled by steps 2 and 4. Several reports assume that the solid-state diffusion step is rate limiting [17].

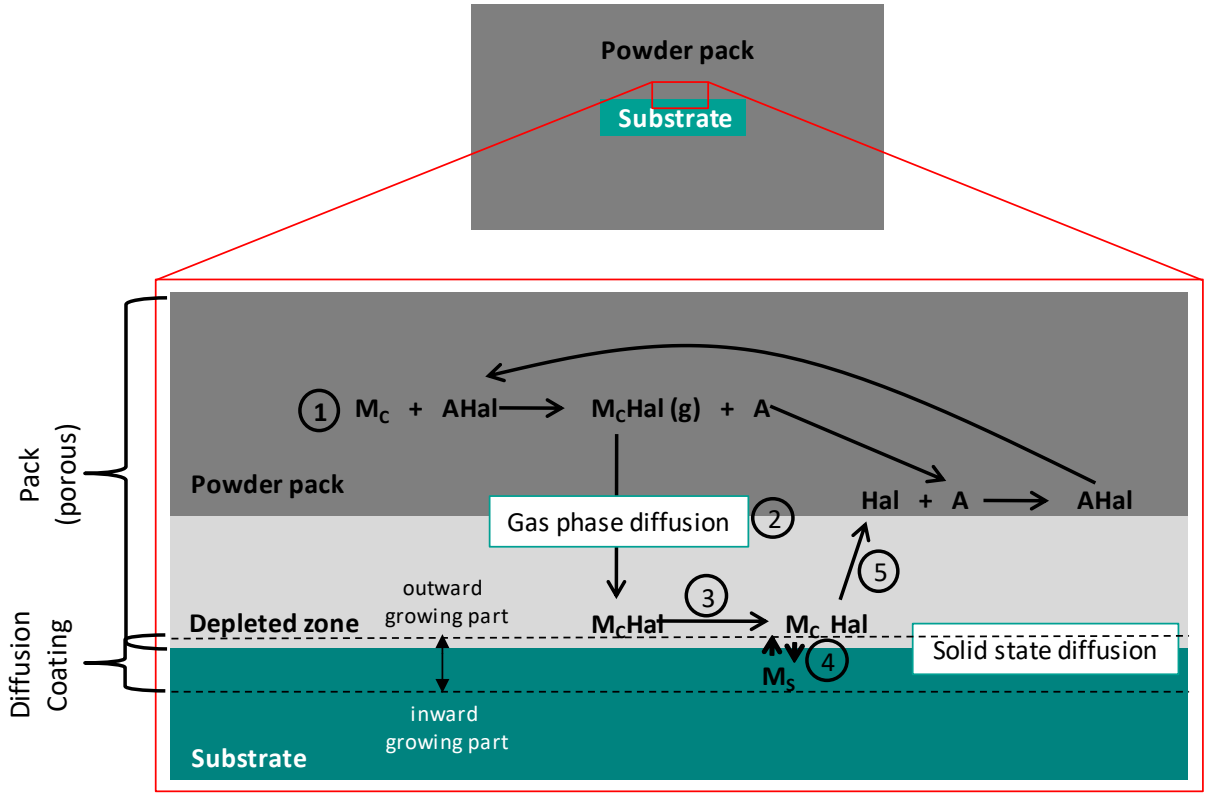


**Figure 2: Schematic representation of the pack cementation process. $M_C$: Coating Metal (e.g. Al), AHal: Activator (e.g. $NH_4Cl$), A: Activator basis, Hal: Halide (e.g. Cl), $M_S$: Substrate Metal (e.g. Fe). Steps 1 to 5 are explained in the text.**

Initially, metal halides formed from the powder that is adjacent to the component, diffuse through the porous powder structure to the components surface. Then, metal halides with a higher distance to the component in the pack begin to diffuse to the substrate surface successively, so that a deposition element depleted zone in the powder around the component grows gradually. The metal halides dissociate at the substrate surface resulting in free metal atoms diffusing into the material due to the concentration gradient between the powder pack and the substrate. In addition to the inward diffusion of the deposition element, outward diffusion of metallic substrate elements can occur to form the diffusion coating.

Since the deposition element is transported to the substrate via gas phase diffusion rather than direct contact of the powder with the component, a uniform coating with a good adhesion to the component is formed. In addition, complex shaped component parts e.g. with small openings can be coated. Disadvantages of the pack cementation process are limitations in the composition of the layer (sufficient partial pressure of the metal halide is needed) and the possible inclusion of filler into the coating.

## 3.3. Single-element Al Diffusion Coatings

According to the pack process parameters, the aluminization of an iron or nickel base alloy leads to the formation of an either *low activity* (LA) coating, which is formed by simultaneous outward Fe/Ni and inward Al diffusion and consists of a β-phase (FeAl or NiAl) or phases with less Al, or a *high activity* (HA) coating, which is formed mainly by inward Al diffusion and consists of phases with higher Al content than the β-phase ($Fe_2Al_5$ or $Ni_2Al_3$) [18, 19, 20]. Figure 3 shows a cross section of an aluminized austenitic steel AISI 321 (X6CrNiTi18 10) with a HA and LA coating.

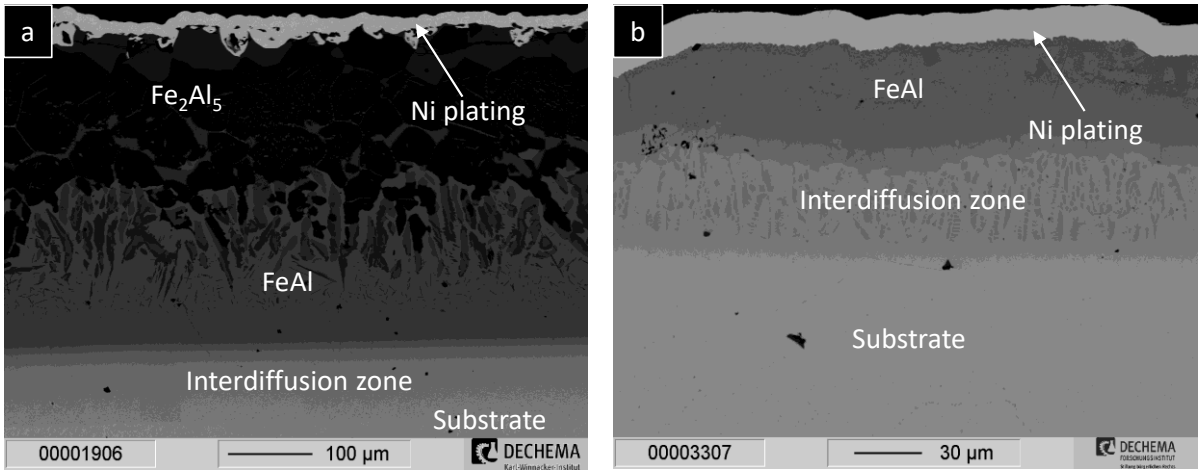


**Figure 3: Cross sections of (a) high activity and (b) low activity coatings on an AISI 321 steel substrate (X6CrNiTi1810), applied at 1000°C and 4 hours with the pack compositions (a) 10 wt.% Al, 1 wt.% $NH_4Cl$, 89 wt.% $Al_2O_3$ and (b) 1 wt.% Al, 1 wt.% $NH_4Cl$, 98 wt.% $Al_2O_3$. The high activity coating consists of the $Fe_2Al_5$ phase with the FeAl phase and the interdiffusion zone beneath it. The low activity coating consists of the FeAl phase with the interdiffusion zone beneath it. The Ni plating provides a contrast between the coating and the granulated carbon (embedding material).**

A large number of binary and multi component innovative aluminides such as Fe-Al, Al-Fe-Ni and Fe-Al-Ni-Cr were developed. The main reason for this huge scientific attention is certainly the widespread application of these intermetallic phases, especially in the aerospace industry, due to their high oxidation resistance, low density and high melting point [21, 22]. Iron aluminides offer good oxidation and sulfidation resistance (due to the formation of a protective alumina scale) and potentially lower costs than many other high temperature structural materials [23]. In the Fe-Al system five intermetallic compounds can be found (Figure 4 a).

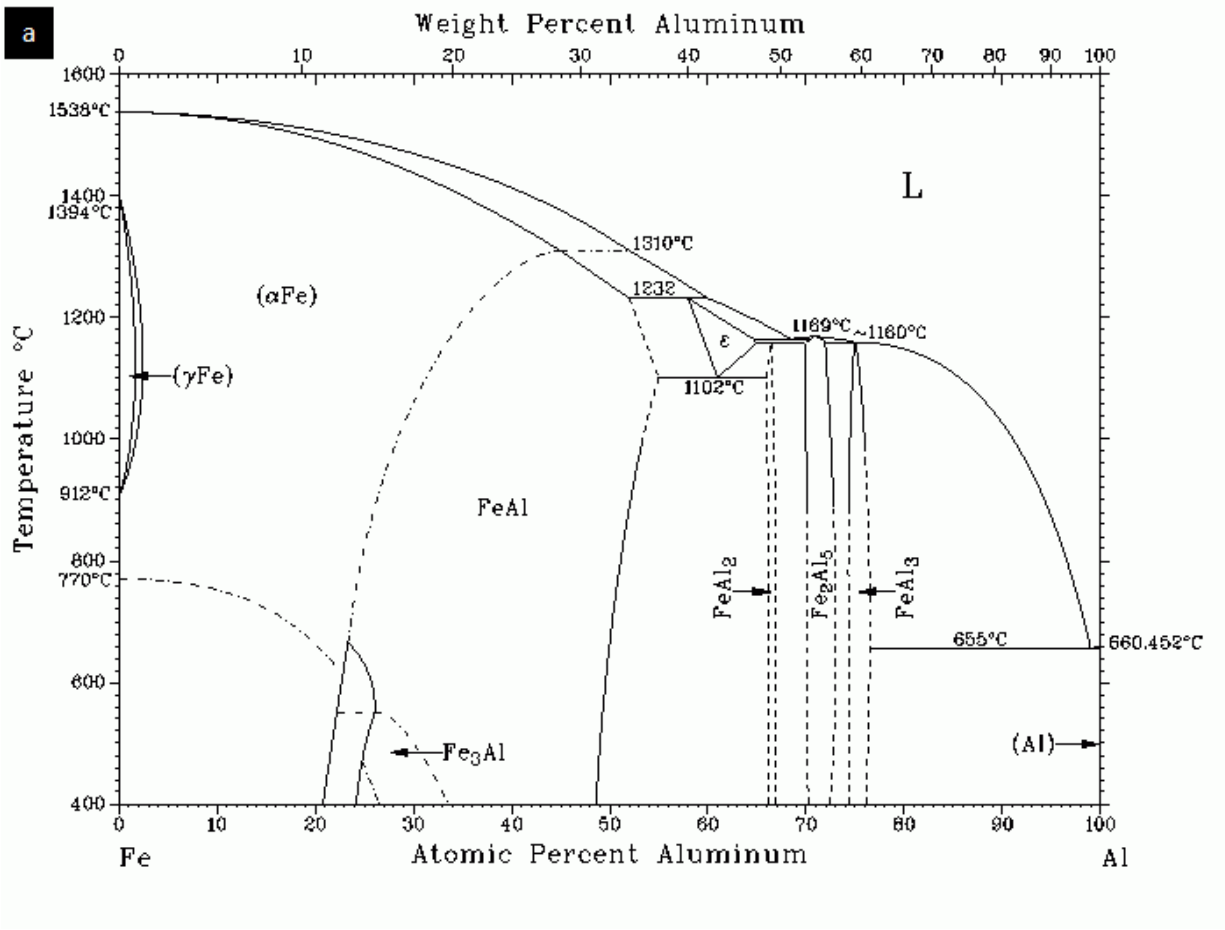


**Figure 4: (a) Fe-Al and (b) Ni-Al phase diagram [24].**

The $FeAl_2$, $Fe_2Al_5$ and $FeAl_3$ compounds have a high Al content, but their application for protection against cyclic oxidation is disadvantageous due to their brittleness [25]. $Fe_3Al$ and FeAl, which have high iron content, still offer a high oxidation resistance, but combined with good tribological properties and strength [26, 27, 28, 29, 30, 31]. Therefore, the application of FeAl and $Fe_3Al$ coatings is preferred when steels are aluminized.

Due to their good mechanical properties and their high resistance against corrosion, Ni-based alloys are materials, which have been used in structural and high temperature application for many years [32]. The Ni-Al system also shows five intermetallic phases. The β-NiAl intermetallic phase is characterized by stability over a large compositional range, a high elastic stiffness, a relatively low density and excellent oxidation resistance up to 1300°C and more [33, 34] (Figure 4 b).

### 3.3.1. Co-diffusion Coatings

There is a strong technical and economical need to further develop the pack cementation process and enable simultaneous deposition of multiple elements such as Al, Cr, Si, Y and Hf on steels and Ni-based superalloys in order to form diffusion coatings with high resistance to oxidation and high temperature corrosion [8].

By adding a second element to the coating metal, the thermodynamics and kinetics are changed compared to a single element diffusion process. In the case of co-diffusion, the deposition source can be either an alloy powder, which consists of the deposition elements, or a mixture of elemental powders. Often, master alloy powders are used because they allow to generate comparable activities of the deposition elements within the pack [35, 36, 37, 38, 39, 40]. In this work a mixture of Al and co-deposition element (Si, Hf, Y) powder is used. The co-deposition of two or more elements in a halide activated pack is challenging, for example when the difference in the Gibbs free energy of the deposition element carrying halides is large, which causes a high difference in the partial pressure of the metal halides [41].

#### 3.3.1.1. Elements for Co-diffusion

The beneficial effects of Si on the high temperature corrosion resistance of stainless steels are due to the ability of Si to form a continuous vitreous silica layer between the oxide scale and the material interface during oxidation [42], which acts as a good diffusion barrier due to its low concentration of defects. This leads to a reduction of the oxide scale growth rate and, thus, a reduction of spallation. Si is also known to enhance the resistance of aluminides on Ni-based superalloys against hot corrosion [43, 44]. Furthermore, Si seems to delay breakaway in the presence of water vapour in the environment and may facilitate Cr diffusion from the bulk which would help to heal the oxide scale. As a consequence, the level of Cr reservoir can be kept lower than for Si-free steels [45]. Fitzer et al. added Si to Al overlay coatings in order to enhance their ductility [46]. These coatings were applied on nickel and iron-based alloys to improve their resistance against high temperature oxidation and hot corrosion.

The addition of reactive elements (RE) such as Y, Hf, Ce and Zr can significantly improve the oxidation behaviour of $Al_2O_3$ forming alloys [47]. This "rare earth effect" was patented by Pfeil in 1937 [48]. Since then, many investigations of the effect of reactive elements on high temperature oxidation resistance, especially under cyclic oxidation were performed. Recently, Pint gave an insight into the reactive element effect, induced by one or more of the following effects [49]:

1. Promotion of the selective oxidation of the oxide forming elements such as aluminium or chromium, and consequently reduction of their content necessary to form the continuous protective scale.
2. Deceleration of the scale growth mechanism by blocking the grain boundaries (due to the larger ion sizes of RE) and, thus, the pathways for both anionic and cationic diffusing species.
3. Enhancement of the oxide scale fracture toughness by reducing the grain size, which could reduce spallation and crack formation.
4. Enhancement of the oxide scale adhesion by promoting the growth of oxide “pegs” beneath the oxide scale and minimizing the development of voids and porosity at the oxide scale/alloy interface, formed due to the Kirkendall effect.

Besides the addition of reactive elements via alloying, they can be applied by ion-implantation. For large scale and industrial applications, the use of reactive elements

via pack cementation was found to be efficient, due to the possibility for large components with complex geometries to be coated. One difficulty of the application of reactive elements is the low reactive element halide partial pressure during pack cementation. Instead of forming metal halides, reactive elements are oxygen affine and thus react with oxygen even from the atmosphere or from the $Al_2O_3$ filler in the pack powder to form thermodynamically stable reactive element oxides. This was shown by I. I. Gab et al., who demonstrated that the contact interaction between $Al_2O_3$ and Zr and Hf at high temperature solid phase pressure welding lead to the reduction of $Al_2O_3$ to pure Al [50].

### 3.3.2. Degradation Mechanism of Diffusion Coatings

During exposure of Al diffusion coated metals, degradation occurs via two mechanisms: Al interdiffusion between coating and substrate and Al loss due to Al outward diffusion from the coating to the surface. The interdiffusion between the coating and substrate is driven by the difference in chemical potential (Al concentration/activity difference) of both. The Al outward diffusion is driven by consumption of Al for oxide formation, spallation or potential evaporation of the oxide scale during exposure. Both mechanisms occur simultaneously on the same component. Depending on the applied temperature and process conditions, interdiffusion may contribute more to the overall Al depletion than Al outward diffusion does, although repeated spallation of $Al_2O_3$ scale may accelerate the loss of Al due to oxidation [3].

#### 3.3.2.1. Degradation of Diffusion Coatings due to Interdiffusion between Coating and Substrate

Since the composition of coatings differs strongly from the composition of the alloys, to which they are applied, a concentration difference between them exists. Coatings, which consist of the β-FeAl or β-NiAl phase, contain about 30 wt.% Al, whereas the $Fe_2Al_5$ or $Ni_2Al_3$ phases contain between 55 and 60 wt.% Al. Typical for Al, the content in steels or Ni-based superalloys is lower than 6 wt.%. Thus, interdiffusion of Al from the intermetallic coating into the interior of the substrate occurs during exposure and increases exponentially as a function of the components service temperature. This is considered as an Al loss, because the interdiffused Al cannot serve for $Al_2O_3$ formation

at the substrate surface anymore. Furthermore, interdiffusion of Al to the interior of the substrate could influence certain properties of the substrates, e.g. mechanical properties, negatively. Interdiffusion of Al from the intermetallic coating into the interior of the material can be decelerated by developing intermetallic phases with less Al amount than the β-FeAl or NiAl-phase.

#### 3.3.2.2. Degradation of Diffusion Coatings during Oxidation

Mechanical stresses during operation can occur due to temperature changes with different heating and cooling rates, which lead to crack formation and spallation of the oxide scale or even the diffusion coating, causing an accelerated consumption of oxide forming elements. Parabolic oxide scale growth can only be maintained if spallation of the oxide scale is prevented. Especially under cyclic operation conditions [51] mechanical stresses in the coating promote the formation of cracks within the coating. Important mechanical properties of a diffusion coating include the brittleness [52, 53] and mismatch of the coefficients of thermal expansion (CTE) between the coating and substrate [53, 54]. In Figure 5 the CTEs of several intermetallic phases and materials are plotted against temperature. It shows that in case of austenitic material, the β-FeAl phase exhibits the most compatible CTE slope over the entire temperature range in comparison with other intermetallic phases ($FeAl_2$ and $Fe_2Al_5$). Especially, below the brittle to ductile transition temperature (BDTT), the CTE is critical, which occurs at about 200°C for FeAl [55]. In the case of Ni base alloys, the CTE mismatch to the β-NiAl phase is the smallest. As a rule of thumb, the brittleness of an intermetallic phase increases with the Al content. Thus, the most appropriate phase for aluminization of austenitic steels and Ni-base alloys is the β-phase FeAl and NiAl, respectively.

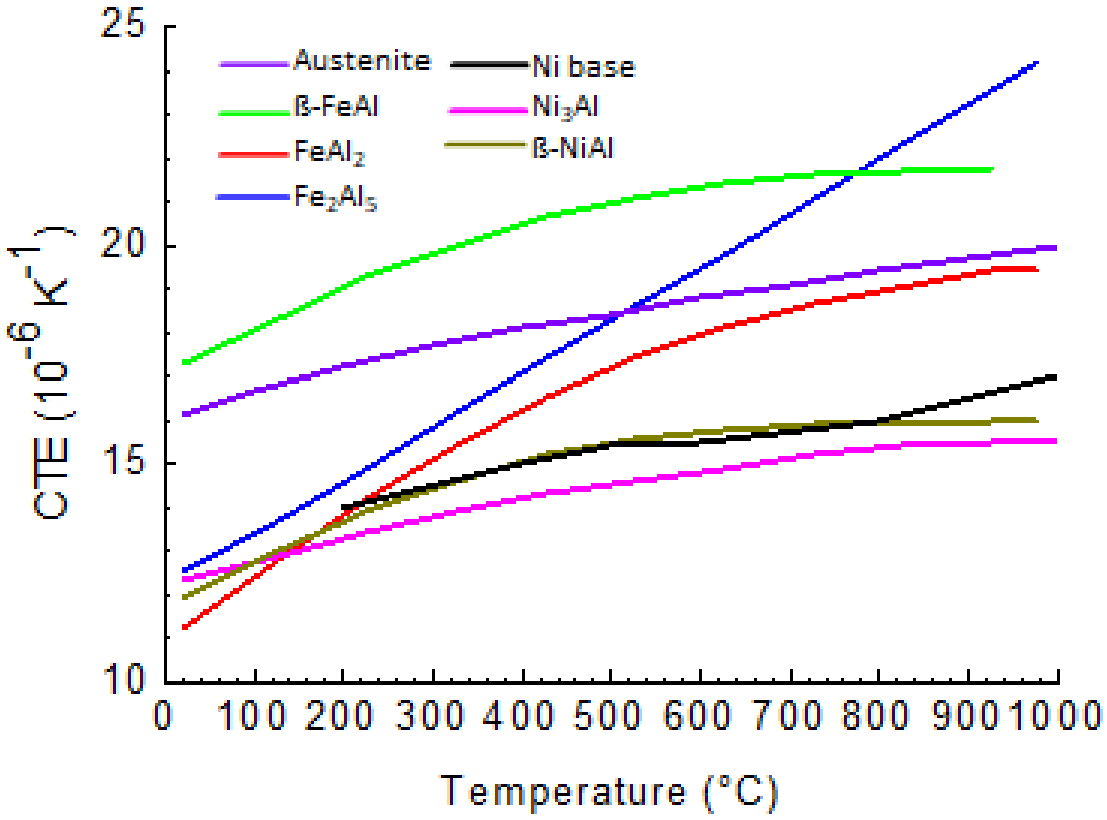


**Figure 5: CTE (coefficient of thermal expansion) of several intermetallic phases and alloys as a function of temperature [24, 56, 57].**

Combustion atmospheres, as they occur, e.g. in reformer systems, engine block heaters, exhaust gas system components and heat exchangers, contain oxygen and a significant water vapour partial pressure. Most technical alloys oxidize faster in water vapour containing atmospheres than in "dry" atmospheres [2]. For example, iron oxides show in dry atmospheres a relatively dense protective oxide scale below 500°C, but in water vapour containing atmospheres the porosity of the scale increases. Also chromium oxide forming systems face the issue, that at temperatures above about 650°C in addition to chromium oxide, non-protective gaseous chromium oxy hydroxide is formed [58, 59]:

$$2\,Cr_2O_3(s) + 3O_2(g) + 4H_2O\,(g) \rightarrow 4CrO_2(OH)_2(g) \qquad (2)$$

Without water vapour in an oxygen containing atmosphere, chromium oxide starts to evaporate above 900°C [60]. Thus, no long-term protection is provided, which makes alumina forming coatings more suitable at elevated temperatures or atmospheres

containing water vapour. In Figure 6 the partial pressure of chromium oxy hydroxide, which occurs by exposure of chromium in an oxygen and water vapour containing atmosphere, is calculated via the thermodynamic calculation program FactSage® as a function of temperature. Vapour pressures above $10^{-9}$ atm are usually considered measurable, showing that non-negligible chromium oxy hydroxide is formed, contributing to a loss of the originally protective $Cr_2O_3$ scale.

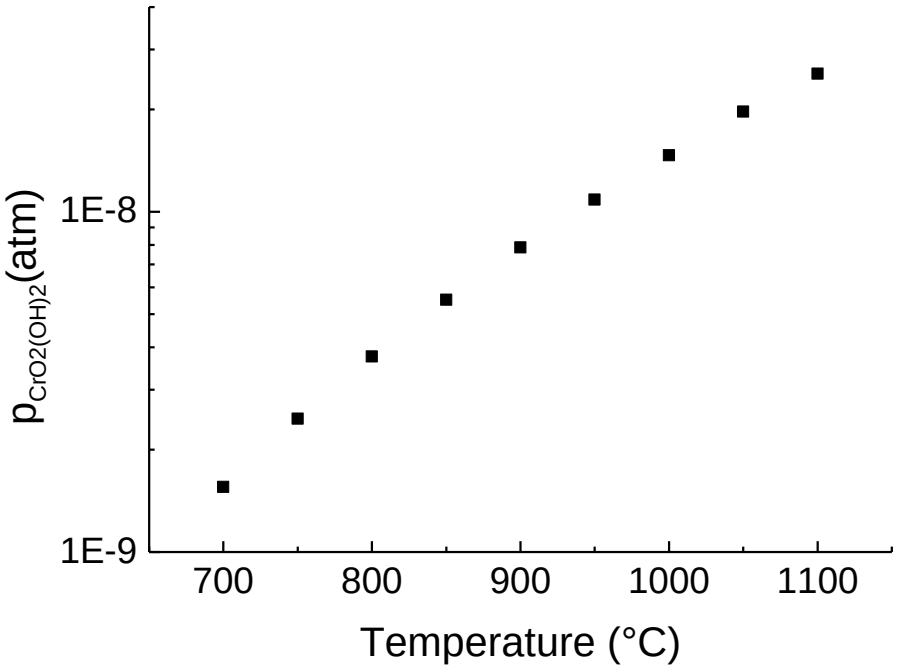


**Figure 6: Thermodynamic calculation of the $CrO_2(OH)_2$ partial pressure $p$ as a function of temperature for pure Cr in 30 vol.% $H_2O$ and 70 vol.% $O_2$.**

In order to provide a long-term protection at high temperatures and atmospheres, which contain a combination of water vapour and oxygen, alumina forming coatings have to be applied on metallic materials such as Fe and Ni-based alloys due to their resistance to these atmospheres. To turn such Fe- and Ni-based alloys into alumina formers, the coating process via pack cementation is the appropriate method for the above-mentioned aluminides on the surface.

## 3.4. Pack Cementation Modelling

It is known that higher operating temperatures of engines such as aircraft turbines require a long coating life time. Therefore, efforts have been made to optimize the Al coatings by the investigation of the correlation between the manufacturing process and resulting coating properties [14, 61, 62, 63].

In 1967, Janssen and Rieck investigated the diffusion coefficients and activation energies in intermetallic phases in the Al-Ni system [64, 65], which is the basis for coating growth considerations. Studies on the mechanism of formation of Al diffusion coatings in Ni-based superalloys and pure nickel in a one-step pack cementation process were performed by Goward et al. [66, 67]. They classified the coating mechanism into two processes: the *low temperature high activity pack* (LTHA) and the *high temperature low activity pack* (HTLA). During the LTHA process, the Al-rich nickel aluminide δ($Ni_2Al_3$) is formed, which can be converted by heat treatment and interdiffusion of Al into the substrate to the β-phase nickel aluminide NiAl. During the HTLA process, β-NiAl is mainly formed by outward diffusion of Ni from the substrate. With the work of Levine and Caves the thermodynamic and kinetic processes of pack cementation were examined quantitatively for the first time using a mathematical approach [68]. Here, the partial pressures of the Al halides have been calculated in dependence of the activator, pack composition, process temperature and process time. Based on this, the effect of these process parameters on the structure and thickness of the aluminide coating of the Ni-based alloy IN 100 was studied. They suggest that the classification into a *high activity* and *low activity* pack, as proposed by Goward and Bone can still be used. The process temperature rather than the Al pack activity controls the coating phase formed. Depending on the process parameters, the rate-controlling step is either the gaseous diffusion of Al compounds from the pack to the substrate surface or the solid state diffusion of Al into the substrate. When the substrate surrounding Al is transported, an Al depleted zone is formed in the powder, with continuous growth with time. Based on this assumption and the fact that the entire transported Al is deposited on the substrate, they derived parabolic coating growth kinetics, regardless of whether the solid state or gas phase diffusion is the rate limiting step.

Shankar and Seigle determined the diffusion coefficient over the entire β(NiAl) composition range via Matano analysis, which made it possible to evaluate the interdiffusion coefficients of Al and Ni as a function of composition with a reasonable

accuracy [69]. They measured the interdiffusion coefficient, using a vapour-solid technique, and found that the interdiffusion coefficient in NiAl varies by several orders of magnitude over the NiAl phase range with a minimum at 48 to 49 at% Al (Figure 7).

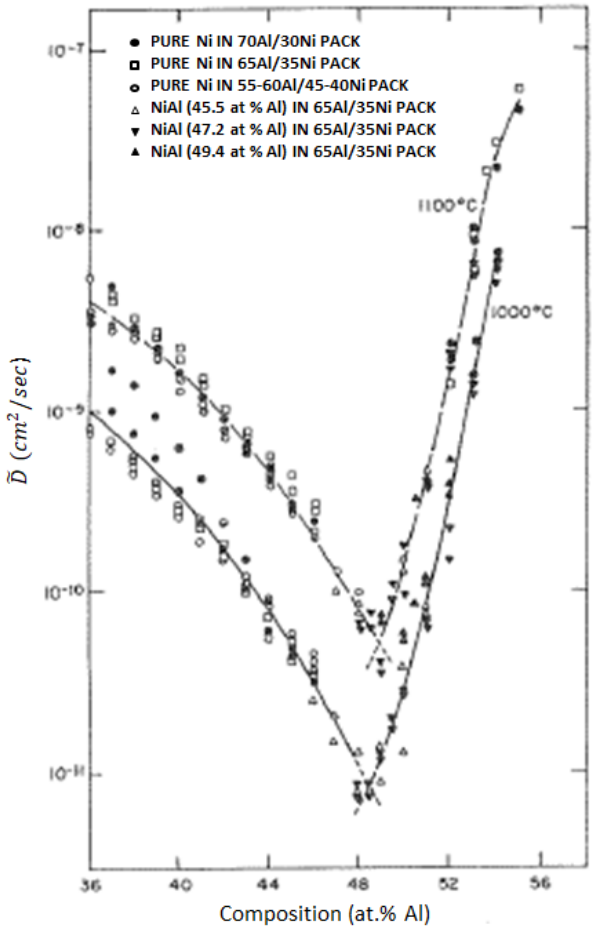


**Figure 7: Variation of the interdiffusion coefficient $D$ of Al with composition in NiAl for 1000 and 1100°C [69].**

Hickl and Heckel studied the pack cementation process by a two-step aluminizing process on Ni [70], in which the Al rich δ($Ni_2Al_3$) phase is initially formed by a high activity pack and then β(NiAl) phase is formed by continuous interdiffusion of Al into the substrate (Figure 8). Step 1 was characterized mainly by the rapid parabolic growth of the $Ni_2Al_3$ coating with concurrent growth of a thinner NiAl layer. Step 2 was characterized by the rapid loss of the Al content in the $Ni_2Al_3$ layer due to homogenization and parabolic growth of the NiAl layer by the dissolution of the $Ni_2Al_3$ phase.

By investigating the resulting coating thickness for a wide process temperature and range, the diffusion coefficients of Ni and Al were determined for several intermetallic

phases and thus concentration profiles were calculated with the limitation that, concentration independent diffusion coefficients were assumed.

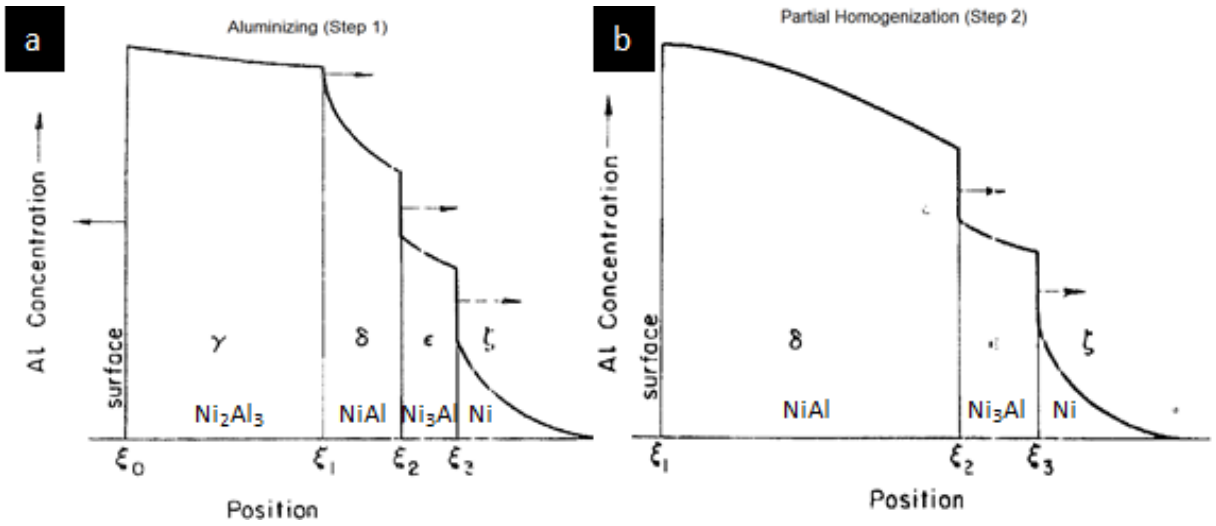


**Figure 8: Schematic representation of the Al concentration profile (a) during aluminizing of Ni and (b) at the end of homogenization treatment. Arrows indicate the motion of the interface. At step 1 the coating consists of $Ni_2Al_3$ (γ), NiAl (δ), $Ni_3Al$ (ε) and a solid solution (ζ). After homogenization the $Ni_2Al_3$ phase has completely dissolved into the NiAl phase. The positions $\xi_0$, $\xi_1$, $\xi_2$, $\xi_3$, indicate the phase boundaries.**

The later work shows that in most cases the structure developed is rather a combination of inward diffusion of Al and outward diffusion of Ni (or Fe) with a tendency of one of the two being dominant, depending on the process parameters.
Gupta et al. formulated a theory of pack aluminizing by combining the gaseous diffusion model of Levine and Caves with a calculation of solid state diffusion rates. They assumed that during the pack process, an Al depleted zone in the powder increases and therefore, the diffusion distance of the Al halides to the substrate increases, leading to a parabolic relationship of transferred Al weight $W_g$ and time $t$:

$$W_g^2 = \frac{2\rho\varepsilon M}{l}\frac{N_{Al}d}{A}t = K_g t \tag{3}$$

where $\varepsilon$ and $l$ designate the correction factors for pack porosity and pore length, and $M$, $\rho$, $d$, $A$, and $N_{Al}$ designate the atomic weight of Al, the pack Al concentration ($g\ cm^{-3}$), the diffusion distance ($cm$), the total area ($cm^2$) and the overall rate of diffusion of Al through the gas phase ($mol\ s^{-1}$), respectively.

Analog to the relationship for gaseous Al transfer, Al transfer via solid state diffusion $W_s$ obeys a parabolic law[1]:

$$W_s^2 = K_s t \tag{4}$$

where $K_s$ is the parabolic rate constant and depends on the surface composition. Hence, a plot of the two rate constants $K_g$ and $K_s$ against surface composition will intersect at a point where the rates are equal. This point defines the surface composition (intermetallic phase) and rate of formation of the coating [71]. It was shown that the Al concentration at the surface reaches a constant value shortly after the commencement of the deposition. While the rate of transport of Al from the pack to the coating surface decreases with increase in Al content at the surface, the rate of diffusion of Al from the surface into the sample increases with increase in Al content at the surface. In the steady state, both rates will be equal [71]. In Figure 9, $K_g$ and $K_s$ are superimposed and plotted against the surface composition.

Nciri and Vandenbulke [72] applied this model for iron aluminide coatings by pack cementation and obtained a good correlation between the theoretical and experimental values of surface composition.

[1] Provided that diffusion takes place into an infinitely extended medium, where the surface of the specimen remains at constant composition.

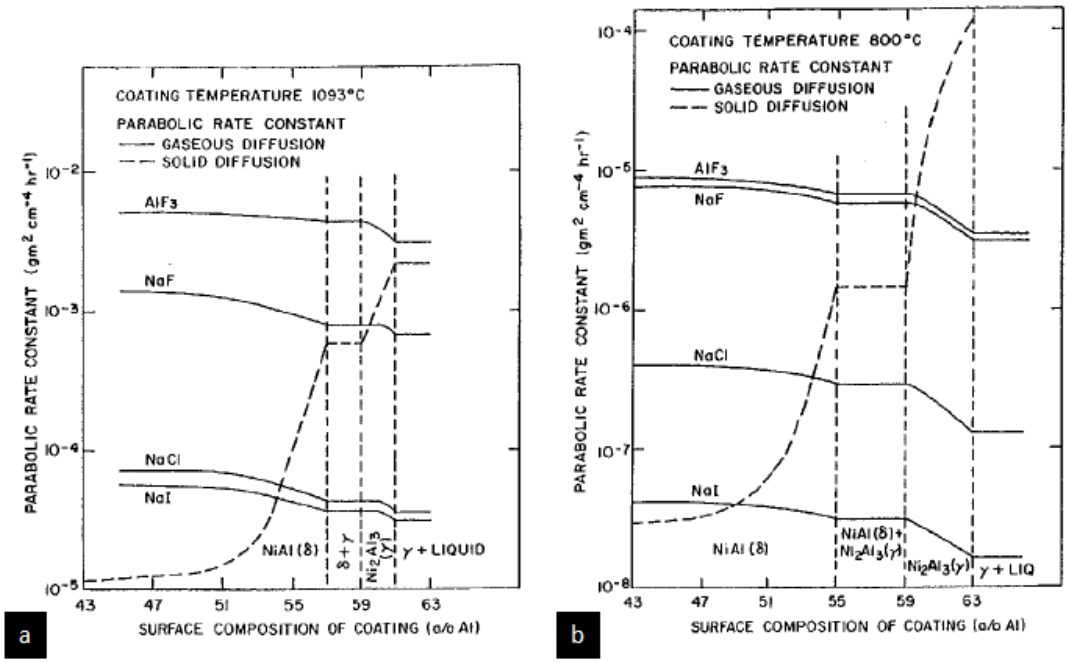


**Figure 9: Parabolic rate constants $K_g$ and $K_s$ for gaseous and solid state diffusion as a function of surface composition for several metal halides and intermetallic phases at (a) 1093°C (calculated) and (b) 800°C (calculated) [73].**

# 4. Development and Concept of Coating Design

Coating design for a material/deposition element (e.g. Al) couple starts with thermodynamic considerations. The thermodynamic consideration consists of comparing the Al activity of the pack (which is generated within the pack powder during the coating process) with the Al activity of the consequently generated intermetallic phase, and thus adjusting the process temperature and process time in order to achieve an Al pack activity, which has a comparable level with the Al activity within the desired intermetallic phase (β-FeAl and NiAl). This is performed by using the thermodynamic calculation software FactSage®, with which the Al activity within the pack powder as a function of temperature and powder composition can be determined and the phase diagrams of the Fe/Ni-Al systems as a function of temperature are calculated.

Based on the Al activity considerations, the resulting coating thickness is determined by means of the interdiffusion coefficient in the material, and depends on the process temperature and time. Since every single material has its particular properties, which affect the microstructure and chemistry of the Al diffusion coating significantly [74], at least three “calibration” experiments at three different temperatures have been performed in order to determine the pre-factor $D_0$ of the diffusion coefficient $D$ and activation energy $E_A$ for the considered material/deposition element couple.

The collection of the thermodynamic and kinetic data for a material/deposition element couple can then be used for the prediction of the resulting coating properties on this couple for a wide range of coating process parameters (process time $t$, process

temperature $T$ and pack powder mixture). Figure 10 shows an illustration of the coating design procedure.

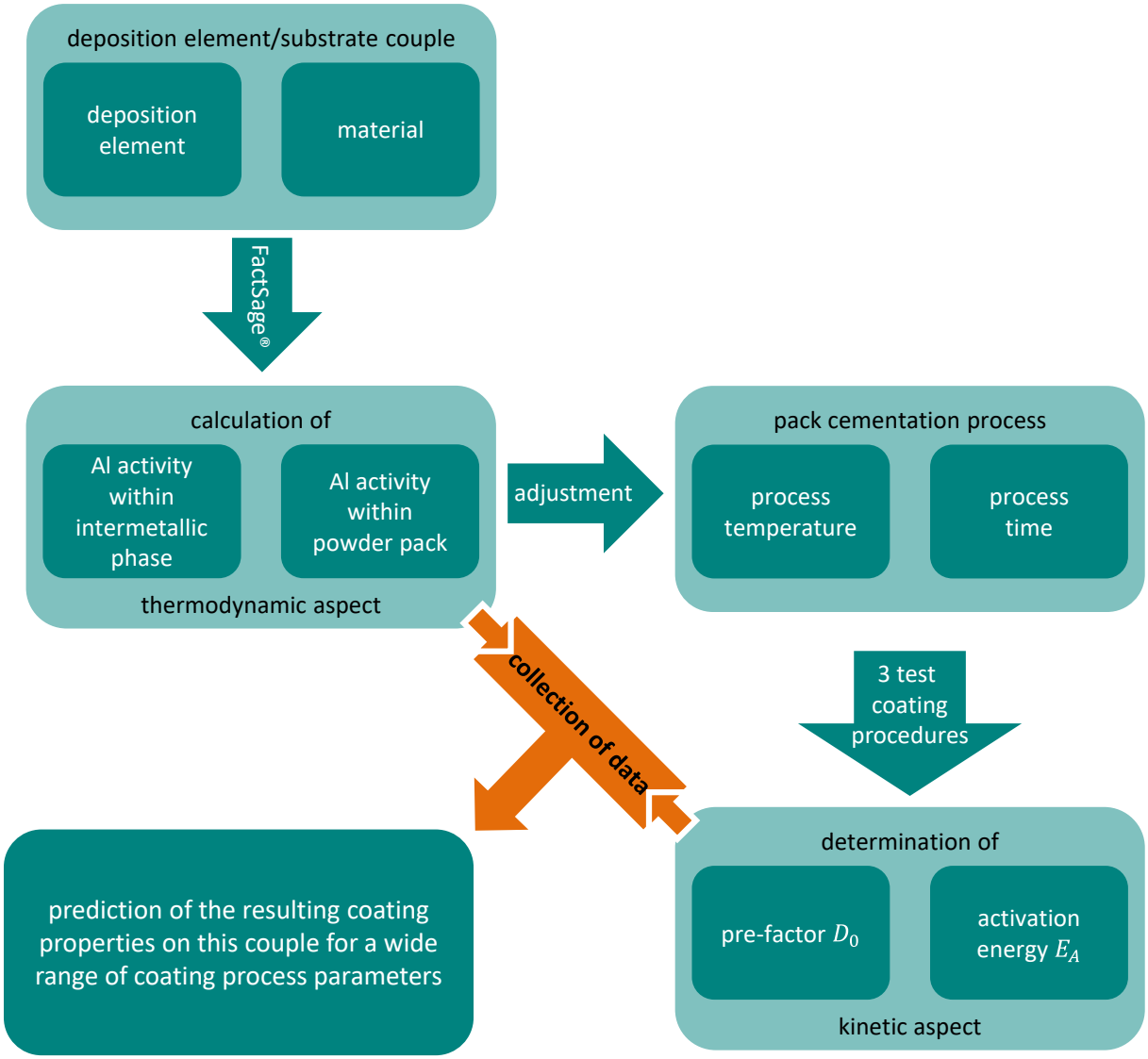


**Figure 10: Illustration of the coating design for a material/deposition element couple.**

## 4.1. Thermodynamic Considerations of Coating Design

The driving force for the gaseous transport of the deposition element (e.g. Al) to the substrate surface during the pack cementation process is the Al activity gradient between the powder pack (total partial pressure of the Al carrying halides) and coating surface. The same applies for the solid state diffusion of the deposited element, where its driving force is the Al activity (Al concentration) gradient between the coating and the substrate.

While the concentration is specified for ideal mixtures (gas, liquid or solid), the activity $a$ is its equivalent for "real" mixtures. The thermodynamic activity $a$ corresponds to the effective concentration of a species in a mixture. The activity is treated as a dimensionless quantity. The activity of pure substances in condensed phases (solid or liquid) is normally taken as unity (the number 1), whereas for mixtures, it depends on the composition, temperature and pressure. For gases, the activity is the effective partial pressure and is referred to as fugacity.

Both the activity within the pack and within the intermetallic phases can be calculated, e.g. via the thermodynamic calculation software FactSage®.

### 4.1.1. Al Activity within the Powder Pack

In contrast to "real" gases, attraction or (electrostatic) repulsion between the gas particles are not considered on ideal gases. The fugacity of a gas $i$ may be higher or lower than its mechanical pressure. The fugacity has the dimension of pressure. Thus, the activity is:

$$a_i = \frac{f_i}{p^\theta} = \emptyset_i y_i \frac{p}{p^\theta} \tag{5}$$

where $\emptyset_i$ is the dimensionless fugacity coefficient of the species $i$, $y_i$ is its fraction in the gaseous mixture ($y = 1$ for a pure gas) and $p$ is the total pressure. The value $p^\theta$ is the standard pressure: it may be equal to 1 atm (101.325 kPa) or 1 bar (100 kPa) depending on the source of data, and should always be quoted.

The Al activity within the pack is calculated by means of the FactSage *Equilib* module, which is the Gibbs energy minimization tool of FactSage® (Figure 11 a). It calculates the concentrations of chemical species when specified elements or compounds react or

partially react to reach a state of chemical equilibrium [75]. The components of the pack are fed to the system either in mole or gram (Figure 11 b), and the corresponding databases have to be chosen with the *Data Search* function (Figure 11 c). The resulting gaseous compositions are dependent on the powder composition and process temperature. The total pressure is set to be 1 atm. (Figure 11 d).

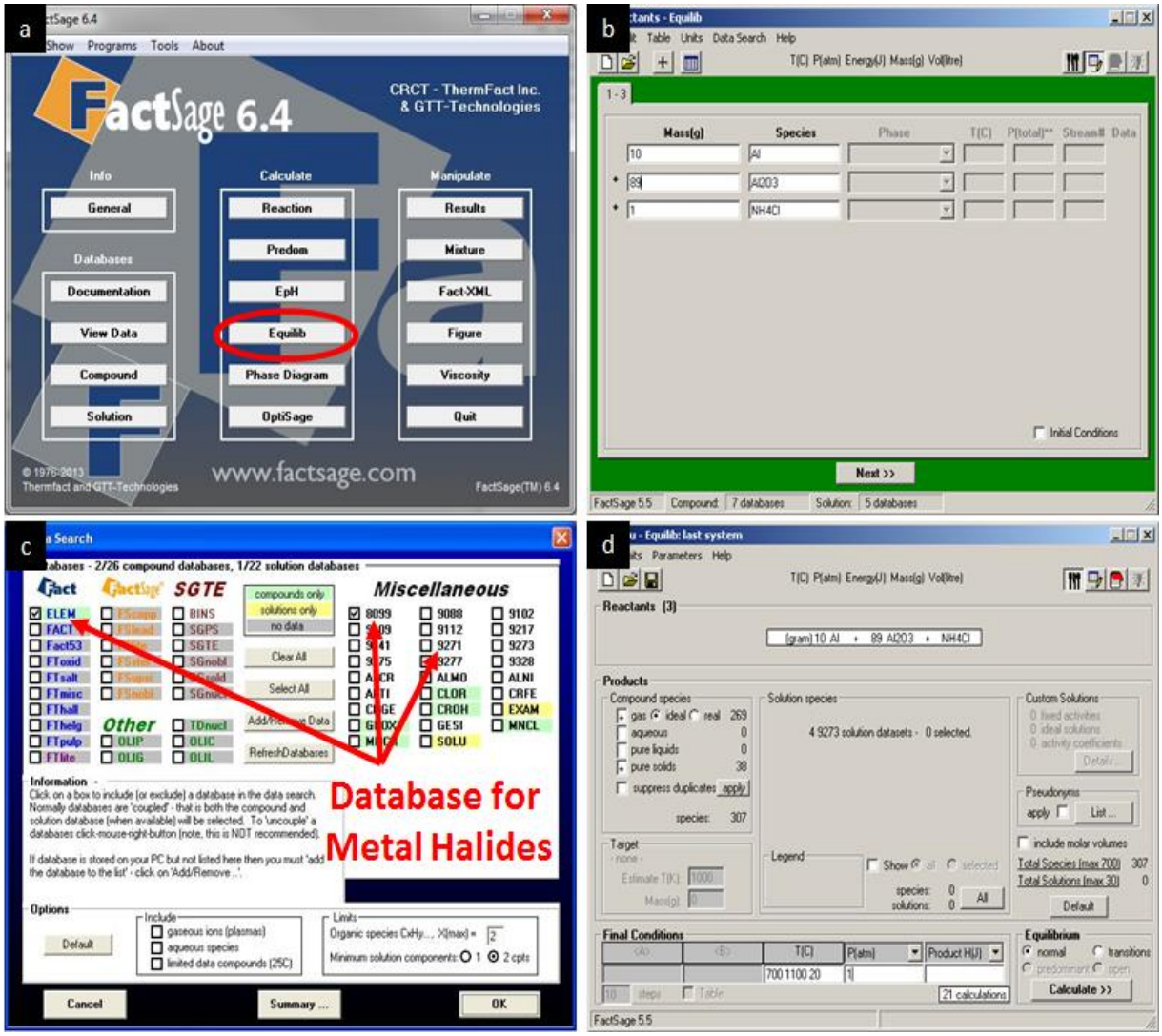


**Figure 11: Operating panels of the FactSage® *Equilib* module to determine the Al activity in the pack.**

#### 4.1.1.1. Contribution of the Metal Chlorides to the Metal Activity within the Pack

The reaction of the deposition element (e.g. Al) with the activator (e.g. $NH_4Cl$) in the pack leads to the formation of different metal halides, where the partial pressure of every metal halide is a function of both the pack composition (amount of deposition element and activator), and the process temperature.

Each metal halide of the type $M_aX_b \begin{cases} a = 1; b = 1,2,3 \\ a = 2; b = 6 \end{cases}$ and $MH_aX_b \begin{cases} a = 1; b = 1,2 \\ a = 2; b = 1 \end{cases}$ $(M: Al, Si, Cr, Hf\ etc.;\ X: F, Cl, Br; H: Hydrogen)$ is a prospective carrier of the deposition element. The sum of partial pressures of the deposition element carrying halides gives an indication for the quantity of deposition element delivery to the substrate. In addition, the sum of the partial pressures of the Al chlorides are considered as Al activity of the pack. This is exemplified by the ratio of the total partial pressure of the deposition element carrying halides to the total pressure:

$$a_{dep.elem.}(pack) = \frac{p(dep.\,elem.\,carrier)}{p(total)}$$

$$= \frac{\sum_i p_i(M_aX_b + MH_aX_b)}{\sum_i p_i} = \frac{\sum_i p_i(M_aX_b + MH_aX_b)}{1\ bar} \tag{6}$$

$$= \sum_i p_i(M_aX_b + MH_aX_b)$$

The calculated partial pressures are plotted over the process temperature (Figure 12). As it can be seen, $AlCl$ and $AlCl_3$ have the largest contribution to the total pressure of Al-chlorides and, thus, are assumed to play an important role in Al-deposition.

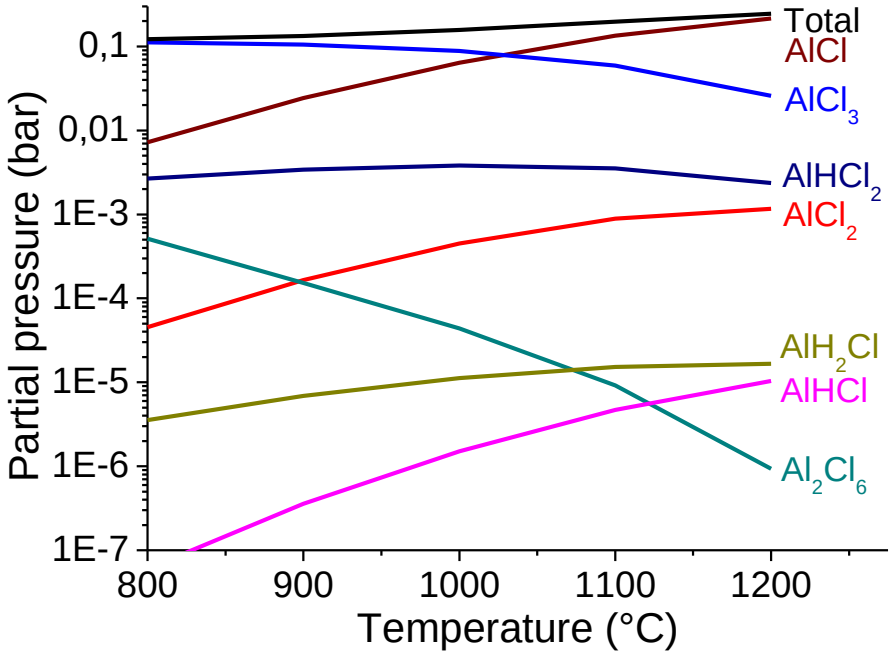


**Figure 12: Calculation of the partial pressure of the deposition elements carrying chlorides for an 1wt.% Al, 1wt.% $NH_4Cl$, 98wt.% $Al_2O_3$ pack as a function of temperature.**

Besides the partial pressure of the metal carrying chlorides, the dissociation energy for the deposition of the metal at the substrate surface provides information about the deposition tendency of a metal at the substrate surface and thus about the resulting coating structure. According to Xiang et al. [10] only the $AlCl$ vapour species is responsible for the Al deposition and is considered in his thermodynamic calculations. Neither the vapour species of higher chlorides $(AlCl_2, AlCl_3, Al_2Cl_6)$ nor vapour species types of $AlH_aCl_b \begin{cases} a = 1; b = 1{,}2 \\ a = 2; b = 1 \end{cases}$ do contribute to Al deposition. Weber et al. [76] stated that for Al deposition the species $AlCl$ and $AlCl_2$ are relevant and undergo dissociation reactions, whereas $AlCl_3$ remains nearly stable and dissociates only to a small amount. According to Weber et al. the same applies to $SiCl_4$, where the tendency for dissociation increases from tri- to mono-chloride.

Our thermodynamic calculations of the dissociation energies for relevant metal chlorides as a function of temperature (Figure 13) show that in the case of Al chlorides, $AlCl_3$ has the highest dissociation energy, which would mean that its contribution to the Al deposition should be rather low. The dissociation energies were calculated via the *Reaction Module* of FactSage®, where the energy of the dissociation of a metal chloride compound to its components was calculated (e.g. $2\ AlCl_3 \rightarrow 2\ Al + 3\ Cl_2$).

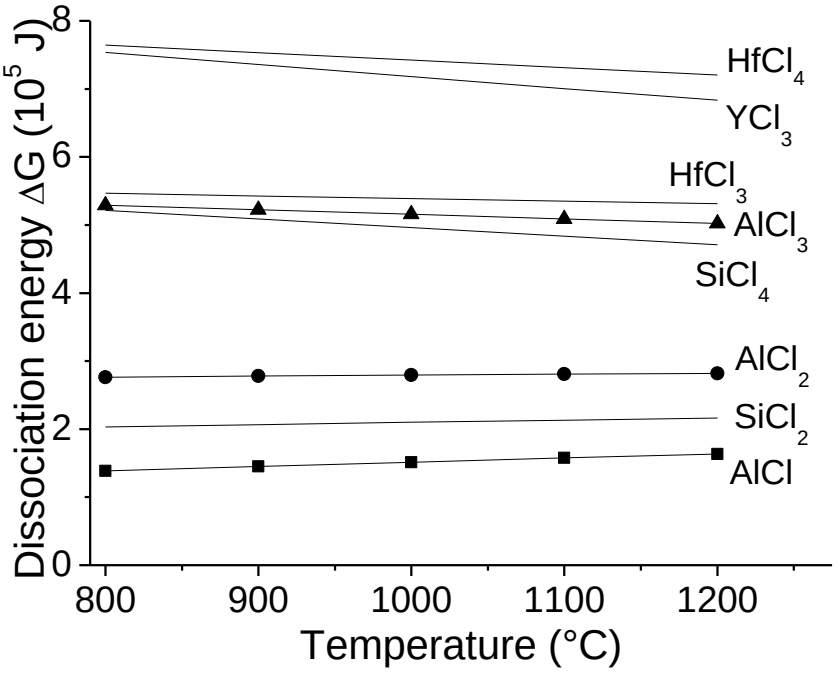


**Figure 13: Thermodynamic calculation of the dissociation energies of relevant deposition elements carrying chlorides as a function of temperature.**

$AlCl$ has the lowest dissociation energy, which would mean that the Al deposition from $AlCl$ would be favored over that from $AlCl_3$. Although the dissociation energies of the Al chlorides are different, the sum of the partial pressures of the Al chlorides has to be considered as the Al activity within the pack, since e.g. $AlCl_3$, which has a high dissociation energy, can also contribute to the Al deposition in an indirect way, by the reaction with Al to $AlCl$:

$$AlCl_3 + 2\,Al \leftrightarrow 3\,AlCl \qquad (7)$$

#### 4.1.1.2. Effect of Argon/5% $H_2$ and Aluminium Oxide on the Thermodynamic Calculations

Usually, the pack cementation process is performed under an Ar/5%$H_2$ flow, with a flow rate of 2L/h. Hydrogen has no effect on the pack cementation process itself, but it serves as a getter for the residual oxygen in the quartz glass tube. Thus, $H_2$ is considered to have no influence on the chemical reactions of the pack process Thermodynamic calculation of the Al activity for pack compositions, consisting of

1 wt.% Al, 1 wt.% $NH_4Cl$ and 98 wt.% $Al_2O_3$, does not change by the addition of $H_2$, Ar and $Al_2O_3$ as shown in Figure 14 a.

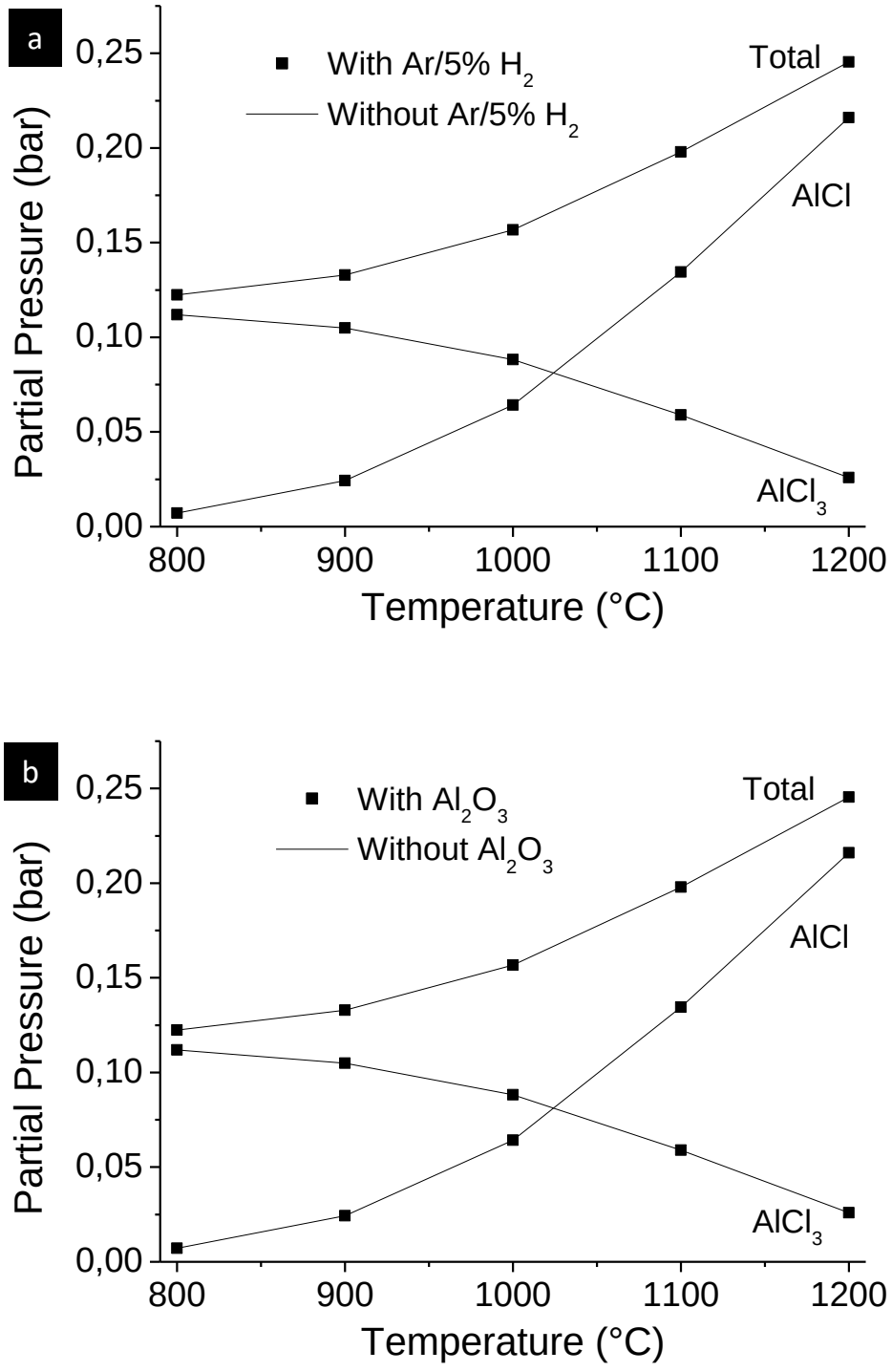


**Figure 14: Comparison of the calculated partial pressures of Al carrying chlorides for a pack composition of 1 wt.% Al, 1 wt.% $NH_4Cl$ and 98 wt.% $Al_2O_3$ as a function of temperature with and without (a) Ar/5%$H_2$ and (b) $Al_2O_3$.**

The same applies for $Al_2O_3$. It serves as inert filler, which prevents the sintering of Al powder during the pack process. As Kung et al. reported, the $Al_2O_3$ filler is extremely stable and does in the most cases not react significantly with other pack components. Therefore, it can be excluded from the thermodynamic calculations [77]. The thermodynamic calculations in Figure 14 b show that the Al activity within the pack is the same, no matter whether $Al_2O_3$ is considered in the calculations or not.
However, this is not valid for every type of activator and deposition element. $Al_2O_3$ could not be considered inert if a more stable, e.g. a reactive element, is included in the pack powder mixture.

#### 4.1.1.3. Effect of Co-deposition

The addition of another element to the main deposition element Al reduces the partial pressure in the pack [78]. In Figure 15 the total and partial pressures of Al, Si and Hf chlorides were calculated for an Al/Si (1wt.% Al, 10wt.% Si, 1wt.% $NH_4Cl$, 88wt.% $Al_2O_3$) and an Al/Hf (1wt.% Al, 3wt.% Hf, 1wt.% $NH_4Cl$, 95wt.% $Al_2O_3$) powder pack mixture as a function of temperature. The thermodynamic calculations show that the difference between the partial pressures of Al carrying chlorides and the Si or Hf carrying chlorides is large. This means that Al deposition should be favored over Hf or Si deposition. This is not necessarily counterproductive, since only low amounts of the co-deposition elements have to be incorporated in the aluminide coatings.

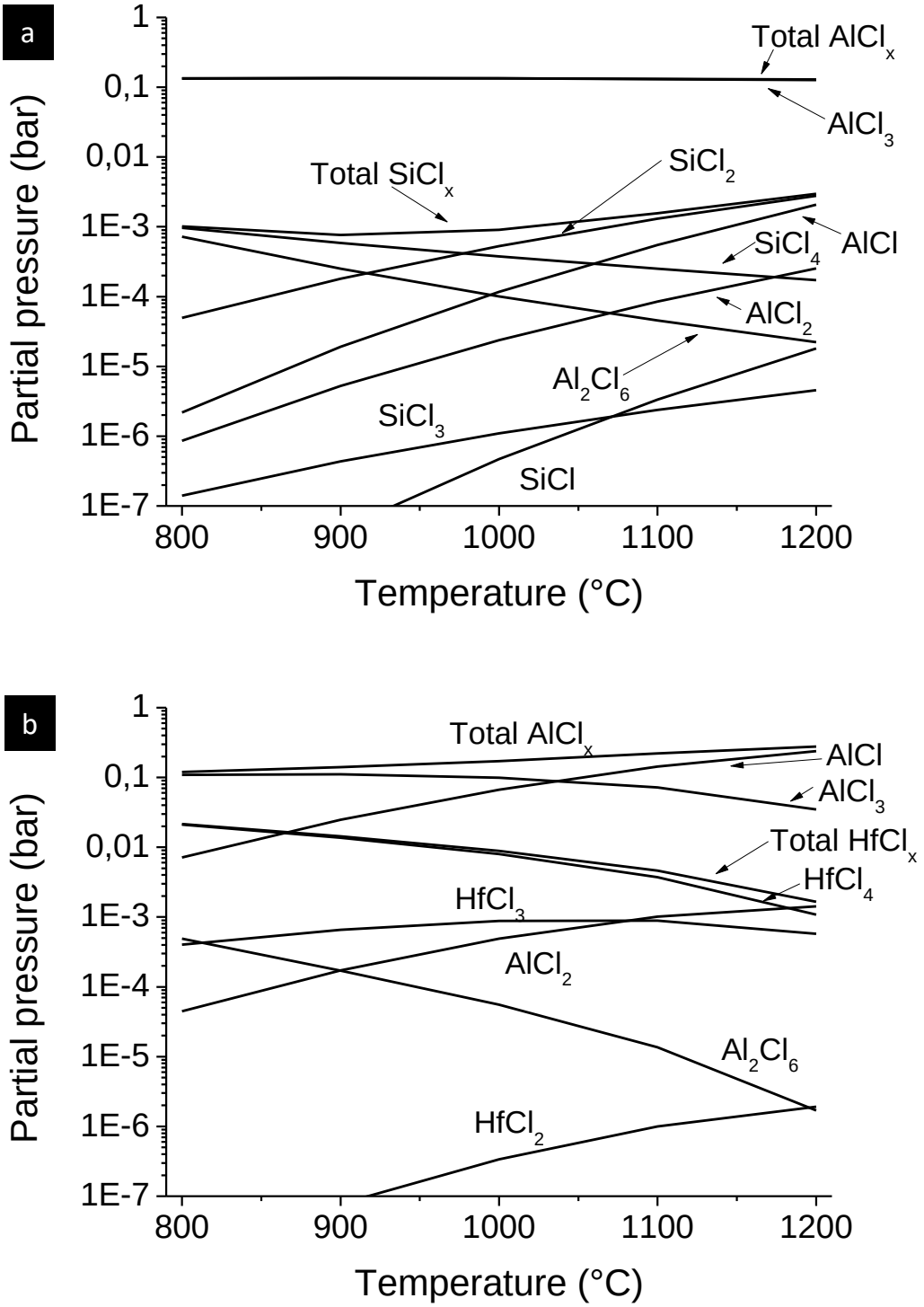


**Figure 15: Thermodynamic calculation of the partial pressures of the deposition elements carrying chlorides as a function of temperature for an a) Al/Si and an b) Al/Hf pack.**

Xiang et al. also calculated the temperature dependence of the partial pressures of these chloride vapours for a pack containing 2 wt.% Al in the series (Figure 16). It shows

that the optimum coating temperature is situated between 925 and 1125°C, where the vapour pressure curve of AlCl intersects that of Si chlorides.

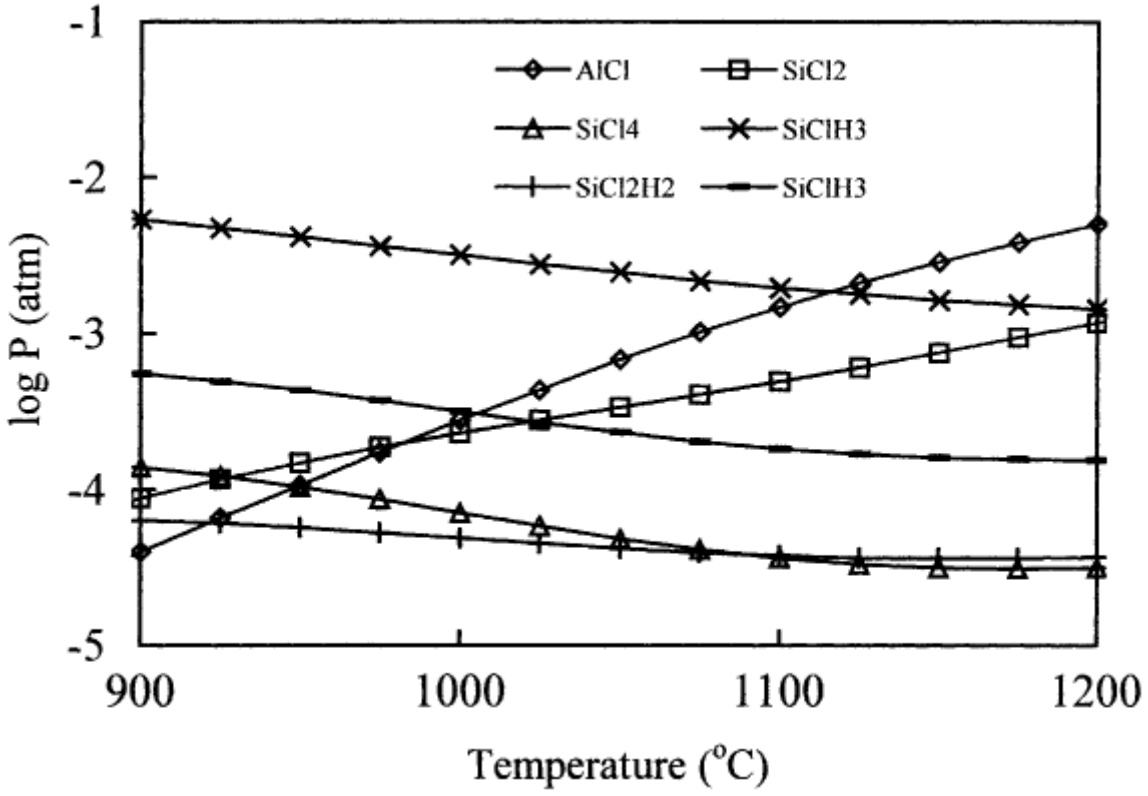


**Figure 16: Dependence of the equilibrium vapour pressure of Al and Si chloride species on temperature for a pack 2 wt.% Al, 5 wt.% Si, 3 wt.% $NH_4Cl$, 90 wt.% $Al_2O_3$ [35].**

The Al activity within the pack is shown to be reduced by adding Si to the Al pack powder mixture (Figure 17), because the activator is consumed by two elements instead of one (Al pack activity: 0.18 at 1000°C; Al/Si pack activity: 0.12 at 1000°C). Both calculated Al activity values for the Al and Al/Si pack are in the level of the Al activity of the β-FeAl intermetallic phase. This means that after a pack cementation process with both pack mixtures at 1000°C for 4 hours, the development of the FeAl intermetallic phase is expected.

Comparable to Si addition to the Al pack, the thermodynamic calculations in Figure 18 show that the Al activity is reduced when Hf is present in the powder.

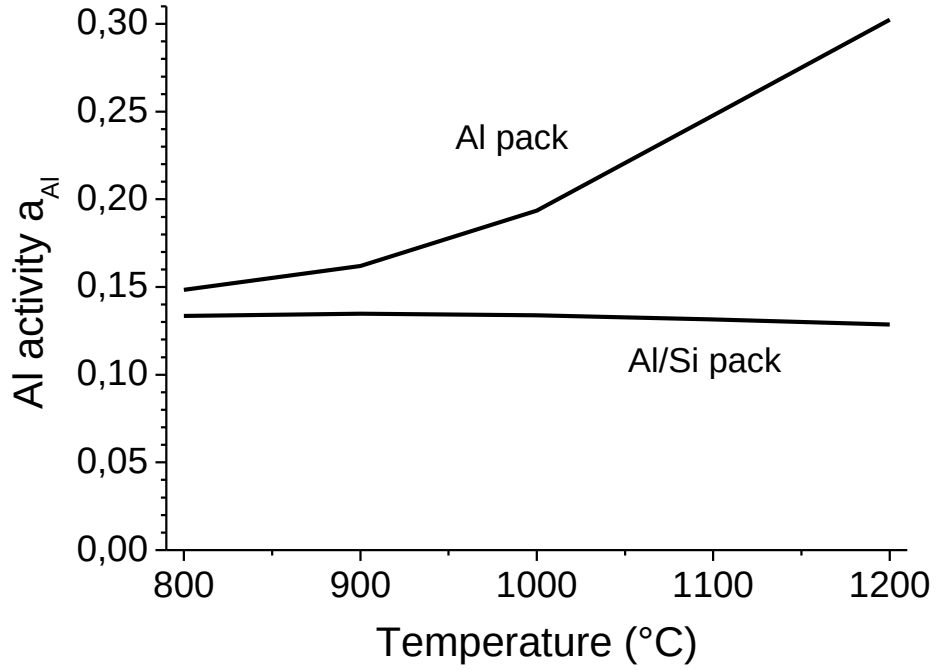


**Figure 17: Calculation of the Al activity for Al pack (1wt.% Al, 1wt.% $NH_4Cl$, 98wt.% $Al_2O_3$) and Al/Si pack (1wt.% Al, 10wt.% Si, 1wt.% $NH_4Cl$, 88wt.% $Al_2O_3$) as a function of temperature.**

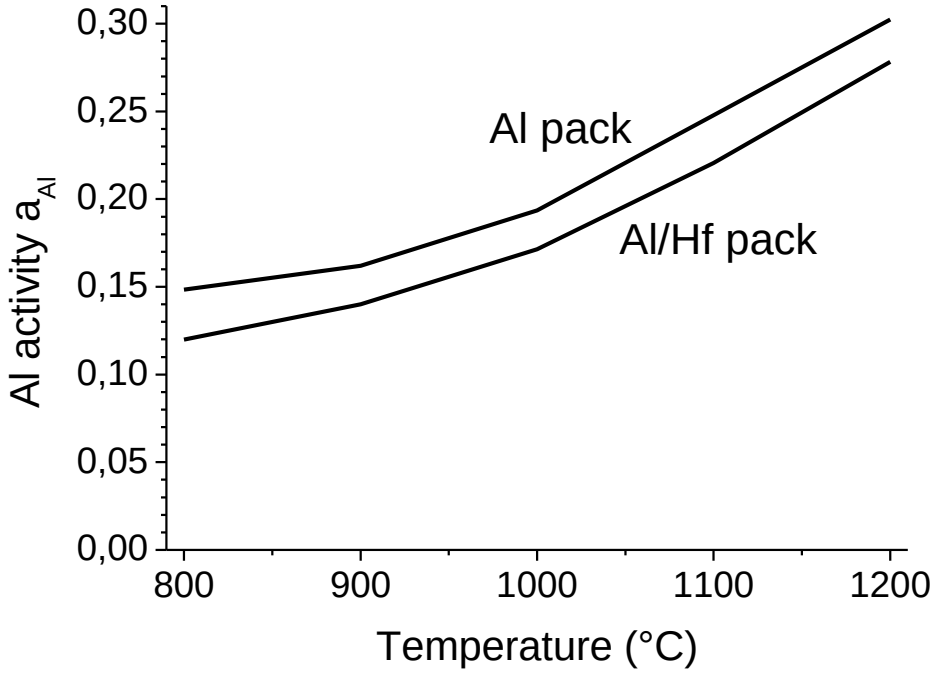


**Figure 18: Calculation of the Al activity for Al pack (1wt.% Al, 1wt.% $NH_4Cl$, 98wt.% $Al_2O_3$) and Al/Hf pack (1wt.% Al, 3wt.% Hf, 1wt.% $NH_4Cl$, 95wt.% $Al_2O_3$) as a function of temperature.**

### 4.1.2. Al Activity within the Intermetallic Phases

Analogous to “real” gases, attractive forces occur between the particles in “real” liquid or solid mixtures. In contrast to the "ideal behaviour", in which the concentration of component *A* of a binary mixture is equal to the mole fraction, the activity of actual mixtures or alloys usually shows a negative deviation. Since in the solid mixtures the attractive forces between the particles are much stronger than in gas mixtures, it is necessary to replace the concentration by the activity:

$$a = x \cdot \gamma \tag{8}$$

where $\gamma$ is the dimensionless activity coefficient, which is a function of the concentration. The activity $a$ of one element of a binary system is between 0 and 1 and is always lower than its mole fraction.

The activity of an element in a binary intermetallic phase is also temperature dependent. If the activity is known for one temperature, it can be extrapolated to other temperatures:

$$ln\left[\frac{a(T_2)}{a(T_1)}\right] = \frac{\Delta\overline{H}}{R} \cdot \left(\frac{1}{T_2} - \frac{1}{T_1}\right). \tag{9}$$

$a(T_1)$ and $a(T_2)$ are the element activities at the temperature $T_1$ and $T_2$, respectively, $R$ is the gas constant, and $\Delta\overline{H}$ is the partial molar enthalpy of the element. $\Delta\overline{H}$ is assumed to increase linearly with increasing temperature.

The Al activities in the Fe-Al and Ni-Al systems are correlated with the phase diagram of these systems. Thus, the calculation of a phase diagram of a binary system and activity of a species in this system via FactSage® are based on the same database. The phase diagrams of the Fe-Al and Ni-Al systems are calculated by the *Phase Diagram* module (Figure 19 a). The corresponding databases have to be chosen with the *Data Search* function (Figure 19 b and c). Finally, the temperature, composition range and considered compound and solution species are chosen and calculation of the phase diagram can be started (Figure 19 d).

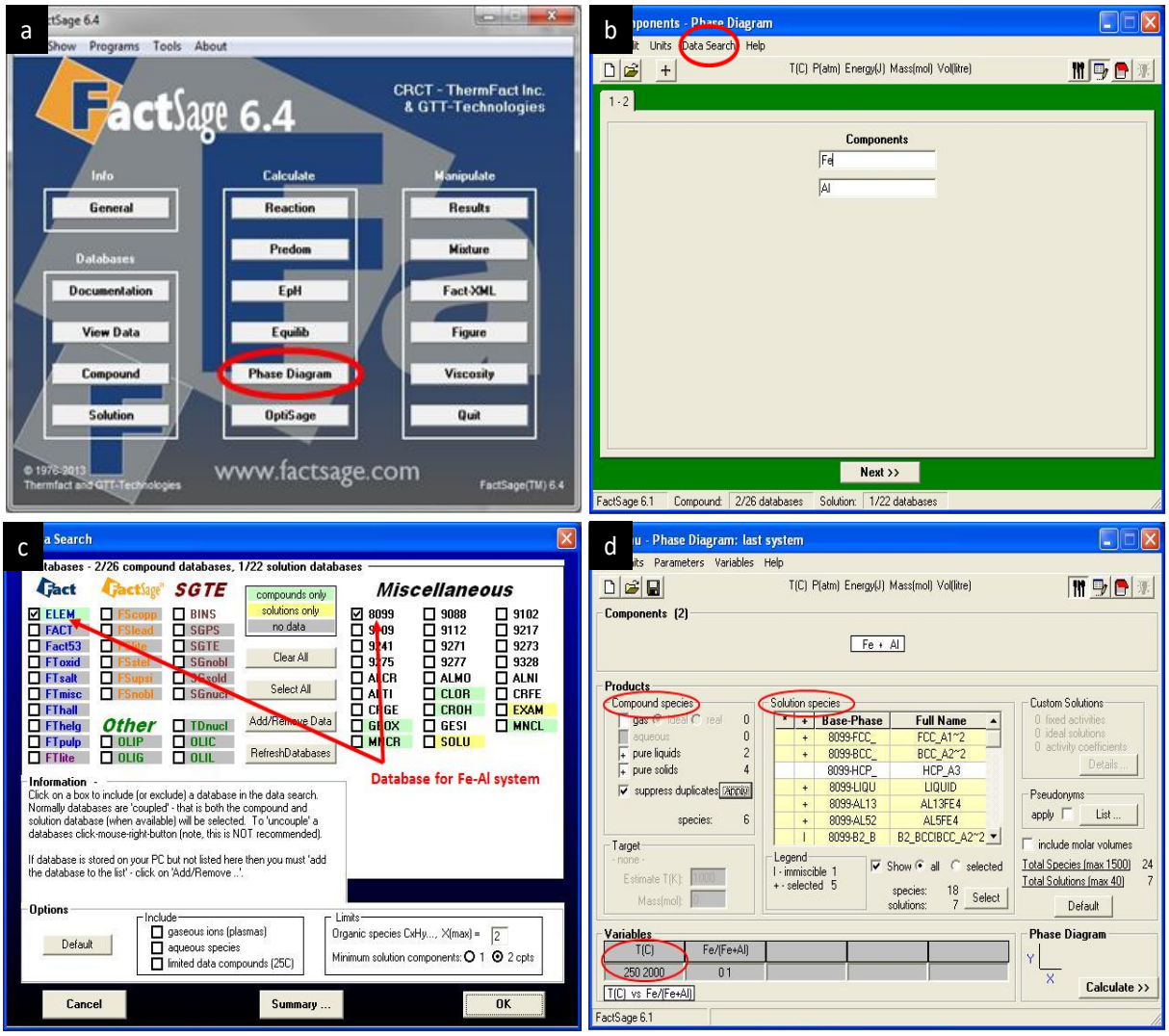


**Figure 19: Operating panels of the FactSage® *Phase Diagram* module.**

The calculated phase diagrams of the Fe-Al and Ni-Al systems show very good agreement to the literature (Figure 20) [24].

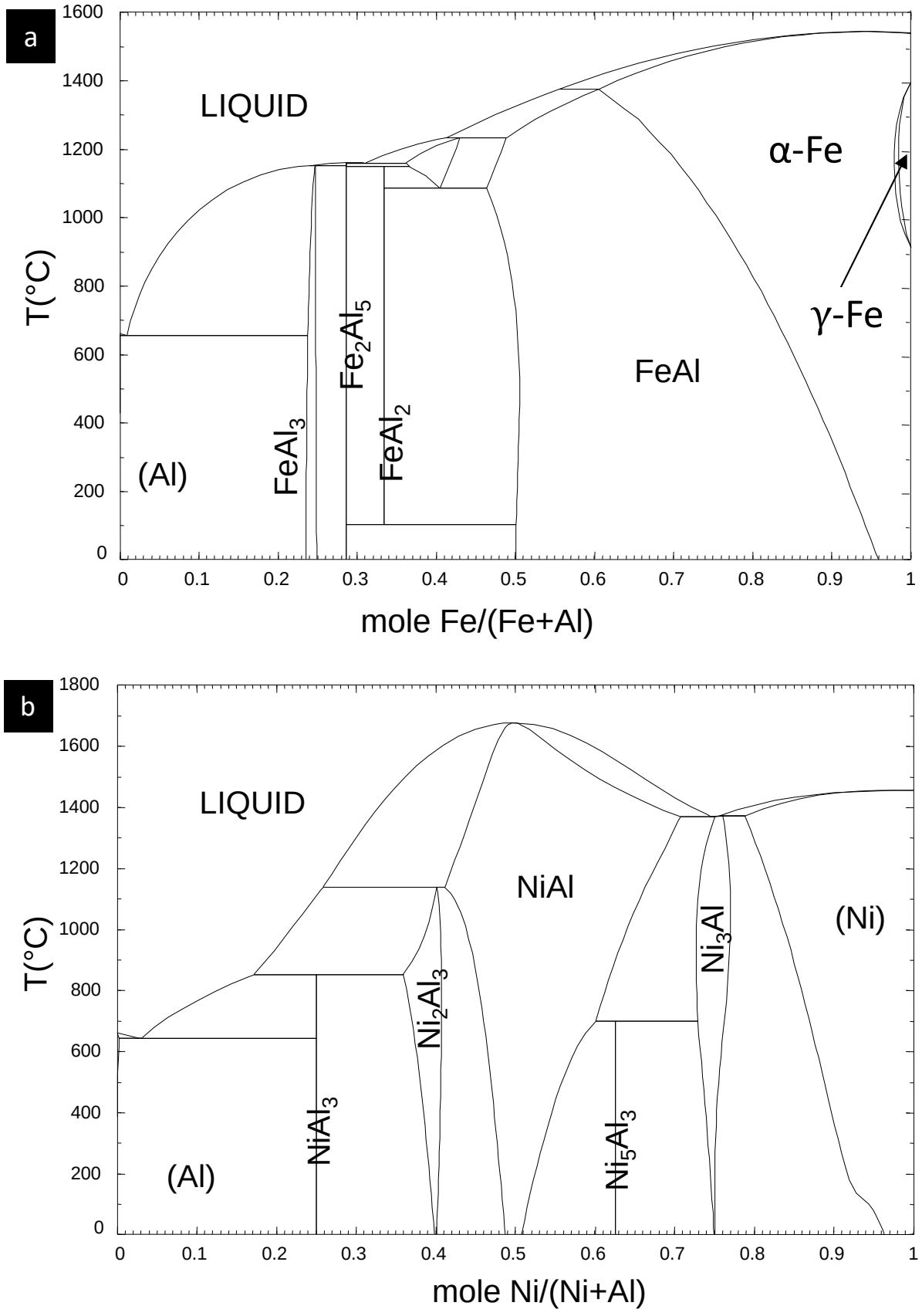


**Figure 20: Via FactSage® calculated phase diagrams of the (a) Fe-Al and (b) Ni-Al systems.**

The Al activities in the phases of the Fe-Al and Ni-Al systems are calculated as a function of the Al mole fraction in the system at 1000°C (Figure 21). The Al activity is not equal

to the mole fraction, and the steps in the curves correspond to the phase transitions in the Fe-Al and Ni-Al phase diagrams. The horizontal lines (e.g. 0.1 to 0.23 moles (Figure 21 a) or 0.2 to 0.4 moles (Figure 21 b)) show that the program FactSage® assumes constant Al activity values in mixed phases.

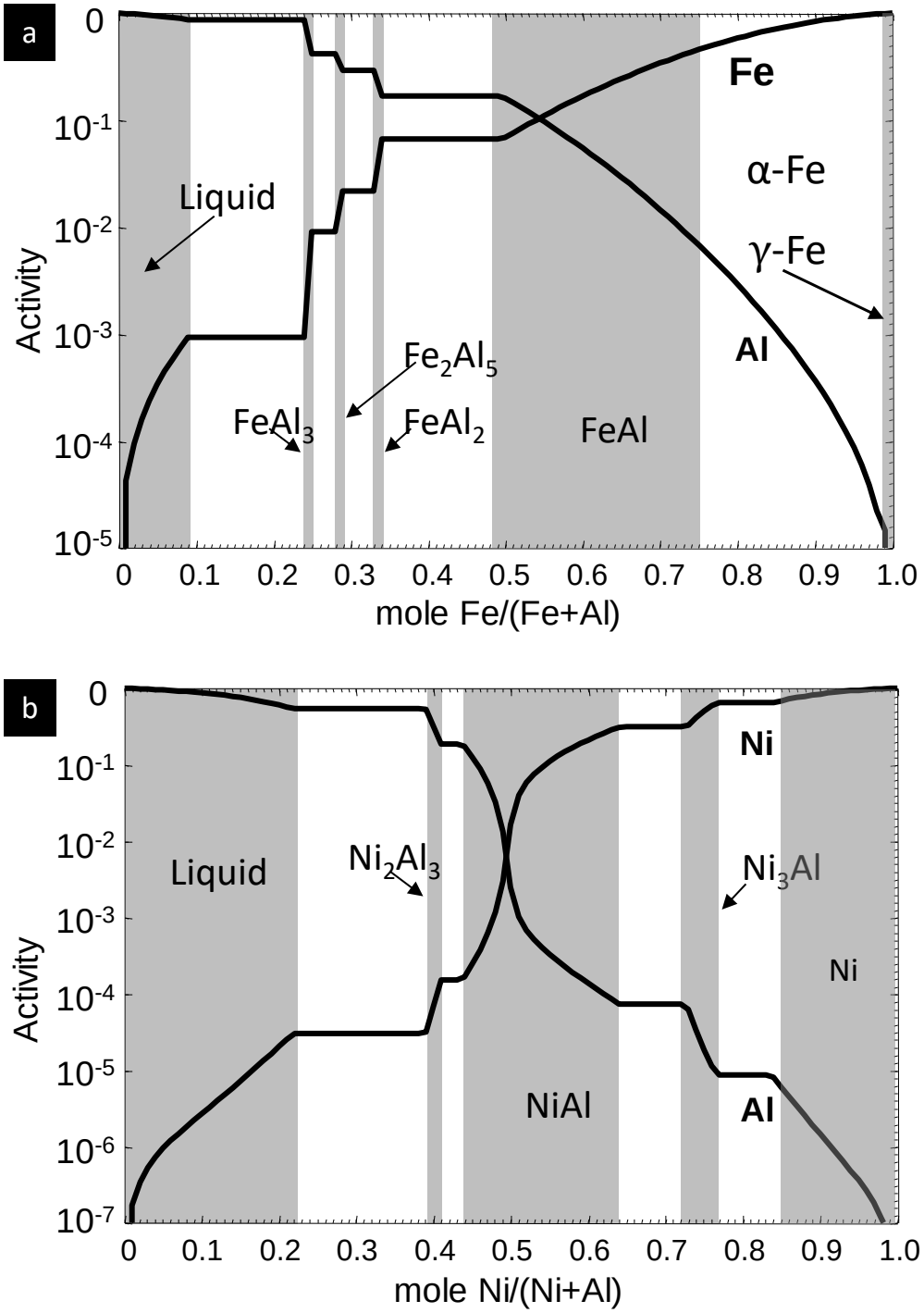


**Figure 21: Via FactSage® calculated Al activities within the phases in the (a) Fe-Al and (b) Ni-Al systems at 1000°C.**

As it is shown in Figure 22 the calculated Al activities within the Fe-Al and Ni-Al systems for different temperatures and Al mole fractions show good agreement with the literature values [22, 79, 80, 81, 82].

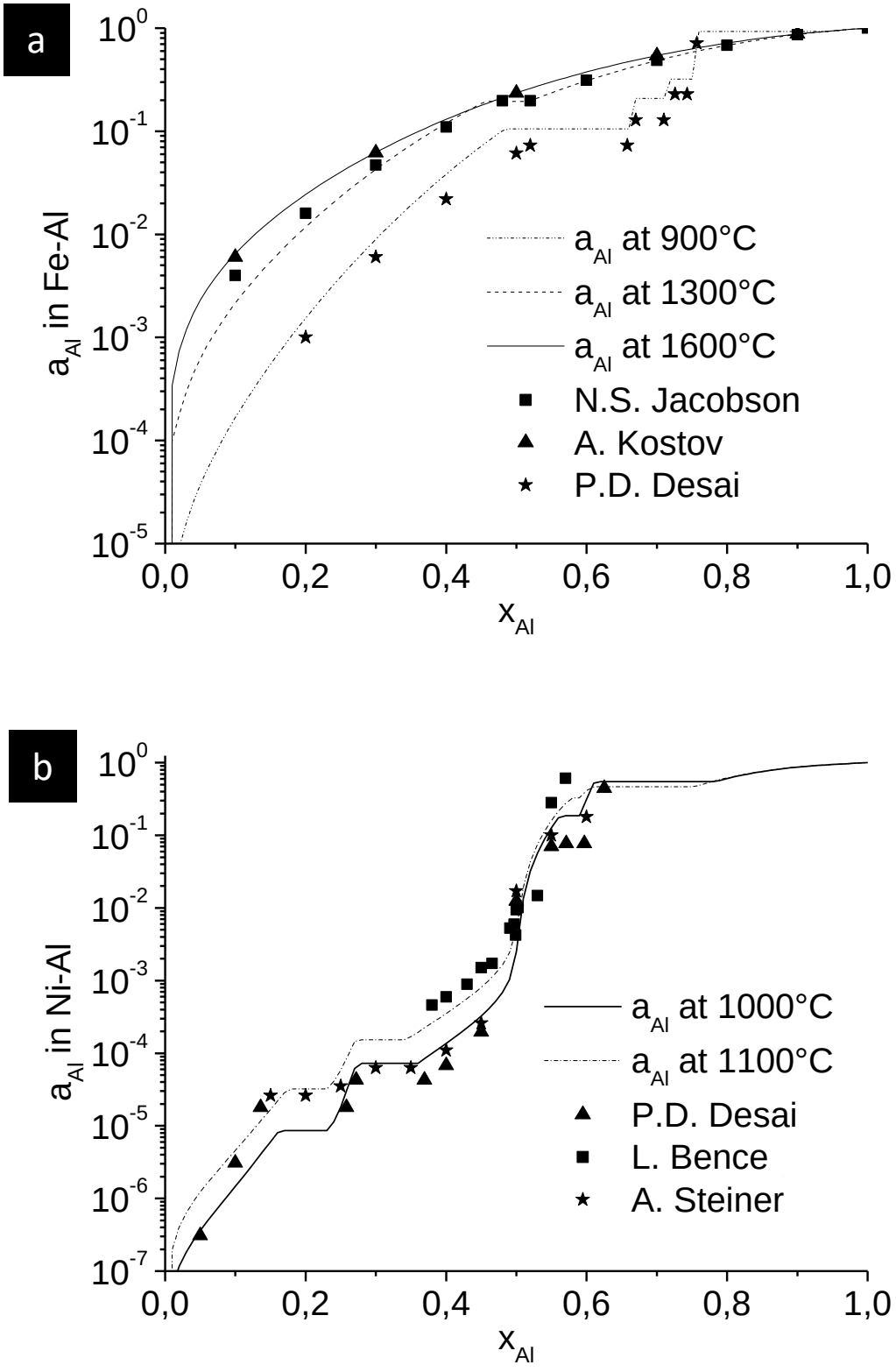


**Figure 22: Comparison of the calculated Al activities in the a) Fe-Al and b) Ni-Al systems (as a function of mole fraction) with literature values.**

## 4.2. Kinetic Considerations of Coating Design

### 4.2.1. Diffusion in Binary Intermetallics

Diffusion also plays a crucial role in the pack cementation process, since it determines both, the gas phase diffusion of the metal halides from the pack to the substrate surface and the solid state interdiffusion of the deposition element into the substrate. Interdiffusion is the diffusion of two different atomic species of formerly separated areas within each other. It is assumed that the diffusion partners are the deposited Al at the substrate surface and Fe or Ni from the substrate steel or Ni-based superalloy.
Fick's first law describes the relationship between the deposition element activity gradient $\partial a/\partial x$ and diffusion flux $j$ (amount of substance per unit area per unit time) $j$, with $D$ as a constant of proportionality:

$$j = D\frac{\partial a}{\partial x} \tag{10}$$

However, since it is difficult to maintain a constant concentration gradient during the experiment, Fick's second law enables the tracing of the concentration along the diffusion path after a certain time, or the time progression of concentration at a certain point [83]:

$$\frac{\partial c}{\partial t} = \frac{\partial}{\partial x}\left(D\frac{\partial a}{\partial x}\right) \tag{11}$$

During the solid state diffusion step of the pack cementation process, a diffusion coating is formed mainly either by inward diffusion of the deposition element (e.g. Al) and secondarily outward diffusion of the material element (assumed to be Fe by coating an Fe-based alloy or Ni by coating a Ni-based alloy), causing a high temperature low activity (HTLA) coating, or mainly by outward diffusion of the substrate element and secondarily inward diffusion of the deposition element, causing a low temperature high activity (LTHA) coating. This results in a diffusion coating, which is formed by the interdiffusion of the two elements with different diffusion coefficients $D_i$ and $D_j$, but the interdiffusion coefficient $D$ is composed of the diffusion coefficients of both elements (Darken equation):

$$D = D_i x_i + D_j x_j. \tag{12}$$

Thus, the resulting intermetallic phase in a coating and its thickness also depend on the diffusion characteristics of the material and deposition element couple (Al/Fe or Al/Ni), which on the other hand depends on the pack process temperature and deposition element activity difference between material and pack. The interdiffusion coefficient of the deposition element in the material follows an Arrhenius like equation:

$$D(T) = D_0 \, exp\left(\frac{E_a}{RT}\right) \tag{13}$$

where $D_0$ is the pre-factor of the diffusion coefficient (temperature-independent material parameter), $E_a$ the activation energy to be overcome for site exchange of the atoms in the lattice, $R$ the gas constant and $T$ is the temperature.

A graphical method for determining the concentration dependent diffusion coefficient is the Matano analysis [83]. The solid-state diffusion step in the pack cementation process can be considered as a heat treatment of a binary diffusion couple (deposition element and material), consisting of two half-spaces. After a period of heat treatment at a given temperature, a concentration profile arises for each element of the diffusion couple. Via the Boltzmann approach [84], Fick's second law is converted, so that an equation for the diffusion coefficient results, which can be solved graphically:

$$D = -\frac{1}{2t}\frac{dx}{dc}\int_0^c xdc\,, \qquad where \int_0^1 xdc = 0 \tag{14}$$

The determination of the tangent $\frac{dx}{dc}$ of the concentration profile $c(x)$ at the Matano-plane and the integral value $\int_0^c xdc$ can be performed graphically (Figure 23). At the Matano-plane, the net particle flux is zero (the particle flux is equal at both the left and right side of the Matano plane), which means that both areas below and beyond the concentration profile are the same.

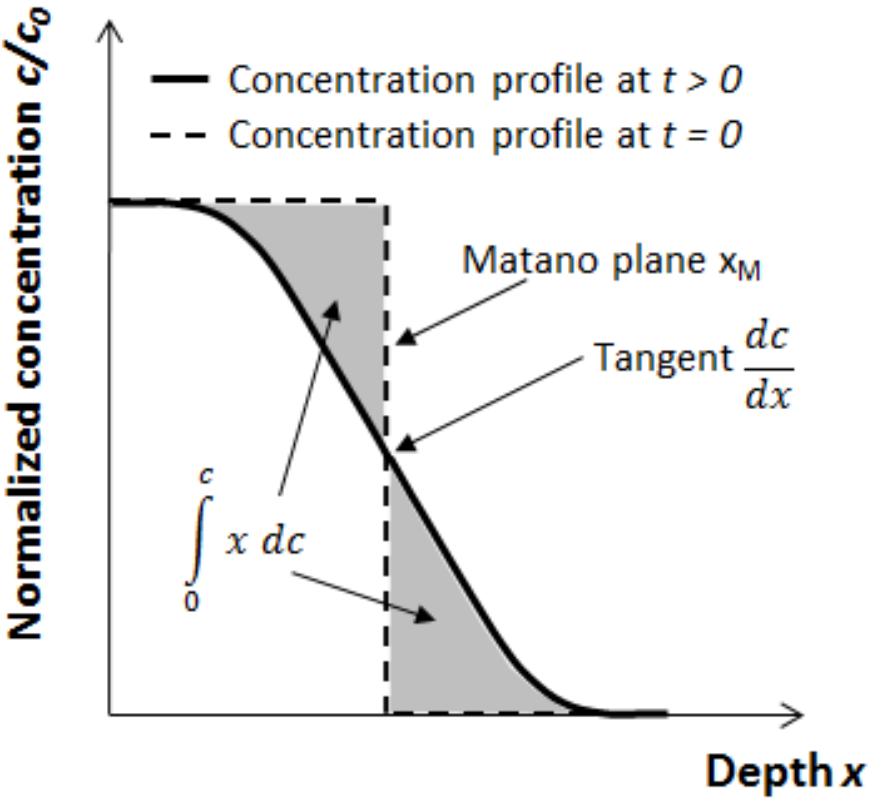


**Figure 23: Schematic representation of the Matano analysis, where the normalized concentration profiles of an element are plotted for $t = 0$ and $t \neq 0$. The location of the Matano plane $x_M$, the tangent $dc/dx$, and the area $\int_0^c x dc$ are needed for the calculation of the diffusion coefficient.**

### 4.2.2. Diffusion in the Pack Cementation Process

The gas phase flux $j$ for metal halide vapour is given by:

$$j_i^g = \left(\frac{D_i}{RT}\right)\frac{\Delta f_i}{\Delta x} \tag{15}$$

where $D_i$ is the gas phase interdiffusion coefficient, $R$ the gas constant, $T$ the temperature, and the derivative $\frac{\Delta f_i}{\Delta x}$ is the partial fugacity gradient of the metal halide $i$ over the diffusion distance $\Delta x$ (depletion zone).

Depending on the pack composition, either gas phase diffusion or solid state diffusion is the rate limiting step. In this work, it is assumed that the solid state diffusion step is the rate limiting step, except when the deposition element amount in the pack is depleted in the final stage of the pack process.

The coating growth consideration is based on the previously performed thermodynamic calculations of the coating design, where it is assumed that the process temperature and powder pack composition are adjusted in a way that the β-FeAl and

β-NiAl phases would be formed. Consideration of the coating growth kinetics is based on Fick's first law, which describes the correlation between the Al flux $j_M$ from the surface (at the coating pack interface) through the coating and the Al activity gradient $\frac{\partial a_M}{\partial x}$ between the coating surface and the material:

$$j_M = -D \frac{\partial a_M}{\partial x} \tag{16}$$

where the constant of proportionality $D$ is the interdiffusion coefficient. Both the Al concentration gradient $\Delta c_{Al}$ for solid state diffusion and the Al fugacity gradient $\Delta f_{Al}$ for gas phase diffusion can be substituted by the Al activity gradient. If the net material flux is directional, coating growth would occur:

$$j_M = q \frac{dx}{dt} \tag{17}$$

where $q$ is the constant of proportionality and $\frac{dx}{dt}$ is the coating growth rate.
Equalization of (16) and (17) results in:

$$-D \frac{\partial a_M}{\partial x} = q \frac{dx}{dt} \tag{18}$$

In order to solve this equation analytically instead of numerically for $x$ (resulting coating thickness) a simplification has to be made: the linearization of the activity gradient from $\frac{\partial a_M}{\partial x}$ to $\frac{\Delta a}{x}$ (Figure 24).

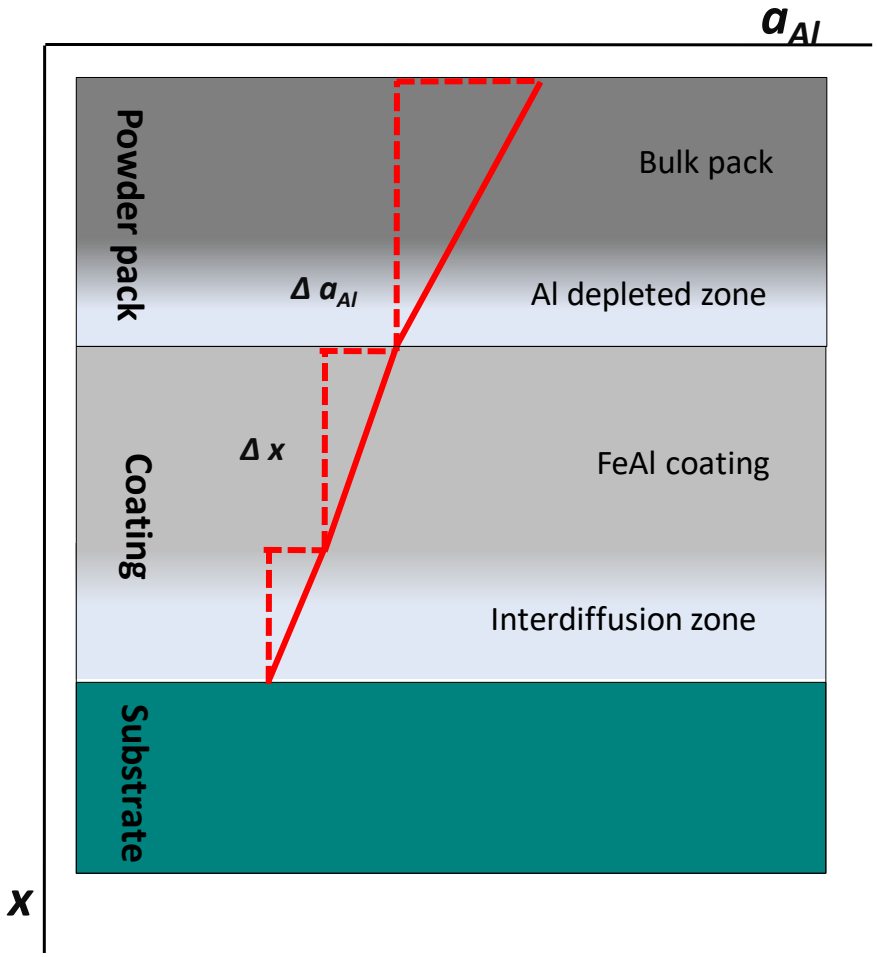


**Figure 24: Schematic illustration of the linearization of the Al activity gradient during the pack cementation process. The linear Al activity profile is plotted against depth $x$, where three zones (powder pack, coating and interdiffusion zone) can be seen.**

Thus, Equation (18) can be written as follows:

$$-D\frac{\Delta a_M}{x} = q\frac{dx}{dt} \tag{19}$$

$\Delta a_M$ is the Al activity difference between the coating surface and substrate. $x_0$ is located at the coating surface and $x$ is the distance which has to be crossed by Al during the coating growth. $\Delta x$ is replaced by $x$, since $\Delta x = x - x_0$ and $x_0 = 0$. This means that $x$ in the differential Equation (16) is the resulting coating thickness (Equation (20)). The process time $t$ and the Al activity difference $\Delta a_M$ are adjusted by the pack cementation process parameters. The interdiffusion coefficient $D$ depends on one hand on the process temperature $T$ and on the other hand on the diffusion properties of the diffusion element in the coating:

$$x = \sqrt{2\,\frac{D}{q}\Delta a t} \tag{20}$$

The Al activity difference $\Delta a_M$ is known from the thermodynamic considerations, whereas $t$ is the process time, which is determined by the operator. The interdiffusion coefficient of the deposition element in the material for a deposition element/material couple can be determined via Matano analysis. Therefore, once a coating process has been performed at a known process time and temperature the EPMA scan of the Al concentration over the depth of the cross section of an Al coated material enables the determination of the diffusion coefficient $D_{Fe}^{Al}$. The diffusion coefficient has an Arrhenius like temperature dependency:

$$D(T) = D_0\, exp\left(\frac{E_a}{RT}\right). \tag{21}$$

The values of $D_0$ (pre-factor), $E_a$ (activation energy) and $q$ (constant) are specific for every material/deposition element couple. The pre-factor can be seen as the diffusion coefficient at infinitely high temperature. The activation energy is the minimum energy, which is required to start the diffusion process. In order to determine $D_0$ and $E_a$, three coating procedures have to be performed at least and $ln\big(D(T)\big)$ has to be plotted against $\frac{1}{T}$. The slope of the line is $\left(\frac{E_a}{R}\right)$ and its Y axis intercept is $D_0$ (Figure 25).

$$ln\big(D(T)\big) = ln\,(D_0) + \left(\frac{E_a}{R}\right)\frac{1}{T} \tag{22}$$

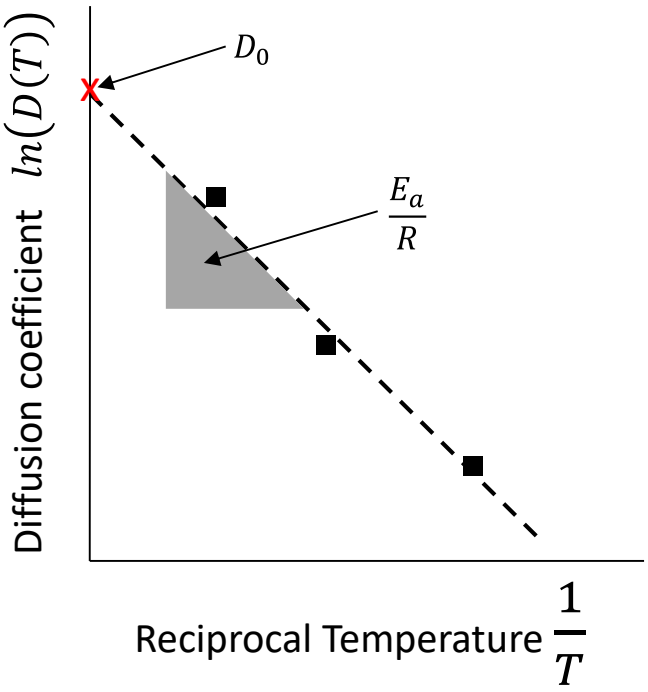


**Figure 25: Plotting of the diffusion coefficient vs. reciprocal temperature in order to determine the pre-factor $D_0$ and the activation energy $E_a$.**

The only remaining unknown variable is the constant $q$. It is determined via boundary conditions of the pack cementation process of one material/deposition element couple, where the process parameters and thermodynamic and kinetic values are known:

$$q = 2\,\frac{D}{x^2}\Delta at \tag{23}$$

Once the interdiffusion coefficient $D$ and the constant $q$ have been determined for a deposition element/material couple by a pack process, the coating structure for this couple can be predicted for a wide range of process parameters.

# 5. Experimental

The experimental part of this work includes the development of Al diffusion and Al/Si, Al/Hf and Al/Y co-diffusion coatings on Fe and Ni-based alloys via the pack cementation process, based on the coating design model. Exposure tests in a fuel and combustion atmosphere of a reformer system were carried out on coated and uncoated specimens of the investigated materials. This was performed in order to optimise and determine the performance of the coatings. The analysis of the specimens after the coating process or exposure procedure includes metallographic and micro analytical (microprobe (WDS), scanning electron microscope (SEM, EDS)) investigations.

## 5.1. Alloy Compositions and Specimen Preparation

Coating and exposure experiments were carried out with austenitic steels (AISi 321, AISI 314, alloy 800) and Ni base alloys (alloy 601, alloy 602, René 80). The chemical composition of the materials is given in Table 1.

**Table 1 Chemical composition (in wt.%) of the tested materials.**

| Alloy | Fe | Ni | Cr | Mn | Ti | Al | Si | C | Co |
|---|---|---|---|---|---|---|---|---|---|
| AISI 321 | Bal. | 11 | 18 | ≤ 2 | ≤ 0,7 | - | ≤ 1,0 | ≤ 0,1 | - |
| AISI 314 | Bal. | 19-22 | 24-26 | ≤ 2 | - | - | 2 | ≤ 0,2 | - |
| Alloy 800 | Bal. | 31 | 21 | ≤ 1,5 | 0,35 | 0,35 | ≤0,1 | 0,05 | ≤ 0,5 |
| Alloy 601 | 18 | Bal. | 21-25 | ≤ 1 | ≤ 0,5 | 1-1,7 | ≤ 0,5 | ≤ 0,1 | ≤ 1 |

In order to simulate real conditions for both the coating as well as the exposure processes, samples were sandblasted, since the combustion chamber in the reformer system is also sand blasted. The sandblasting was conducted with fused silica (90 micron average particle size) at 3 bar pressure. To achieve a good comparability, each surface was treated for 20 seconds so that for a square shaped specimen, the total treatment time was 2 minutes. The distance between sample and nozzle was 50 mm. The specimens are rectangular and have the dimensions $17 \times 10 \times (1{,}5 - 2)\ mm^3$. Specimens were weighed and measured before coating or exposure in order to determine the mass change kinetics.

## 5.2. Pack Cementation Setup

The specimen to be coated is embedded in an alumina crucible with a powder mixture. The crucible is covered with a lid and is inserted into a quartz tube of an electrically heated furnace (Figure 26). The pack process is conducted in an argon-hydrogen atmosphere (Ar/5% $H_2$), where the hydrogen acts as an oxygen getter for the residual oxygen in the atmosphere. Before the coating process, the furnace is evacuated and purged several times. A drying-process is performed before the actual coating step for several hours (6 h) at 200°C to remove any humidity in the furnace, which could cause undesirable oxidation during the powder pack process.

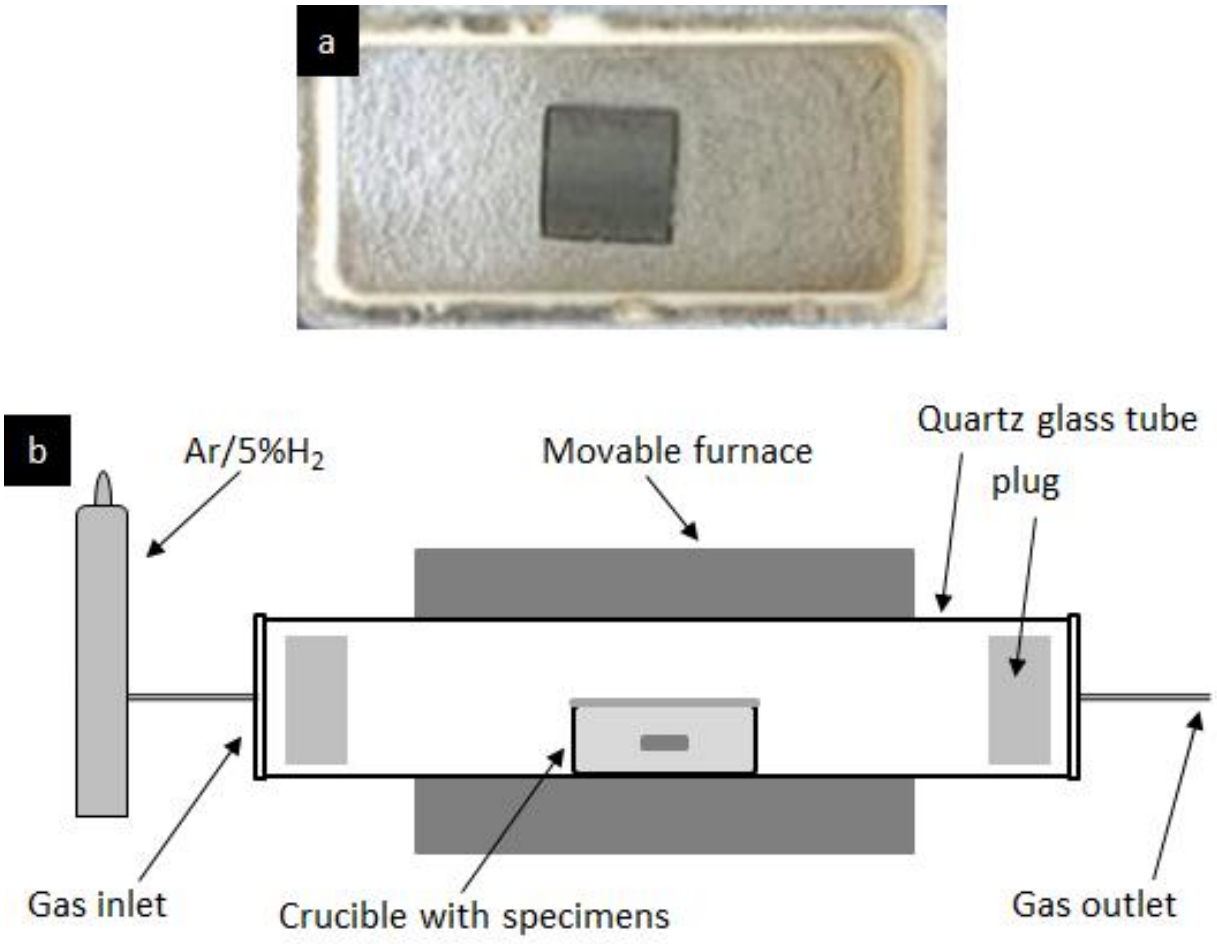


**Figure 26: (a) Photo of a specimen, partially embedded in a pack mixture and (b) schematic picture of the pack cementation experimental setup.**

## 5.3. Exposure Test Setup

In order to simulate the degradation processes in the combustion chamber, a test stand was constructed according to the ISO standard 13573:2012. By means of a movable, electrically heated furnace ($T$ = 1000°C) the heating and cooling phases are simulated. The heating and cooling processes are not included in the hot and cold period dwell time. The hot phase begins when 97% of the desired temperature is reached during the heating process and the cooling time is defined to finish when the temperature drops below 50°C. The temperature is measured with thermocouples that are very close to the specimen to be as accurate as possible. The specimens were exposed in a combustion atmosphere (51.6% $N_2$, 31.9% $H_2O$, 13.3% $CO_2$, 3.2% $O_2$). The gas flows through the thermostat and is enriched with water vapour. The flushing gas for the cooling cycle consists of synthetic air. The magnetic valves open or close automatically when the furnace moves in order to switch the atmospheres. Figure 27 shows a schematic representation of the experimental setup.

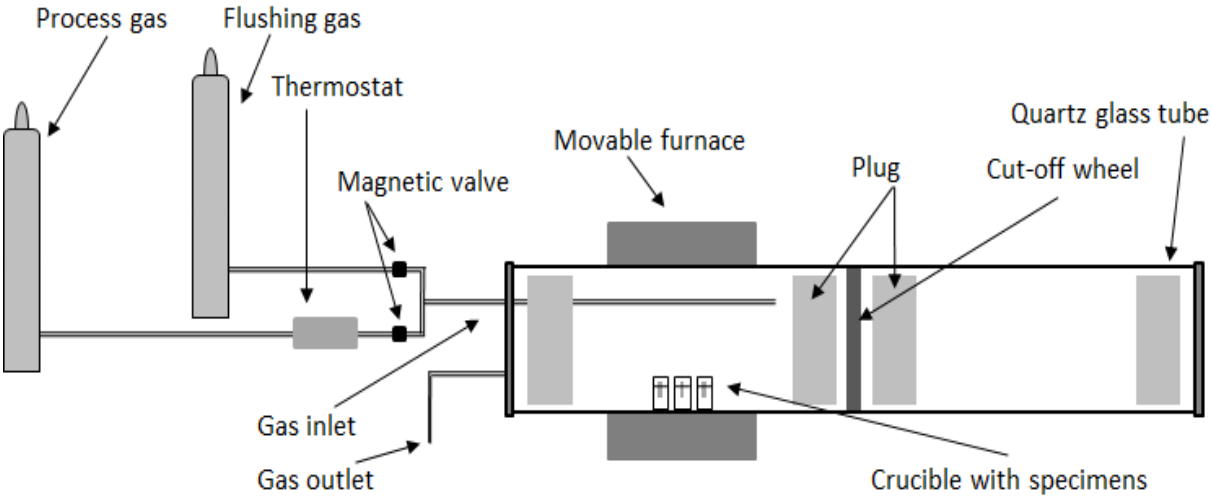


**Figure 27: Schematic of the high temperature exposure experimental setup.**

After certain time intervals, the exposed samples are removed from the furnace and weighed in order to determine the mass change kinetics of the materials, by which the oxide scale growth rates and the interval when spallation occurs can be determined.

## 5.4. Analysis Methods

After completing the pack procedure, the specimens were removed from the powder pack, cleaned with a brush, put into an ultrasonic bath and weighed in order to determine the mass gain. However, after exposure the specimens were only cleaned by a brush and weighed. Cross sections of each sample were mounted in epoxy resin with granulated carbon as a conductive mount. Grinding was performed with silicon carbide papers that ranged from 500 to 1200 grit. The samples were then polished using 5µm and 3µm alumina suspensions sequentially. The microstructure of the coatings was investigated by optical microscope (Leica DFC 420), scanning electron microscope (SEM), and electron probe micro analyser (EPMA), manufactured by JOEL (model JXA-8100). The step size of the EPMA line scan for the element composition measurement of cross sections was 1µm.

# 6. Results and Discussion

## 6.1. Structure of High Activity (HA) and Low Activity (LA) coatings on steels and Ni-based Superalloys

The plotting of the calculated Al activities within the pack of the type 1 wt.% Al, 1 wt.% $NH_4Cl$, 98 wt.% $Al_2O_3$ and the stability range of intermetallic phases (as a function of temperature) shows that in the case of aluminizing an Fe-based alloy in the temperature range between 700 and 1000°C the $FeAl_3$ and $Fe_2Al_5$ phases are formed within the coating, whereas in the case of aluminizing a Ni-based superalloy only the $Ni_2Al_3$ intermetallic phase is formed in the entire temperature range (Figure 28).
The thermodynamic calculations of the coating design model predict that a low process temperature promotes the formation of the HA coating, because the Al activities within the intermetallic phases of the coatings increase stronger with increasing process temperature than the Al activity in the gas phase of the pack (for $NH_4Cl$ activator) as it is shown in Figure 28.

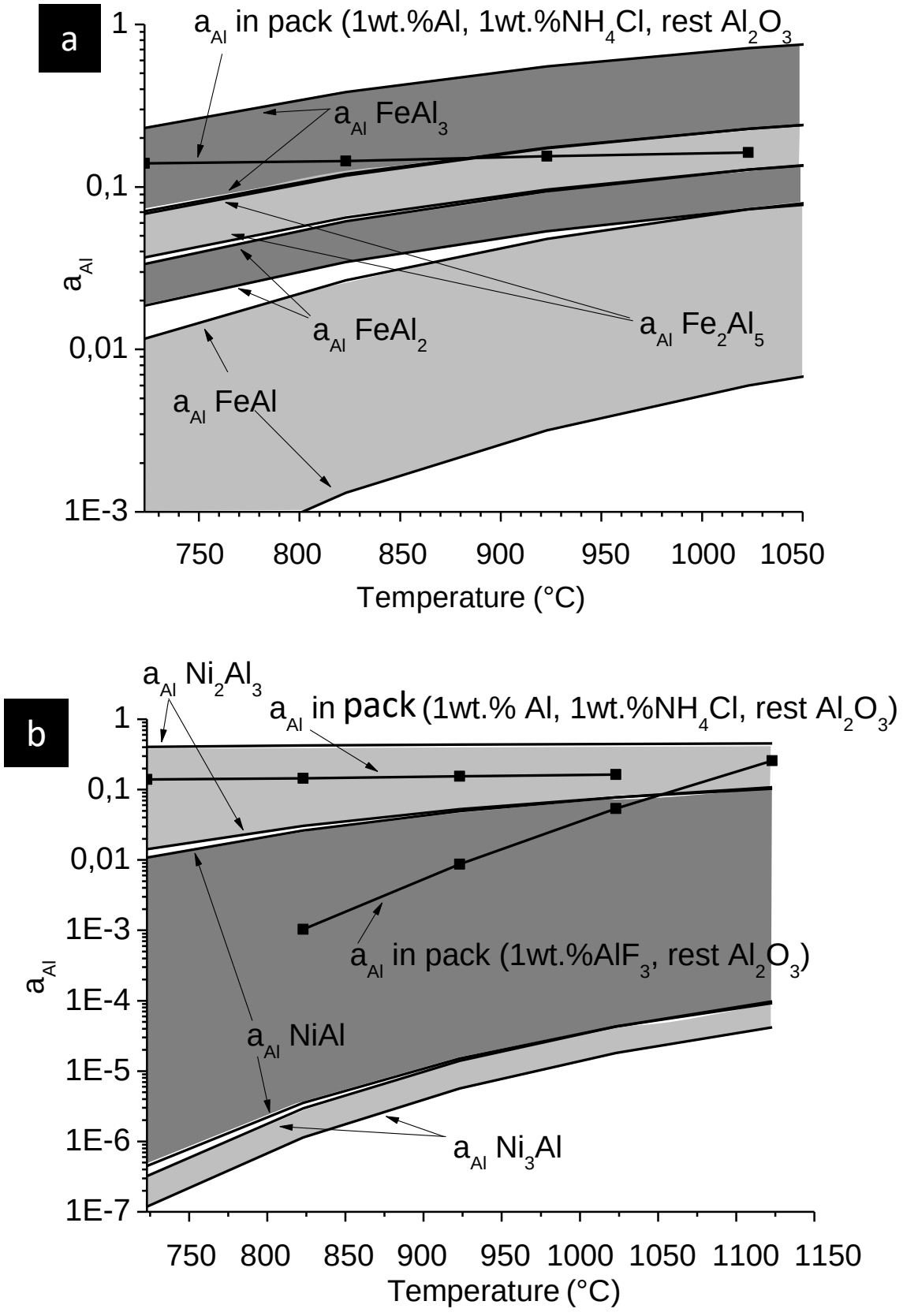


**Figure 28: Thermodynamic calculation of the Al activity ranges for intermetallic phases of the a) Fe-Al and b) Ni-Al system and the Al activities in the pack (for several pack mixtures) as a function of process temperature.**

At low process temperatures (700 to 900°C) the Al activity of the gas phase in the pack is at the same level as the Al activity within the Al rich phase ($Fe_3Al$, $Fe_2Al_5$ or $Ni_2Al_3$), which leads to the formation of the HA coating. But, since the Al activity in the pack increases less with increasing process temperature than the Al activity within the intermetallic phases, the Al activity in the pack at higher process temperatures is at the same level as the Al activity of the intermetallic phases with lower Al content. The Al and Fe concentration profiles (measured via EPMA) of the cross sections of the aluminized austenitic steels (AISI 321, AISI 314 and alloy 800H) coated at 800, 900 and 1000°C confirm that for the steels LA coatings are developed only at a process temperature of 1000°C (Figure 29 - Figure 32).

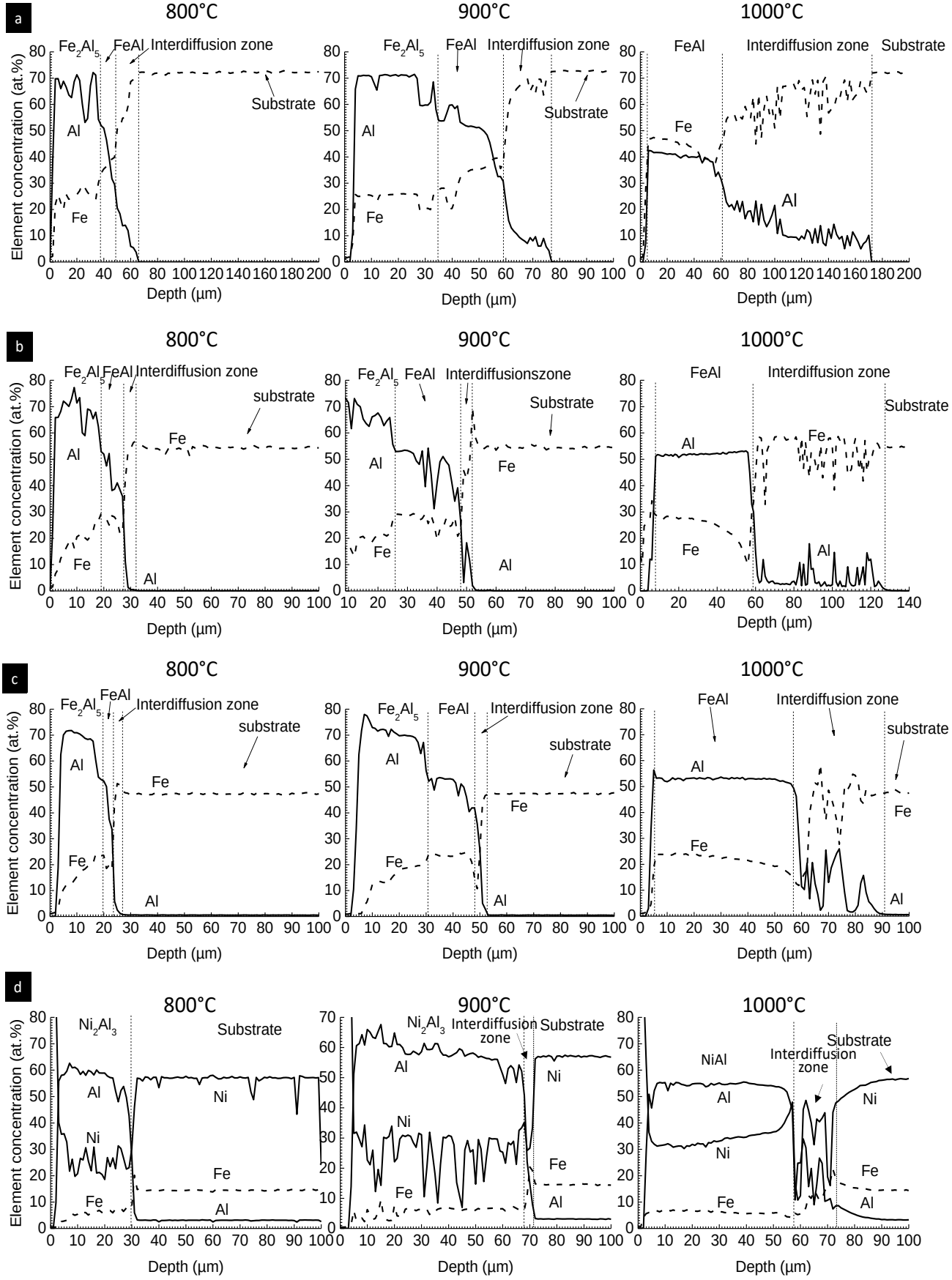


**Figure 29: EPMA concentration profiles of Al, Fe and Ni measured on a cross section of aluminized a) AISI 321, b) AISI 314, c) Alloy 800 and d) Alloy 601 at 800, 900 and 1000°C (pack composition: 1 wt.% Al, 1 wt.% $NH_4Cl$, 98 wt.% $Al_2O_3$).**

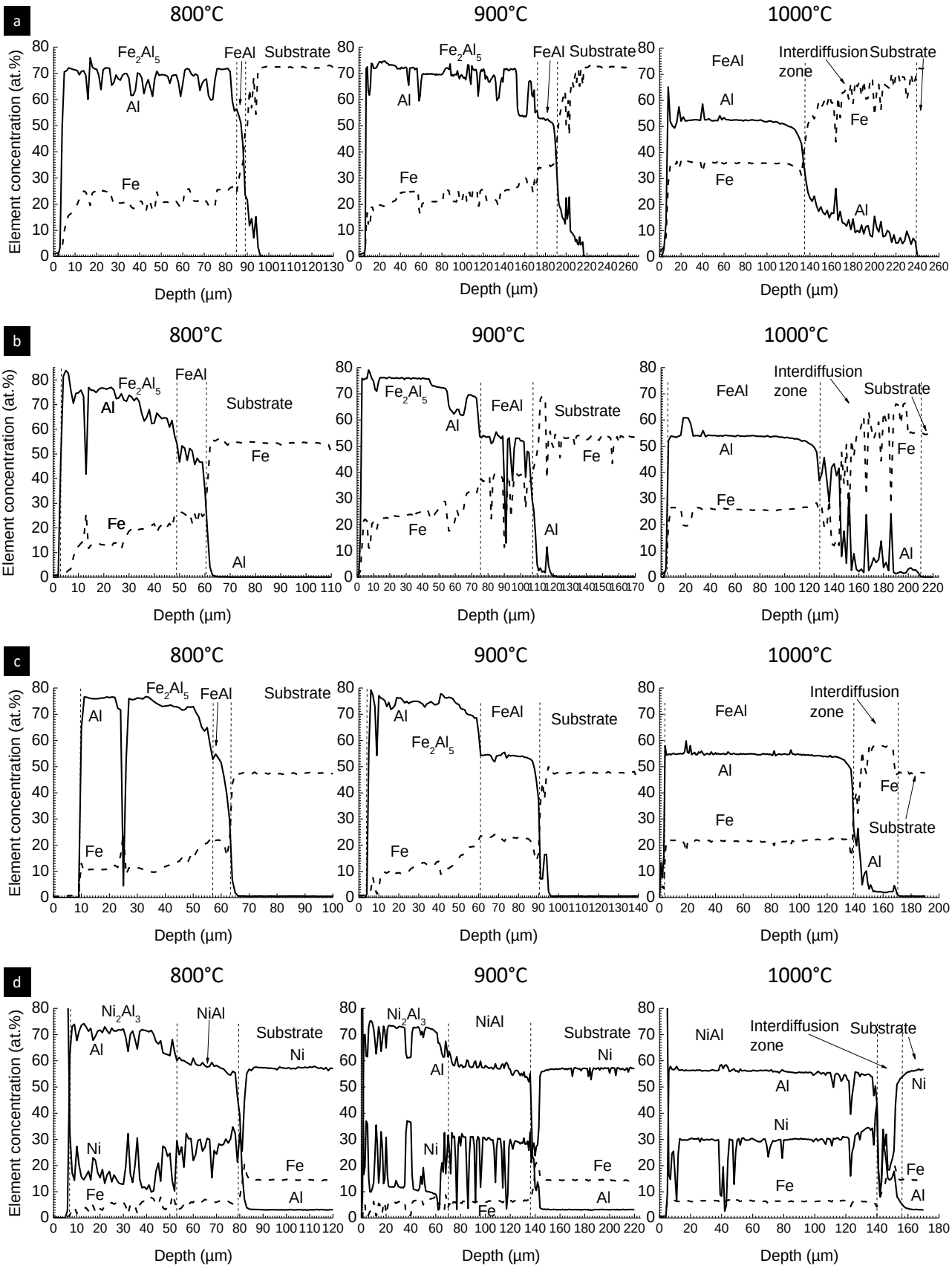


**Figure 30: EPMA concentration profiles of Al, Fe and Ni measured on a cross section of aluminized a) AISI 321, b) AISI 314, c) Alloy 800 and d) Alloy 601 at 800, 900 and 1000°C (pack composition: 10 wt.% Al, 1 wt.% $NH_4Cl$, 89 wt.% $Al_2O_3$).**

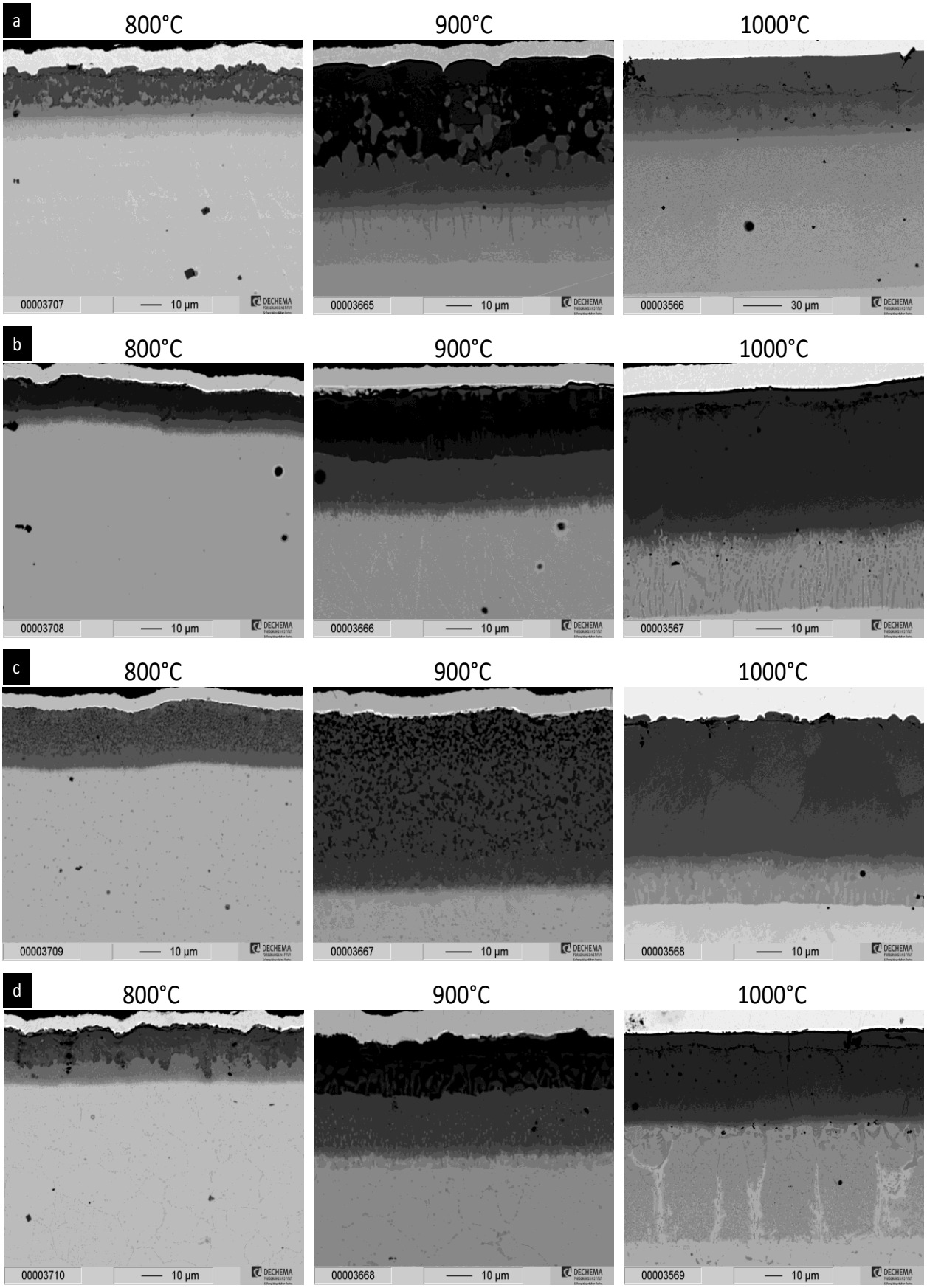


**Figure 31: BSE (backscattered electron) image of the cross sections of aluminized a) AISI 321, b) AISI 314, c) Alloy 800 and d) Alloy 601 at 800, 900 and 1000°C (pack composition: 1 wt.% Al, 1 wt.% $NH_4Cl$, 98 wt.% $Al_2O_3$).**

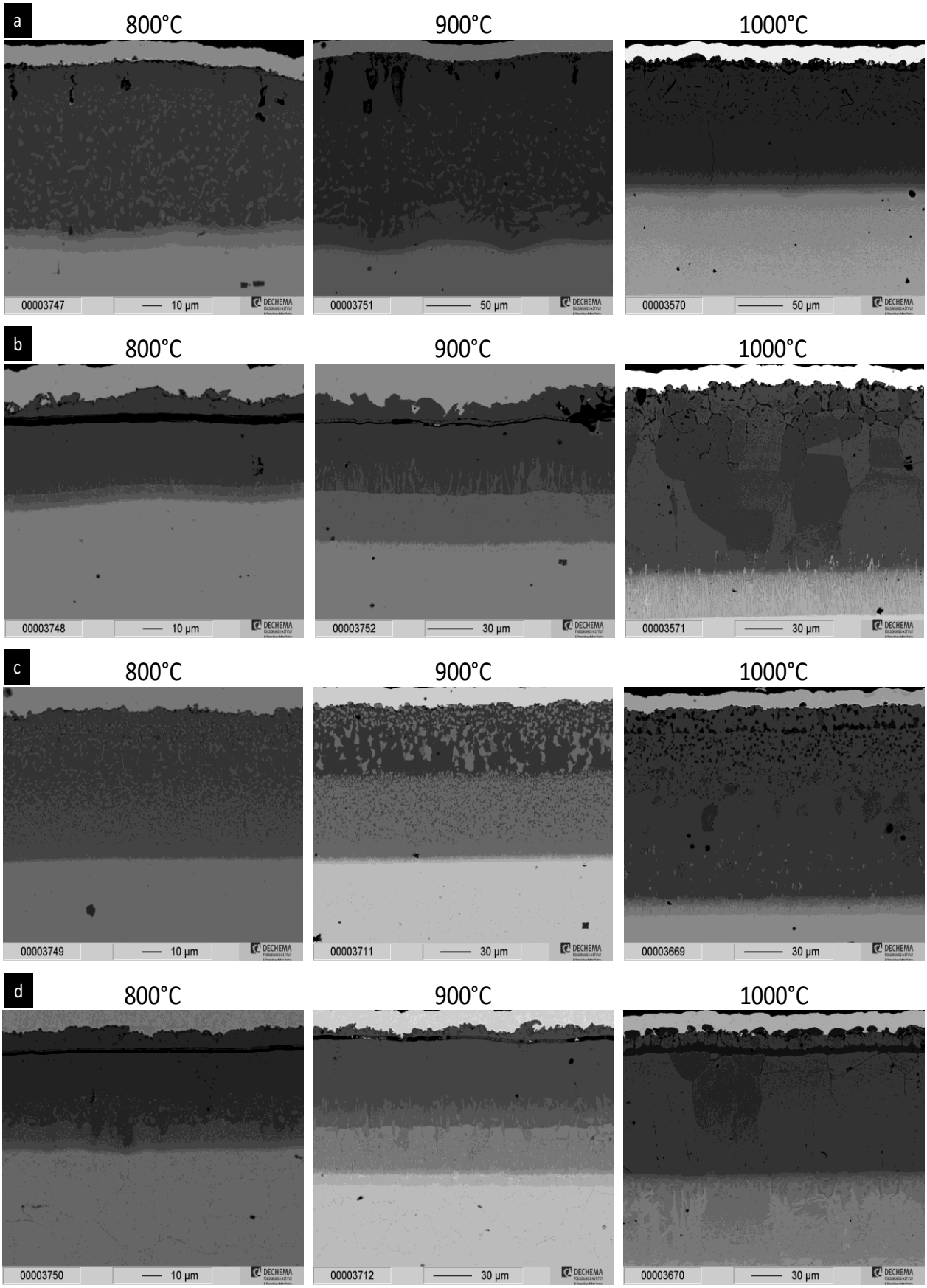


**Figure 32: BSE (backscattered electron) image of the cross sections of aluminized a) AISI 321, b) AISI 314, c) Alloy 800 and d) Alloy 601 at 800, 900 and 1000°C (pack composition: 10 wt.% Al, 1 wt.% $NH_4Cl$, 89 wt.% $Al_2O_3$).**

Nevertheless, it can be seen in Figure 28 that the calculated Al activity in the pack is higher than the calculated Al activity within the FeAl and NiAl phases over the entire temperature range, but still the β-FeAl and β-NiAl phase are formed at 1000°C in the experiment. This indicates that other effects (e.g. kinetic effects, aluminium chloride loss within the pack etc.) have also to be considered in this modelling.

Furthermore, the calculations (Figure 28 b) show that a change of the activator in the pack composition (from Al + $NH_4Cl$ to $AlF_3$) leads to a lower Al activity in the pack, which is on the same level as the Al activity within the NiAl phase. Furthermore, the lower Al activity in the pack, due to pack mixture change, leads to a lower coating thickness. Figure 33 and Figure 34 show an EPMA line scan and a cross section of aluminized Alloy 601 with an optimized Al coating, consisting of the required NiAl intermetallic phase.

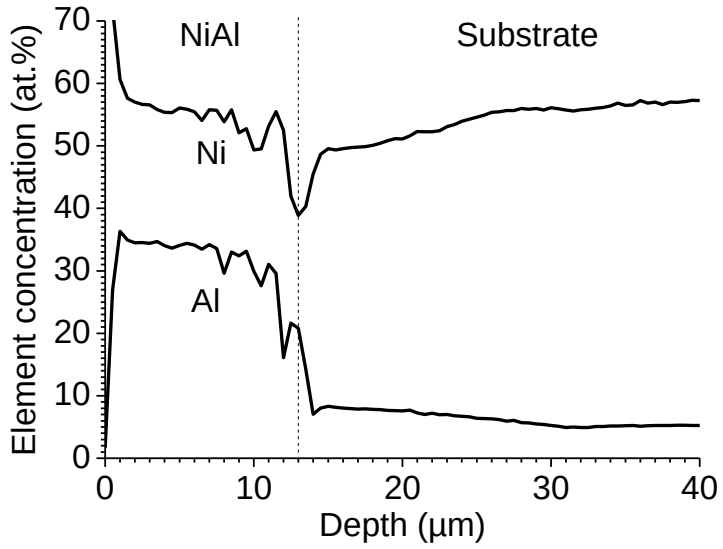


**Figure 33: EPMA (electron probe micro analysis) concentration profiles of Al and Ni measured on a cross section of aluminized Alloy 601 at 1000°C (pack composition: 1 wt.% $AlF_3$, 99 wt.% $Al_2O_3$).**

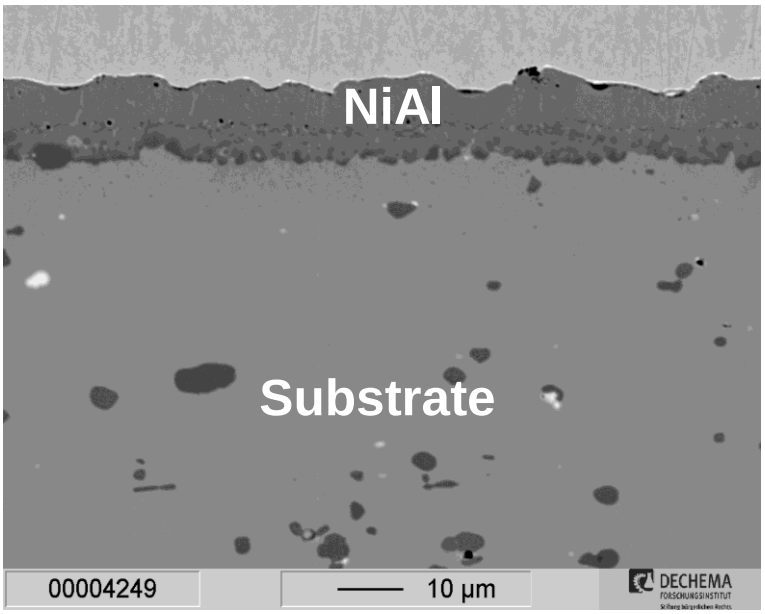


**Figure 34: BSE (backscattered electron) image of the cross sections of aluminized Alloy 601 at 1000°C (pack composition: 1 wt.% $AlF_3$, 99 wt.% $Al_2O_3$).**

Generally, the thermodynamic calculations and the experiments show a tendency of preferred HA coating formation at lower process temperatures and LA coating formation at higher process temperatures, when using the same pack composition. During the pack cementation procedure, the FeAl layer grows due to the deposition of Al from the pack. On the other hand, the FeAl layer loses Al due to the interdiffusion of Al into the substrate interior. Furthermore, Al interdiffusion could lead to dissolution of a phase if the interdiffusion rate is higher than the deposition rate. This could be a positive effect, if interdiffusion leads to a transformation of the $Fe_2Al_5$ phase into the FeAl phase. In order to determine the Al increase or loss in a layer due to Al interdiffusion, the Al activity differences between the intermetallic phases and the diffusion of Al through the intermetallic phases must be known. Then, the real growth or depletion of specific intermetallic phases during the coating process can be determined. However, Al loss within a coating due to interdiffusion and successive decrease of coating thickness can be determined mathematically as a reverse coating growth process, which is considered as a depletion process and is also depending on the Al activity of both in the interdiffusion involved intermetallic phases and the diffusion coefficient of the diffusing element in the phase.

### 6.1.1. Evaluation of Kinetic Values for Al Coating of Fe and Ni base Alloys

Three pack cementation procedures were performed at temperatures between 800 and 1000°C in order to determine the kinetic values $D_0$, $E_a$ and $q$ for Al/material (AISI 321, AISI 314, Alloy 800 and Alloy 601) couples. The experiments showed that at process temperatures of 800 and 900°C the $Fe_2Al_5$ and $Ni_2Al_3$ phases are developed. Thus, for the determination of the diffusion coefficient of Al through the β-FeAl and β-NiAl phase at 800 and 900°C, the considered driving force for the diffusion is the Al concentration gradient between the $Fe_2Al_5$ phase and β-FeAl, and the $Ni_2Al_3$ phase and β-NiAl, respectively. At 1000°C the driving force is the Al concentration gradient between the pack and the β-phase. This circumstance could make the determination of the diffusion coefficient as a function of temperature difficult, because beside the temperature the concentration gradient changes for the three process temperatures. Thus, it could be advantageous to choose process temperatures with minor variation in order to ensure that the resulting coating consists of the same intermetallic phase at all three process temperatures. Therefore, coating experiments were performed at 882, 945 and 1000°C with grinded AISI 321 specimens in order to examine the process temperature effect on the determined kinetic values. In Table 2 the coated materials, the process temperature, process times and the pack mixture are listed with the determined kinetic and thermodynamic values.

**Table 2: Determined Kinetic Values of several Materials.**

| Material | Temperature [°C] | Powder Pack Composition | $t$ [h] | x (FeAl) [µm] | Diffusion Coefficient [ms$^{-2}$] | $D_0$ [ms$^{-2}$] | $E_A$ [Jmol$^{-1}$] | $\Delta a$ | $q$ |
|---|---|---|---|---|---|---|---|---|---|
| AISI 321 | 800 | 1 wt.% Al, 1 wt.% $NH_4Cl$, 98 wt.% $Al_2O_3$ | 4 | 11 | $1.53 \cdot 10^{-15}$ | 0.025064 | 279718 | 0.15 - 0.026 | 0.0546 |
| AISI 321 | 800 | 10 wt.% Al, 1 wt.% $NH_4Cl$, 89 wt.% $Al_2O_3$ | 4 | 2.5 | $1.07 \cdot 10^{-15}$ | 0.006181 | 263079 | 0.15 - 0.026 | 0.0074 |
| AISI 321 | 882 | 1 wt.% Al, 1 wt.% $NH_4Cl$, 98 wt.% $Al_2O_3$ | 4 | 22 | $4.71 \cdot 10^{-15}$ | 0.017555289 | 274806 | 0.155 – 0.043 | 0.0434 |
| AISI 321 | 900 | 1 wt.% Al, 1 wt.% $NH_4Cl$, 98 wt.% $Al_2O_3$ | 4 | 24 | $5.20 \cdot 10^{-15}$ | 0.025064 | 279718 | 0.16 - 0.048 | 0.042 |
| AISI 321 | 900 | 10 wt.% Al, 1 wt.% $NH_4Cl$, 89 wt.% $Al_2O_3$ | 4 | 18 | $8.57 \cdot 10^{-15}$ | 0.006181 | 263079 | 0.16 - 0.048 | 0.122 |
| AISI 321 | 945 | 1 wt.% Al, 1 wt.% $NH_4Cl$, 98 wt.% $Al_2O_3$ | 4 | 51 | $17.50 \cdot 10^{-15}$ | 0.017555289 | 274806 | 0.175 – 0.058 | 0.0339 |
| AISI 321 | 1000 | 1 wt.% Al, 1 wt.% $NH_4Cl$, 98 wt.% $Al_2O_3$ | 4 | 50 | $9.56 \cdot 10^{-14}$ | 0.025064 | 279718 | 0.18 - 0.072 | 0.198 |

| Material | Temper-ature [°C] | Powder Pack Composition | $t$ [h] | x (FeAl) [µm] | Diffusion Coefficient [$ms^{-2}$] | $D_0$ [$ms^{-2}$] | $E_A$ [$Jmol^{-1}$] | $\Delta a$ | $q$ |
|---|---|---|---|---|---|---|---|---|---|
| AISI 321 | 1000 | 10 wt.% Al, 1 wt.% $NH_4Cl$, 89 wt.% $Al_2O_3$ | 4 | 128 | $9.12 \cdot 10^{-14}$ | 0.006181 | 263079 | 0.18 - 0.072 | 0.0288 |
| AISI 321 | 1000 | 1 wt.% Al, 1 wt.% $NH_4Cl$, 98 wt.% $Al_2O_3$ | 4 | 35 | $12.00 \cdot 10^{-14}$ | 0.017555289 | 274806 | 0.18 – 0.072 | 0.508 |
| AISI 314 | 800 | 1 wt.% Al, 1 wt.% $NH_4Cl$, 98 wt.% $Al_2O_3$ | 4 | 8 | $5.87 \cdot 10^{-16}$ | 0.020335 | 281522 | 0.15 - 0.026 | 0.0396 |
| AISI 314 | 800 | 10 wt.% Al, 1 wt.% $NH_4Cl$, 89 wt.% $Al_2O_3$ | 4 | 17 | $7.44 \cdot 10^{-16}$ | 0.019890 | 278011 | 0.15 - 0.026 | 0.011 |
| AISI 314 | 900 | 1 wt.% Al, 1 wt.% $NH_4Cl$, 98 wt.% $Al_2O_3$ | 4 | 22 | $2.60 \cdot 10^{-15}$ | 0.020335 | 281522 | 0.16 - 0.048 | 0.0248 |
| AISI 314 | 900 | 10 wt.% Al, 1 wt.% $NH_4Cl$, 89 wt.% $Al_2O_3$ | 4 | 33 | $5.89 \cdot 10^{-15}$ | 0.019890 | 278011 | 0.16 - 0.048 | 0.0249 |
| AISI 314 | 1000 | 1 wt.% Al, 1 wt.% $NH_4Cl$, 98 wt.% $Al_2O_3$ | 4 | 51 | $8.95 \cdot 10^{-14}$ | 0.020335 | 281522 | 0.18 - 0.072 | 0.178 |
| AISI 314 | 1000 | 10 wt.% Al, 1 wt.% $NH_4Cl$, 89 wt.% $Al_2O_3$ | 4 | 129 | $6.14 \cdot 10^{-14}$ | 0.019890 | 278011 | 0.18 - 0.072 | 0.0191 |

| Material | Temper-ature [°C] | Powder Pack Composition | $t$ [h] | x (FeAl) [µm] | Diffusion Coefficient [$ms^{-2}$] | $D_0$ [$ms^{-2}$] | $E_A$ [$Jmol^{-1}$] | $\Delta a$ | $q$ |
|---|---|---|---|---|---|---|---|---|---|
| Alloy 800 | 800 | 1 wt.% Al, 1 wt.% $NH_4Cl$, 98 wt.% $Al_2O_3$ | 4 | 3.5 | $9.75 \cdot 10^{-17}$ | 0.008274 | 289650 | 0.15 - 0.026 | 0.0344 |
| Alloy 800 | 800 | 10 wt.% Al, 1 wt.% $NH_4Cl$, 89 wt.% $Al_2O_3$ | 4 | 6 | $1.03 \cdot 10^{-16}$ | 0.005510 | 283285 | 0.15 - 0.026 | 0.0124 |
| Alloy 800 | 900 | 1 wt.% Al, 1 wt.% $NH_4Cl$, 98 wt.% $Al_2O_3$ | 4 | 18.5 | $7.35 \cdot 10^{-16}$ | 0.008274 | 289650 | 0.16 - 0.048 | 0.01 |
| Alloy 800 | 900 | 10 wt.% Al, 1 wt.% $NH_4Cl$, 89 wt.% $Al_2O_3$ | 4 | 29.5 | $1.09 \cdot 10^{-15}$ | 0.005510 | 283285 | 0.16 - 0.048 | 0.0058 |
| Alloy 800 | 1000 | 1 wt.% Al, 1 wt.% $NH_4Cl$, 98 wt.% $Al_2O_3$ | 4 | 54 | $6.57 \cdot 10^{-15}$ | 0.008274 | 289650 | 0.18 - 0.072 | 0,0117 |
| Alloy 800 | 1000 | 10 wt.% Al, 1 wt.% $NH_4Cl$, 89 wt.% $Al_2O_3$ | 4 | 135 | $1.25 \cdot 10^{-14}$ | 0.005510 | 283285 | 0.18 - 0.072 | 0.0036 |
| Alloy 601 | 800 | 1 wt.% Al, 1 wt.% $NH_4Cl$, 98 wt.% $Al_2O_3$ | 4 | 6 | $6.94 \cdot 10^{-17}$ | 0.007032 | 291865 | 0.15 - 0.026 | 0.0083 |

| Material | Temperature [°C] | Powder Pack Composition | $t$ [h] | x (FeAl) [µm] | Diffusion Coefficient [$ms^{-2}$] | $D_0$ [$ms^{-2}$] | $E_A$ [$Jmol^{-1}$] | $\Delta a$ | $q$ |
|---|---|---|---|---|---|---|---|---|---|
| Alloy 601 | 800 | 10 wt.% Al, 1 wt.% $NH_4Cl$, 89 wt.% $Al_2O_3$ | 4 | 3 | $8.14 \cdot 10^{-17}$ | 0.017185 | 296045 | 0.15 - 0.026 | 0.0391 |
| Alloy 601 | 900 | 1 wt.% Al, 1 wt.% $NH_4Cl$, 98 wt.% $Al_2O_3$ | 4 | 10.5 | $1.29 \cdot 10^{-16}$ | 0.007032 | 291865 | 0.16 - 0.048 | 0.0054 |
| Alloy 601 | 900 | 10 wt.% Al, 1 wt.% $NH_4Cl$, 89 wt.% $Al_2O_3$ | 4 | 16 | $7.34 \cdot 10^{-16}$ | 0.017185 | 296045 | 0.16 - 0.048 | 0.0132 |
| Alloy 601 | 1000 | 1 wt.% Al, 1 wt.% $NH_4Cl$, 98 wt.% $Al_2O_3$ | 4 | 54 | $3.14 \cdot 10^{-15}$ | 0.007032 | 291865 | 0.18 - 0.072 | 0.0056 |
| Alloy 601 | 1000 | 10 wt.% Al, 1 wt.% $NH_4Cl$, 89 wt.% $Al_2O_3$ | 4 | 137 | $8.55 \cdot 10^{-15}$ | 0.017185 | 296045 | 0.18 - 0.072 | 0.0024 |

In Figure 35 $\ln(D(T))$ of the tested materials is plotted against the reciprocal process temperature in order to determine the activation energy $E_a$ and the pre-factor $D_0$. The plot shows that the regression line corresponds very well with the data. The $\ln(D(T))$ values at 900°C seem to deviate for all materials, whereas the $\ln(D(T))$ data for AISI 321 seem to fit well for the other temperatures (882, 945 and 1000°C). This could be caused by an experimental error, since the specimens of all three materials were coated together in the furnace at 900°C, and $\ln(D(T))$ of all three materials is lower than the regression line. Furthermore, the data for AISI 321 show good agreement for both measurements (800 to 1000°C and 882 to 1000°C). The activation energy $E_A$ and the pre-factor $D_0$ are listed in Table 2. They both show good agreement with literature values (Table 3).

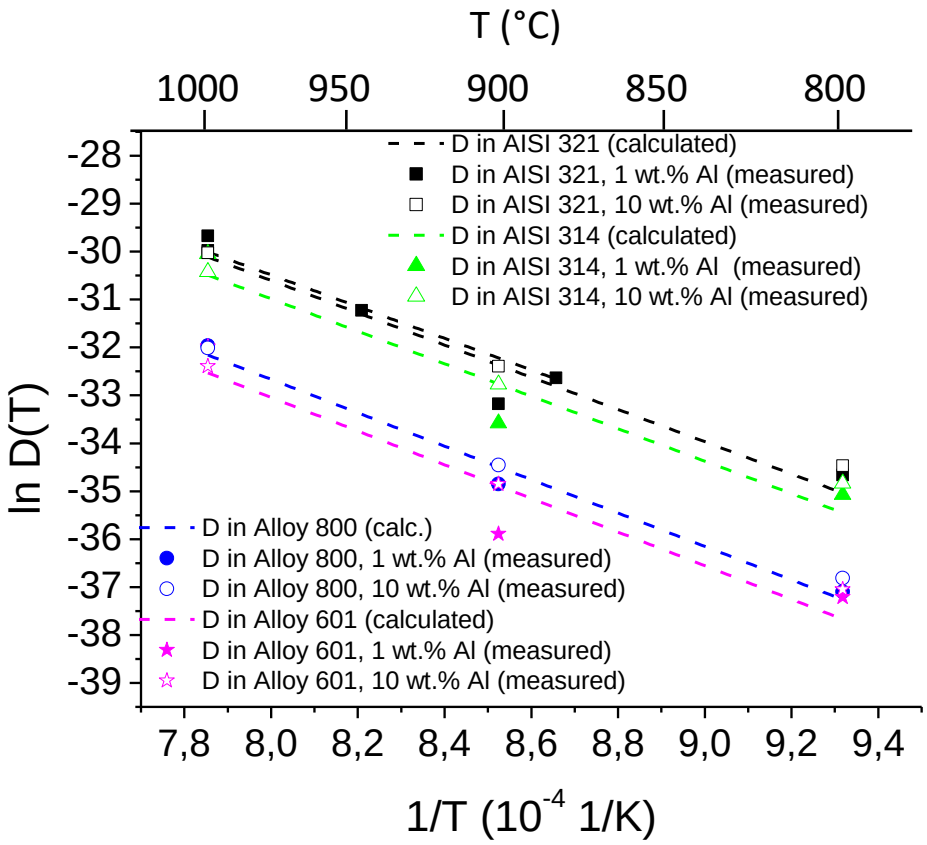


**Figure 35: Plotting of $\ln(D(T))$ vs. $^1/_T$ for the determination of the activation energy $E_A$ and the pre-factor $D_0$.**

The diffusion coefficient of the deposition element in the substrate material is not only influenced in pack cementation experiments by temperature, but also by the Al activity difference between the pack and the substrate material. The Al activity within the pack

increases with the process temperature and, thus, the Al activity difference between the pack and the substrate material increases, which also influences the diffusion coefficient besides the process temperature. Thus, the Al activity change in the pack with temperature is considered by the determination of the diffusion coefficients.

**Table 3: Comparison of the activation energies $E_A$ and pre-factors $D_0$ of this work with reported literature values.**

| Material | $E_A$ [kJ/mol] | $D_0$ $[m^2 s^{-1}]$ | Reference |
|---|---|---|---|
| AISI 321 | 234 | $2.5 \cdot 10^{-2}$ | this work |
| $Fe_{52}Al_{48}$ | 250 | $0.6 \cdot 10^{-2}$ | R. Nakamura [85] |
| $Fe_{52}Al_{48}$ | 260 | $1.7 \cdot 10^{-2}$ | M. Salamon [86] |
| $Fe_{52}Al_{48}$ | 251 | $1.2 \cdot 10^{-2}$ | M. Eggersmann [87] |
| EN-3 Steel | 238 | $0.8 \cdot 10^{-3}$ | R. Sivakumar [88] |

In Figure 36 the determined pre-factors $D_0$ of the diffusion coefficients of Al in the FeAl phase for the different materials are compared. As it can be seen the diffusion coefficient is increasing with decreasing Ni amount in the materials and reaches its maximum when the Ni amount approaches zero, where the literature value is given for a single phase FeAl couple (Table 3). This shows that the amount of other elements within the material has an influence on the diffusion properties of the coated material. Bangaru et al. have proofed in their work that the microstructure and chemistry of Al diffusion coatings on heat-resistant stainless steels are strongly sensitive to the substrate [74]. Thus, the Matano analysis is an important procedure for the coating design. It makes it possible to determine the interdiffusion coefficient for each alloy, depending on the specific alloying elements and microstructure.

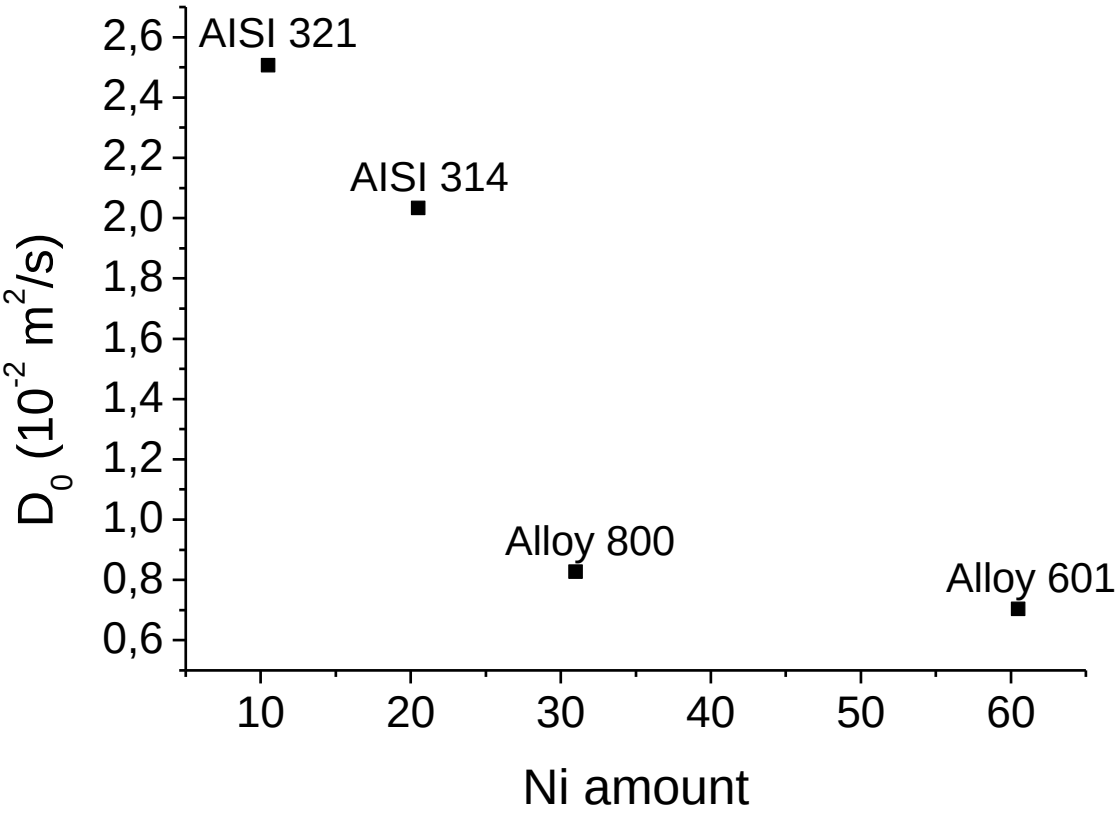


**Figure 36: Diffusion coefficients of Al in FeAl/NiAl determined by Matano analysis at 1000°C plotted vs. the Ni amount of the different materials.**

By means of the determined pre-factor $D_0$ and activation energy $E_a$ the diffusion coefficients of the considered materials can be calculated as a function of temperature, as shown in Figure 37 (dashed lines). The measuring points correspond to the experimentally measured diffusion coefficients, which were determined by means of the Matano analysis. It can be seen that there is a good agreement between measured and calculated diffusion coefficients and that the diffusion coefficients increase exponentially with temperature for all materials, according to the Arrhenius equation. Furthermore, the measurements show that the specified activity differences for the process temperatures below and beyond 900°C lead to a correct diffusion coefficient prediction and are in agreement with the thermodynamic considerations.

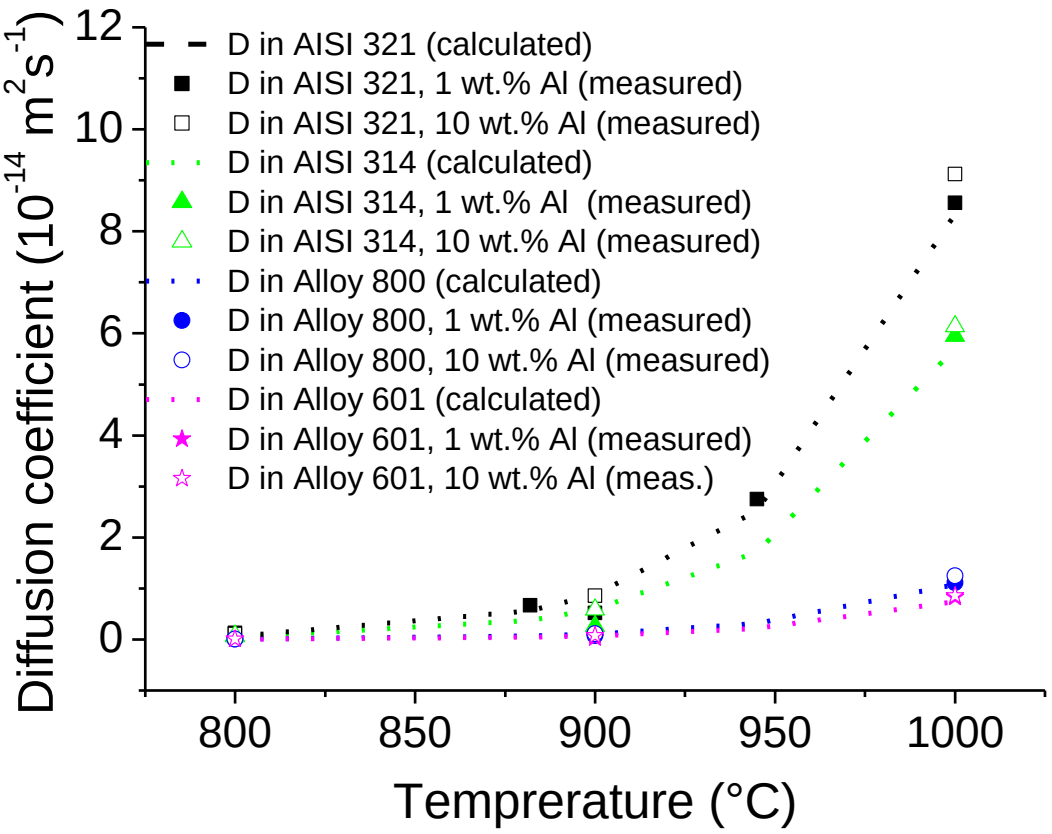


**Figure 37: Comparison of measured and calculated diffusion coefficients of Al in FeAl/NiAl as a function of temperature for AISI 321, AISI 314, Alloy 800 and Alloy 601. Values for the diffusion coefficient calculations ($D_0$ and $E_A$) we obtained by plotting $ln(D(T))$ vs $1/T$.**

Collection of the entire information about the thermodynamics and kinetics of a diffusion element/substrate couple enables the prediction of the resulting coating microstructure, which includes the intermetallic phase and its thickness. Figure 38 shows the correlation between the coating process time and the resulting thickness of the intermetallic phases for a diffusion element/substrate couple and several Al pack activities. The regimes of the intermetallic phases show that in a certain Al activity range, a specific intermetallic phase is formed and the coating growth curve has a parabolic like shape ($x = \sqrt{2\,\frac{D}{q}\Delta a t}$).

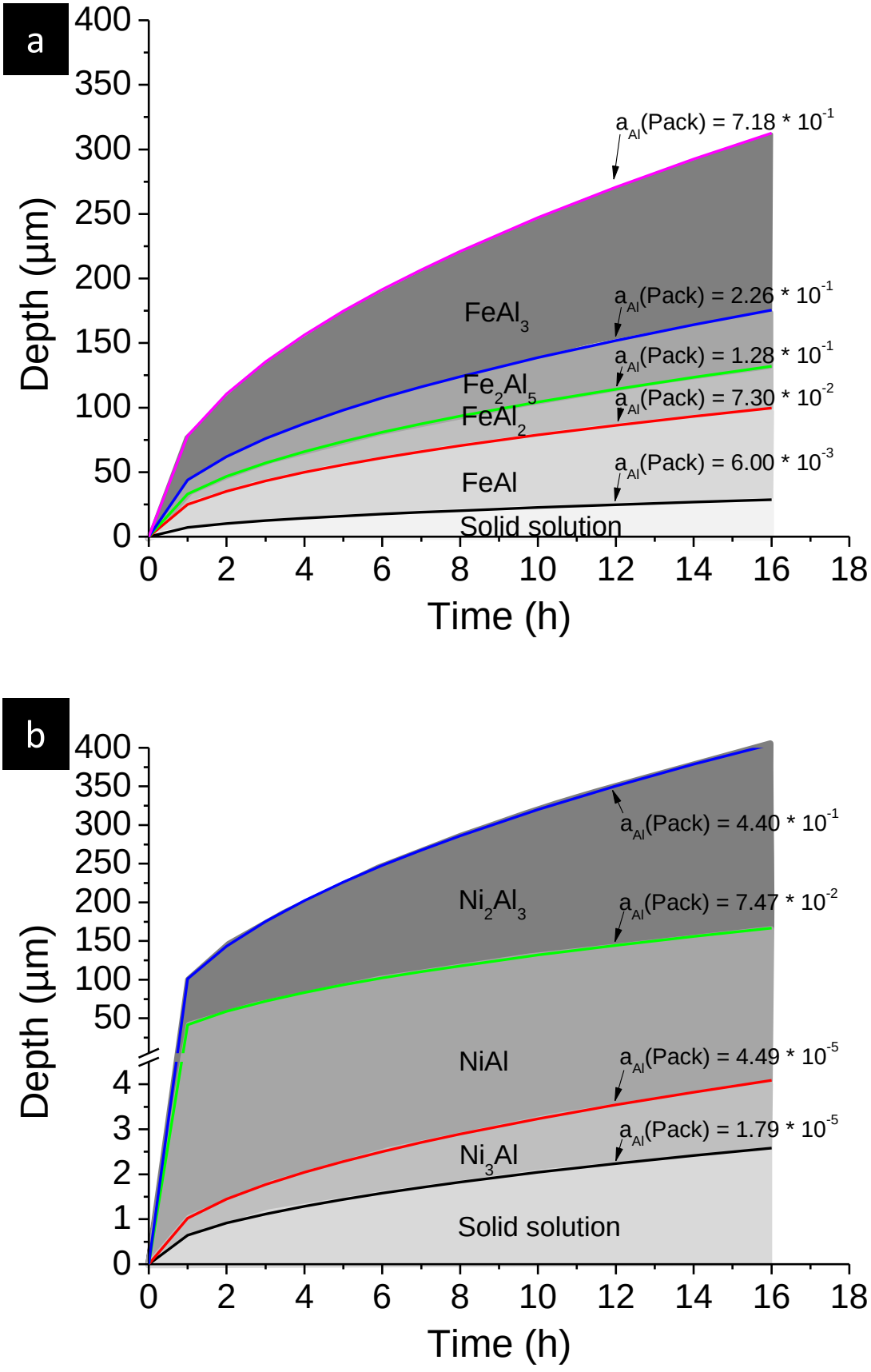


**Figure 38: Calculated coating growth curves as a function of process time for different Al activities during the pack cementation process (coloured lines) for the a) Fe-Al and b) Ni-Al systems. The areas correspond to a set of curves, in which the coating consists of the intermetallic phases whose activities are below the activity of the pack.**

The constant $q$ has not previously been described in the literature. The constant $q$ is the constant of proportionality between the deposition element flux (e.g. Al) and the coating growth rate:

$$j_M = q\frac{dx}{dt} \tag{24}$$

After determination of the diffusion coefficient for a material/deposition element couple the constant $q$ is determined by considering the boundary conditions of the pack cementation process:

$$q = 2\,\frac{D}{x^2}\Delta a t \tag{25}$$

According to Equation (24) $q$ has the dimension of $1/m^3$, whereas it has no dimension according to Equation (25). The reason is that in Equation (25) the concentration gradient $\Delta c$, which has the dimension $1/m^3$ is substituted by the activity $a$, which has no dimension, which means that as a result $q$ has no dimension. For the calculation of $q$ the activity differences $\Delta a$ are obtained from Figure 28, where for process temperatures below 900°C the Al activity differences between the $Fe_2Al_5$/$Ni_2Al_3$ phase and the β-phase at the given temperatures are considered. For temperatures beyond 900°C the Al activity differences between the pack and the resulting FeAl phase are considered at given temperatures.

The results in Figure 36 and Figure 37 have shown that the Matano analysis is a good method for diffusion coefficient determination. Furthermore, the diffusion coefficient determinations revealed that although the resulting diffusion coefficients $D_{Al}^{FeAl}$ for two specimens, consisting of the same material and coated with the same process parameters are the same, they exhibit different resulting coating thicknesses. This is due the specimen pre-treatment. Specimens were either grinded or sandblasted. Grinded specimens of the AISI 321 steels exhibited a 100 µm thick FeAl coating at 1000°C and 4 hours, whereas sandblasted specimens exhibited a 50 µm thick coating. These boundary conditions are considered in the constant $q$. When the Matano analysis is applied under ideal conditions, both diffusion couples exhibit complete solubility into each other, which results in a smooth element concentration profile of both elements. Since in the pack cementation process the pack powder (e.g. Al) and the substrate (e.g. Fe) can be considered as a diffusion couple with limited solubility of Al in the substrate, precipitations occur. This results in non-smooth element

concentration profiles. When precipitation occurs the lattice structure is changed, which influences the diffusion coefficient. Therefore, the constant $q$ can be seen as a correction factor. If the diffusion couples have ideal solubility the constant $q$ would be unity.

## 6.2. Prediction of the Coating Structure of Al Coated Steels and Ni-based Superalloys

In order to test the applicability of the coating design procedure, the coating process parameters were calculated in order to achieve FeAl coatings with coating thicknesses of 20 microns ($T$ = 882°C and $t$ = 4 h, $T$ = 1000°C and $t$ = 69 min) and 50 microns ($T$ = 945°C and $t$ = 4 h, $T$ = 1000°C and $t$ = 11 min) of specimens of AISI 321 steel. After this, the calculated process parameters were used for an experimental coating procedure and the coating thicknesses were compared. Figure 39 shows the Al concentration profiles of the cross sections of the coated specimens of AISI 321 steel for the mentioned process parameters.

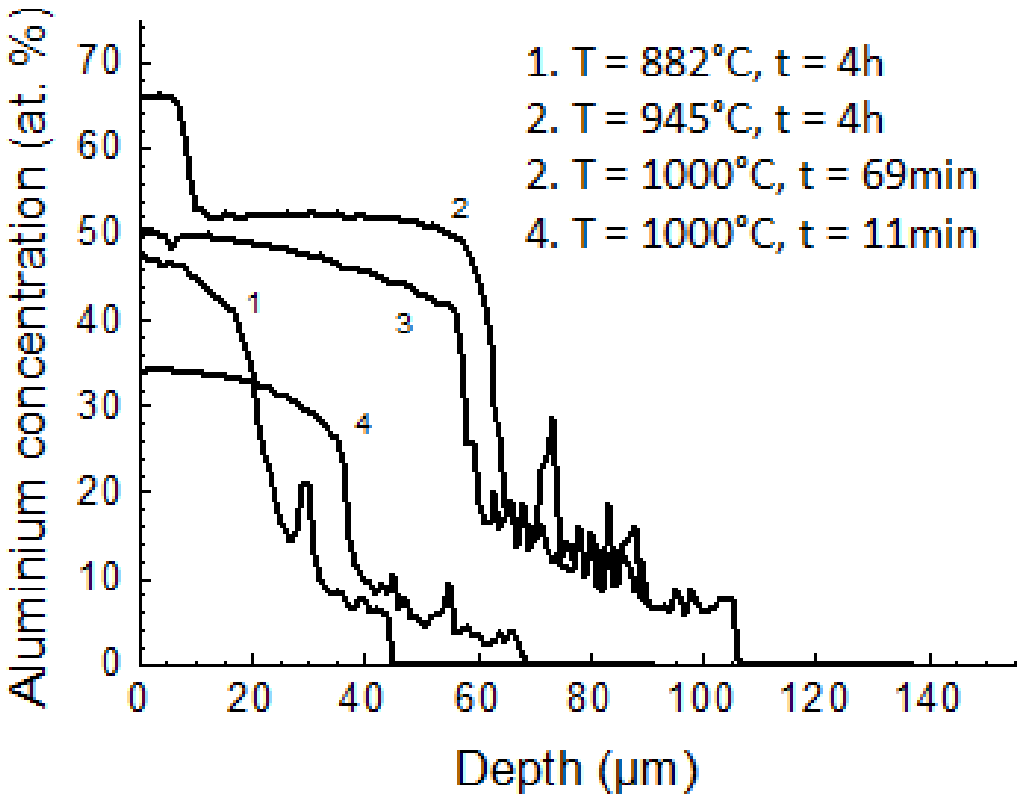


**Figure 39: EPMA (electron probe micro analysis) line scans of the cross sections of the Al-coated samples of AISI 321 for several process times and process temperatures.**

Table 4 compares the thicknesses of the experimentally developed coatings with the predicted thicknesses of the FeAl intermetallic phase for the coating process parameters, which are mentioned above and for the pack processes at 800, 900 and 1000°C for AISI 321, AISI 314, Alloy 800 and Alloy 601. The coating thicknesses

obtained by applying the calculated coating parameters are in good agreement with the predicted coating thicknesses except for 1000°C and 11 minutes. For this short process time the coating growth during heating and cooling cannot be neglected.

**Table 4: Predicted and experimentally formed coating thicknesses.**

| Material | Temperature [°C] | t | Pack mixture | Predicted FeAl-coating thickness | Experimentally formed FeAl-coating thickness |
|---|---|---|---|---|---|
| AISI 321 | 800 | 4 h | | 12 µm | 11 µm |
| AISI 321 | 882 | 4 h | | 20 µm | 22 µm |
| AISI 321 | 900 | 4 h | | 25.3 µm | 24 µm |
| AISI 321 | 945 | 4 h | | 50 µm | 51 µm |
| AISI 321 | 1000 | 4 h | | 50 µm | 50 µm |
| AISI 321 | 1000 | 11 min | 1 wt.% Al, 1 wt.% $NH_4Cl$, 98 wt.% $Al_2O_3$ | 20 µm | 35 µm |
| AISI 321 | 1000 | 69 min | | 50 µm | 55 µm |
| AISI 314 | 800 | 4 h | | 9 µm | 8.5 µm |
| AISI 314 | 900 | 4 h | | 23µm | 22 µm |
| AISI 314 | 1000 | 4 h | | 51 µm | 51 µm |
| Alloy 800 | 800 | 4 h | | 3.9 µm | 3.5 µm |
| Alloy 800 | 900 | 4 h | | 19.9 µm | 18.5 µm |
| Alloy 800 | 1000 | 4 h | | 54 µm | 54 µm |

A comparison of the cross sections of the coated samples (Figure 40), analysed by back-scattered electron (BSE) imaging, shows that coatings developed at high temperature (1000°C) exhibit cracks caused by growth stresses due to fast coating growth and differences in the CTE (coefficient of thermal expansion) between the intermetallic phase of the coating and the material (Figure 40 a and b), whereas coatings developed

at lower temperatures do not exhibit cracks (Figure 40 c and d) because coating growth stresses are lower at lower temperatures.

Thus, by means of the present coating design model growth stresses within the coating can be minimized by reducing the process temperature, while the process time can be extended adequately in order to achieve the same coating structure.

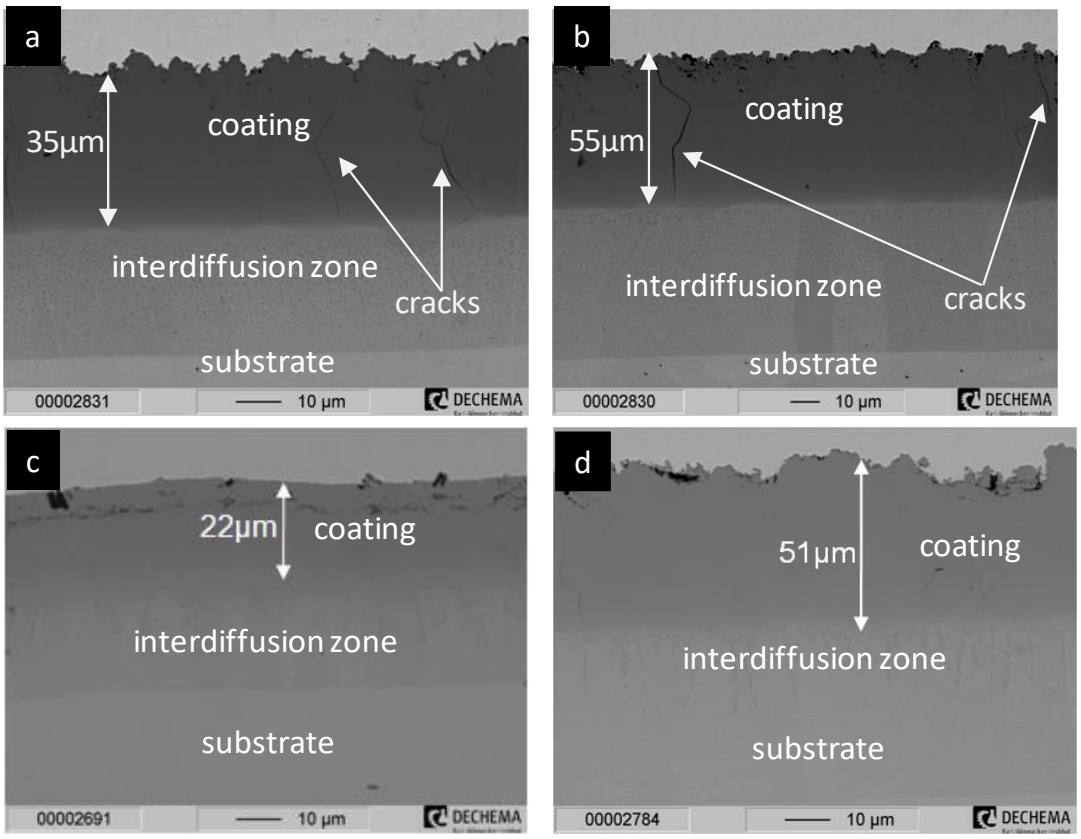


**Figure 40: Back-scattered electron (BSE) images of cross sections of the coated samples. a) *T* = 1000°C, *t* = 11min b) *T* = 1000°C, *t* = 69min. c) *T* = 882°C, *t* = 4h d) *T* = 945°C, *t* = 4h.**

### 6.2.1. Determination of the Diffusion Coefficient

The Matano analysis gives a graphical instruction for the determination of the diffusion coefficient. Thereby, the concentration profile is assumed to be smooth, which is not given in real concentration profiles, were a number of peaks occur due to precipitations. This complicates the determination of the slope $\frac{dx}{dc}$ in $D = -\frac{1}{2t}\frac{dx}{dc}\int_0^c xdc$. The concentration values of the peaks are composed of the concentration of the precipitations and the background, respectively. By means of the image editing program ImageJ® the element concentration profile can be smoothened by determining the phase fractions of a given area.

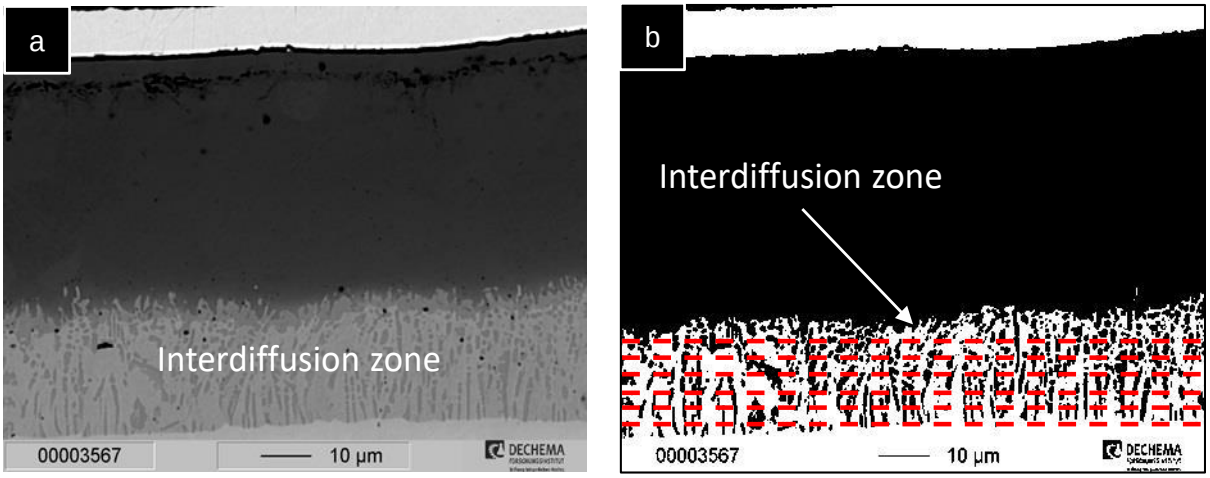


**Figure 41: a) BSE (backscattered electron) image of the cross section of an Al coated specimen of Alloy 800 and b) an image after its editing with Image J®. By means of this program the volume ratio of two phases in the two-phase regime can be determined, which enables the determination of the mean Al concentration.**

After determining the mean Al concentrations for the different depths in the interdiffusion zone the Al concentration curve can be smoothened (Figure 41 and Figure 42).

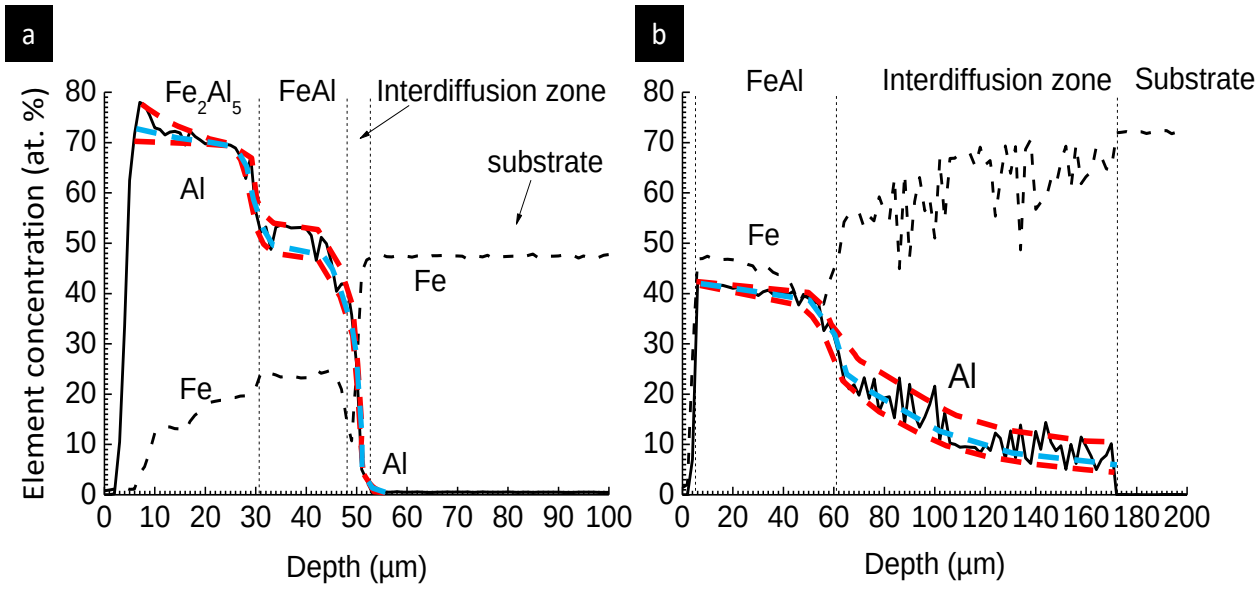


**Figure 42: EPMA (electron probe micro analysis) line scan of the cross section of an Al coated specimen of Alloy 800 at 900°C and of a specimen of b) AISI 321 at 1000°C. The top and bottom red dashed lines correspond to the Al concentrations of the precipitations and the background. The blue dashed line corresponds to the mean Al concentration determined via Image J®.**

### 6.2.2. Rate Limiting Step of the Pack Cementation Process

From a kinetics point of view the pack cementation process can be considered as a gas phase diffusion step followed by a solid state diffusion step. The experiments show that for a sufficient Al amount in the pack solid state diffusion is the rate limiting step. A high Al amount in the pack means a secured supply of the substrate with Al. Figure 43 shows the mass gain $\Delta m/A$ of Al coated specimens of AISI 321 steels with 0.5, 1, 3 and 10 wt.% Al in the pack (1 wt.% $NH_4Cl$, rest $Al_2O_3$) and a process time of 0, 1, 2, 4, 8, 16 hours at 1000°C. It can be seen that the mass gain, which is proportional to the coating growth, deviates from the parabolic coating growth $x = \sqrt{2\,\frac{D}{q}\Delta a t}$ with a tendency to lower values. This indicates that the Al supply of the pack mixture decreases with process time. When the Al supply of the pack mixture decreases to a certain point, the driving force (Al activity difference between bulk pack and coating surface) for the gaseous transport of Al will decrease, and gaseous diffusion will be the rate limiting step.

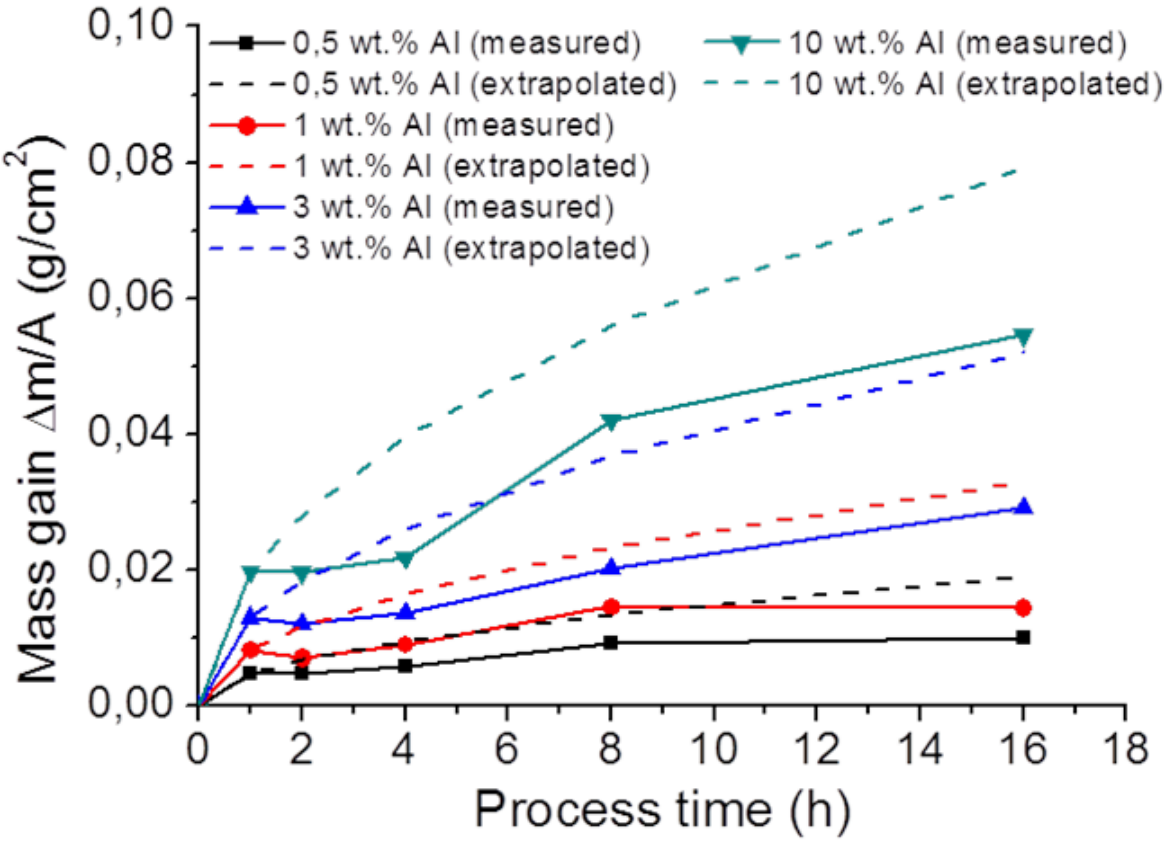


**Figure 43: Measured mass gains of coated AISI 321 specimens for several process times and pack compositions at 1000°C. The solid lines show the mass gains as a function of the pack process time and the dashed lines show the extrapolation of the first measured mass gain values based on a parabolic law.**

## 6.3. Extension of the Coating Design to Co-deposition

Al activity reduction can be achieved by the addition of another element to the main deposition element Al, as predicted by thermodynamic calculations (Chapter 4.1.1), which was confirmed by pack cementation experiments with Al/Si and Al/Hf packs. Figure 44 and Figure 45 show an EPMA element map of the cross section of an Al/Si coated AISI 321 and a comparison of the EPMA line scans of an Al and an Al/Si coated AISI 321 at 1000°C for 4h (Al powder mixture: 1wt.% Al, 1wt.% $NH_4Cl$, 98wt.% $Al_2O_3$; Al/Si powder mixture: 1wt.% Al, 10wt.% Si, 1wt.% $NH_4Cl$, 88wt.% $Al_2O_3$). It can be seen that Si is deposited in the Al/Si coating besides Al, whereas the coating thickness is reduced in comparison to the Al mono-element coating, where no Si is deposited.

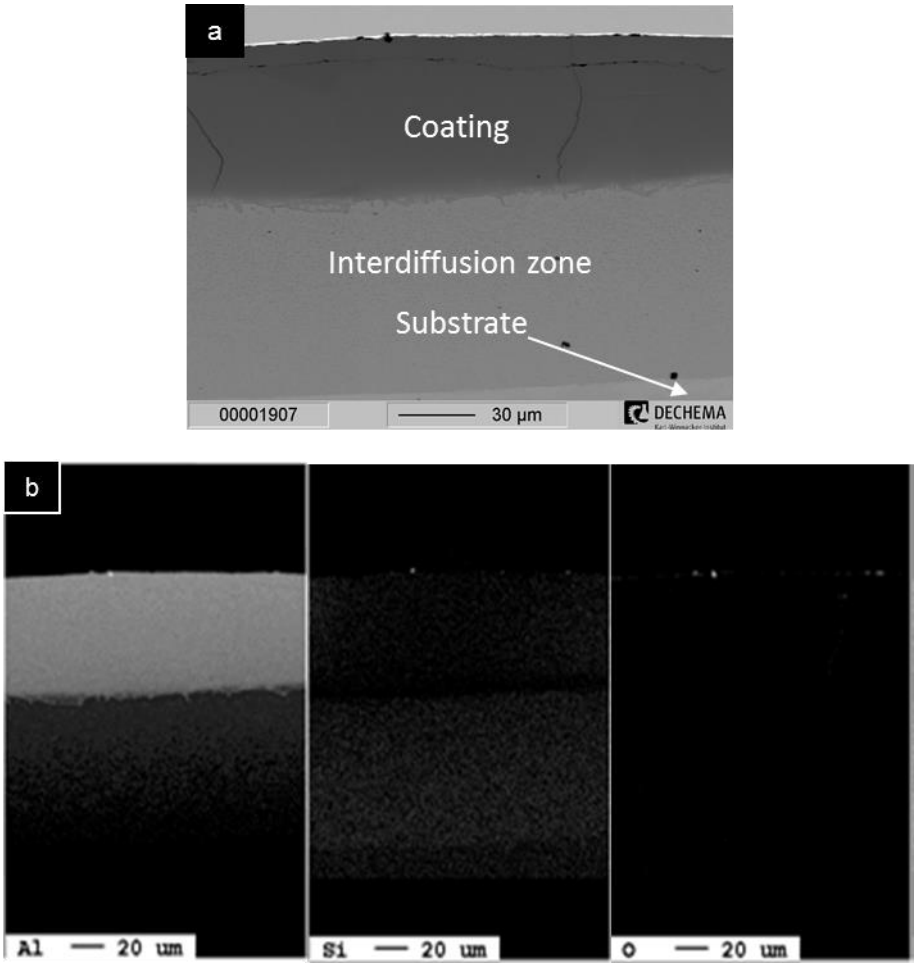


**Figure 44: a) BSE (backscattered electron) image and b) EPMA element map of the cross section of an Al/Si coated specimen of AISI 321 steel (1wt.% Al, 10wt.% Si, 1wt.% $NH_4Cl$, 88wt.% $Al_2O_3$, *T* = 1000°C, *t* = 4h).**

The decrease in coating thickness has two reasons:

1. The total partial pressure of the Al carrying chlorides (Al activity within the pack) is reduced due to co-deposition, which is in accordance with the thermodynamic calculations.
2. The diffusion coefficient of Al in a material is reduced when another element (co-deposition element) diffuses beside Al through the material and occupies a lattice site in the aluminide.

The EPMA line scan of Al on the cross section of the Al and Al/Si coated AISI 321 (Figure 45 a) shows that both the Al and the Al/Si pack form a coating, consisting of the β-FeAl intermetallic phase with an interdiffusion zone beneath it. Furthermore, it can be seen that the slope of the Al concentration profile drops within the FeAl phase between 0 and 65µm distance from the surface for the Al/Si coating, whereas it is almost flat for the Al coating between 0 and 102.5 µm distance. Compared to the pure Al coating, the Al transport by solid state diffusion through the FeAl phase of the coating is reduced due to Si co-deposition and co-diffusion. The slope of the Al concentration profile at the interdiffusion zone is the same for the Al and Al/Si coating, since Si incorporation in the interdiffusion zone deriving from the substrate is similar as can be seen in the magnification (Figure 45 b). The Si concentration profile in Figure 45 b shows that Si is incorporated (0.7 at.%) in the Al/Si diffusion coating, and that the Al diffusion coating contains a Si amount of 0.1 at.%, although Si was not included in the Al coating process. The 0.1 at.% Si in the Al coated AISI 321 comes from the outwards diffusion of the Si of the AISI 321 steel, which contains a Si amount of 1.2 at.%.

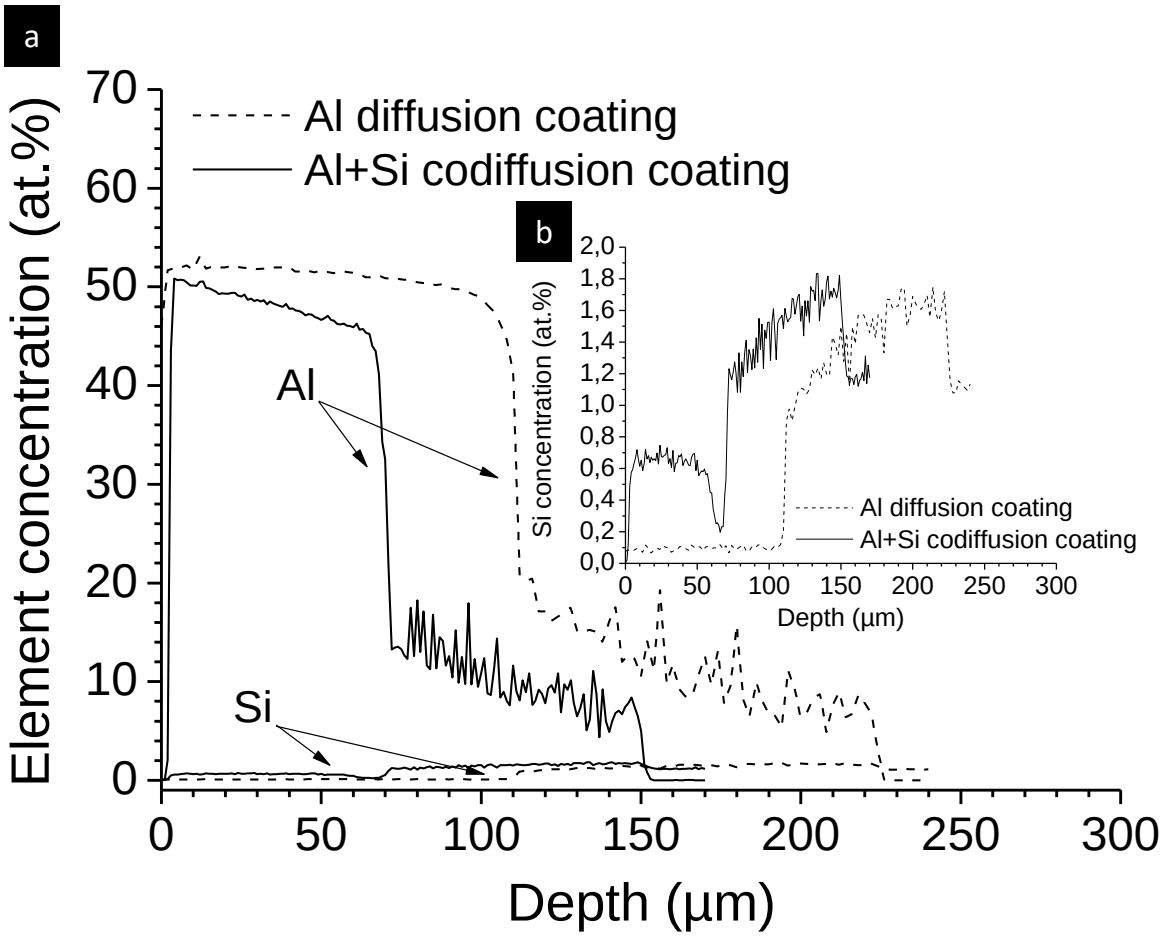


**Figure 45: a) EPMA (electron probe micro analysis) line scan and its b) magnification of the cross section of an Al and Al/Si coated AISI 321 steel (*T* = 1000°C, *t* = 4h).**

The Matano analysis of both the Al and Al/Si coating shows that the interdiffusion coefficient of Al in AISI 321 is reduced (Al pack: $D_{Al}^{AISI\,321} = 14.88 \cdot 10^{-14}\,\frac{m^2}{s}$; Al/Si pack: $D_{Al}^{AISI\,321} = 7.78 \cdot 10^{-14}\,\frac{m^2}{s}$) due to co-diffusion, as it was expected. Concerning Equation 20 the reduction of the Al activity difference between the pack and the substrate $\Delta a$ and the reduction of the diffusion coefficient *D* of Al by adding a co-deposition element causes a reduction of the resulting coating thickness $x$. Table 5 compares the experimentally determined and the calculated coating thickness ratios for Al and Al/Si coatings. Since AISI 321 contains no Al, the Al activity difference between pack and substrate is equal to the Al activity within the pack. By comparing the ratio of the resulting Al coating thicknesses for an Al pack $x_{Al,exp.}$ and an Al/Si pack $x_{Al/Si,exp.}$ with the calculated coating thicknesses for an Al $x_{Al,calc.}$ and an Al/Si pack $x_{Al/Si,calc.}$ it can be seen that the ratios of the coating thicknesses match very well. The

following calculation demonstrates the reduction of the resulting coating thickness by co-deposition:

$$\frac{x_{Al,exp.}}{x_{Al/Si,exp.}} \approx \frac{x_{Al,calc.}}{x_{Al/Si,calc.}} = \frac{\sqrt{2 \cdot \frac{D_{Al}}{q} \cdot \Delta a_{Al} \cdot t}}{\sqrt{2 \cdot \frac{D_{Al/Si}}{q} \cdot \Delta a_{Al/Si} \cdot t}} = \sqrt{\frac{D_{Al} \cdot \Delta a_{Al}}{D_{Al/Si} \cdot \Delta a_{Al/Si}}} \qquad (26)$$

where $D_{Al}$ and $D_{Al/Si}$ are the Al diffusion coefficients of Al in AISI 321 for an Al and Al/Si pack, $\Delta a_{Al}$ and $\Delta a_{Al/Si}$ are the Al activities of the pack for an Al and Al/Si powder mixture. This calculation requires the same pack process time $t$ for both packs (Al and Al/Si). The constant $q$ is assumed to be equal in both cases, since the resulting coating consists of the same intermetallic phase (β-FeAl).

**Table 5: Comparison of the values for the Al and Al/Si coating process and their coating thickness ratios (calculated and experimentally determined).**

| | $\Delta a_{Al}$ | $D_{Al}^{FeAl}\left[\frac{m^2}{s}\right]$ | $x_{exp.}$ | $\Delta a$ | $q$ | $\frac{x_{Al,exp.}}{x_{Al/Si,exp.}}$ | $\frac{x_{Al,calc.}}{x_{Al/Si,calc.}}$ |
|---|---|---|---|---|---|---|---|
| Al coating | 0.19 | $14.88 \cdot 10^{-14}$ | 102.5 | 0.18-0.072 | 0.49 | 1.58 | 1.68 |
| Al/Si coating | 0.13 | $7.78 \cdot 10^{-14}$ | 65.0 | 0.12-0.072 | 0.63 | | |

It can be seen that the ratio of the experimentally determined Al coating thicknesses on AISI 321 for Al and Al/Si pack powder mixture are similar to the calculated ones (Table 5). This means that the Si effect on the activity as well as the diffusion coefficient can be used to optimize the coating thickness.

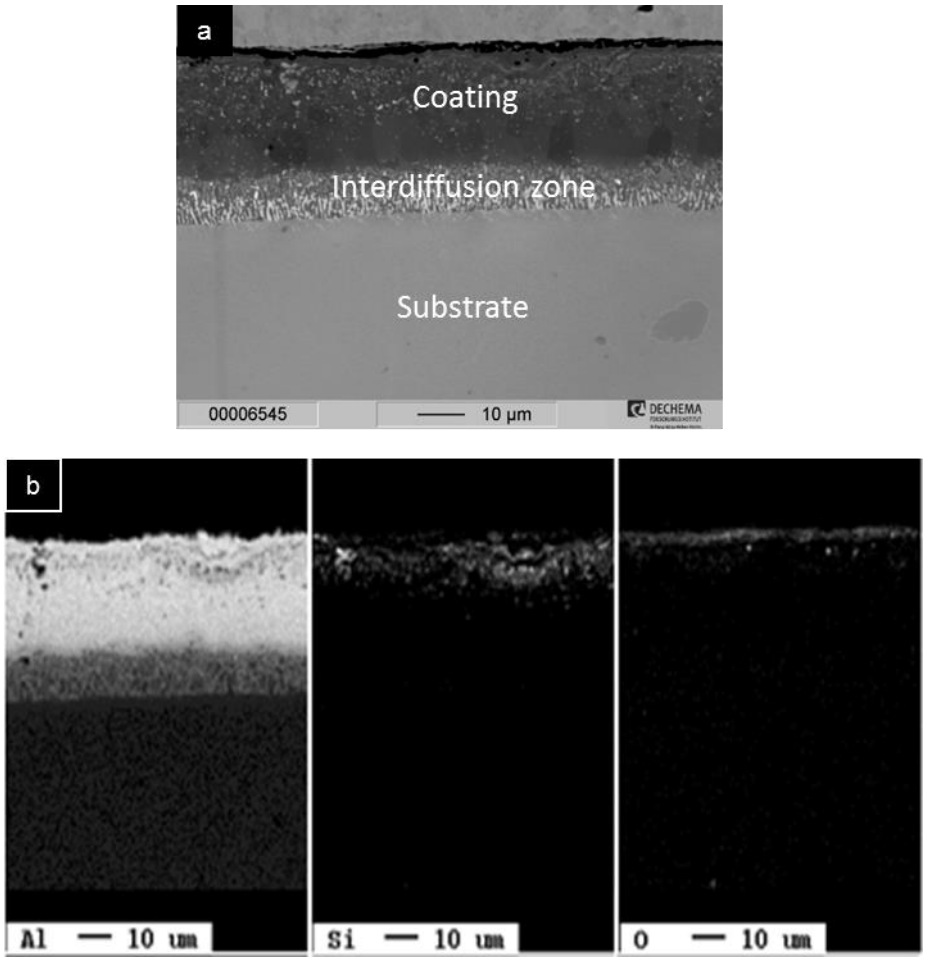


**Figure 46: a) BSE (backscattered electron) image and b) EPMA element map of the cross section of an Al/Si coated specimen of René 80 (*T* = 1000°C, *t* = 4h).**

Since the Si amount of the interdiffusion zone in the case of Al/Si coated AISI 321 (0.6 at.%) is lower than it is in the material (1.2 at.%) (Figure 40), additional Al/Si co-deposition pack cementation experiments at 1000°C for 4 hours were performed on René 80, which contains no Si (Figure 46 and Figure 47), in order to prove that Si can be incorporated into a material by an Al/Si pack cementation process.

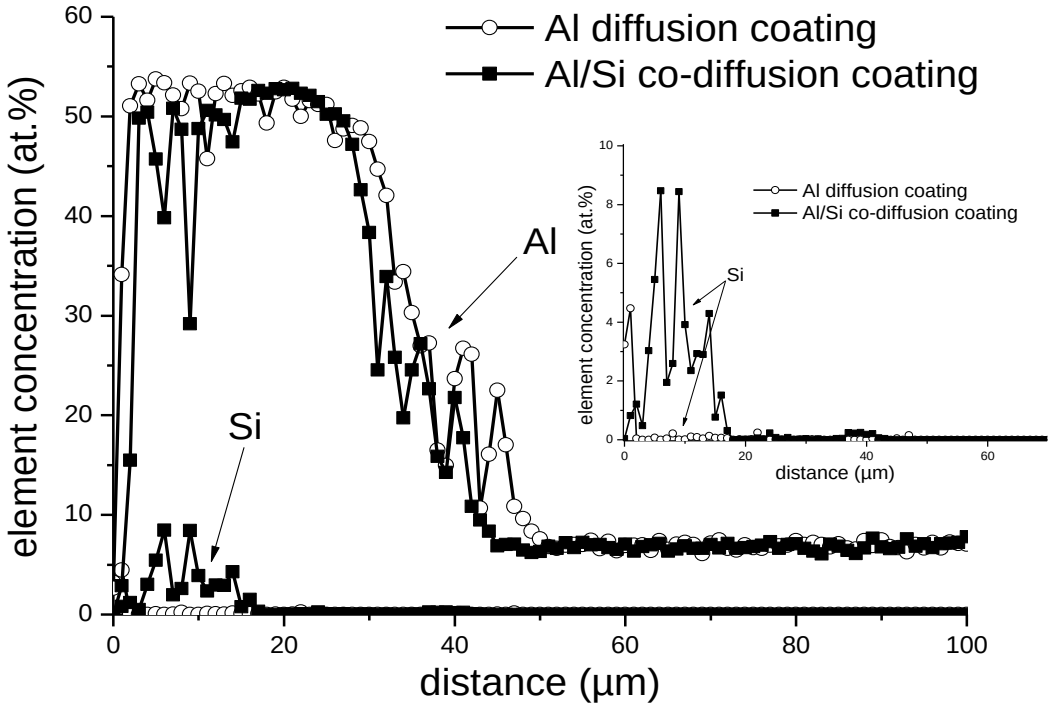


**Figure 47: EPMA (electron probe micro analysis) line scan of the cross section of an Al and Al/Si coated specimen of René 80 (*T* = 1000°C, *t* = 4h).**

The Al activity reduction and the Al incorporation in a coating produced by a powder pack mixture, which contains only Hf as a deposition element, were confirmed by pack cementation experiments on an Alloy 800 steel. Specimens were embedded in a pack powder mixture containing only Hf as a deposition element as well as a pack containing Al and Hf as deposition elements (Figure 48 and Figure 49) (Hf powder mixture: 3wt.% Hf, 1wt.% $NH_4Cl$, 96wt.% $Al_2O_3$; Al/Hf powder mixture: 1wt.% Al, 3wt.% Hf, 1wt.% $NH_4Cl$, 95wt.% $Al_2O_3$).

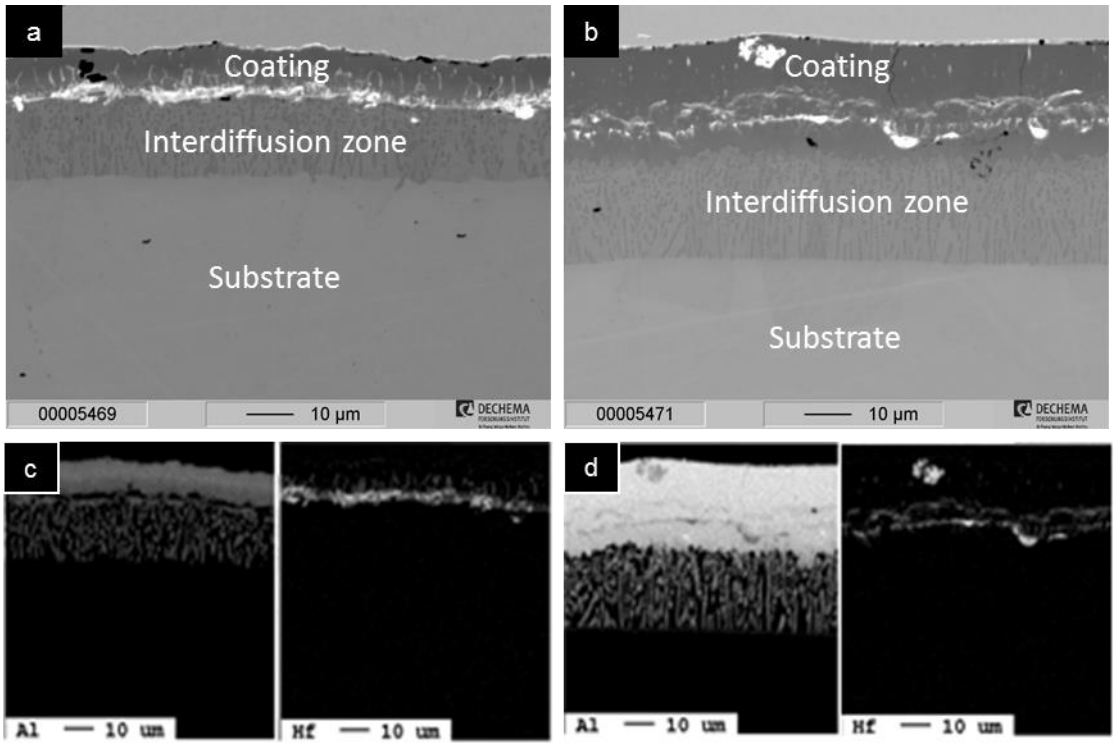


**Figure 48: BSE (backscattered electron) image (a, b) and EPMA element map (c, d) of the cross section of an a, c) Hf and an b, d) Al/Hf coated specimen of René 80 (*T* = 1000°C, *t* = 4h). The element maps show qualitatively the Al and Hf amounts within the cross sections.**

Interestingly in both cases β-phase is formed on the substrate. The resulting Al coating thickness derived from the Al/Hf powder pack is higher than for the Hf powder pack, as it was expected. The Hf deposition is higher in the case of Hf mono-element deposition than for the Al/Hf powder mixture (magnification of Figure 49).

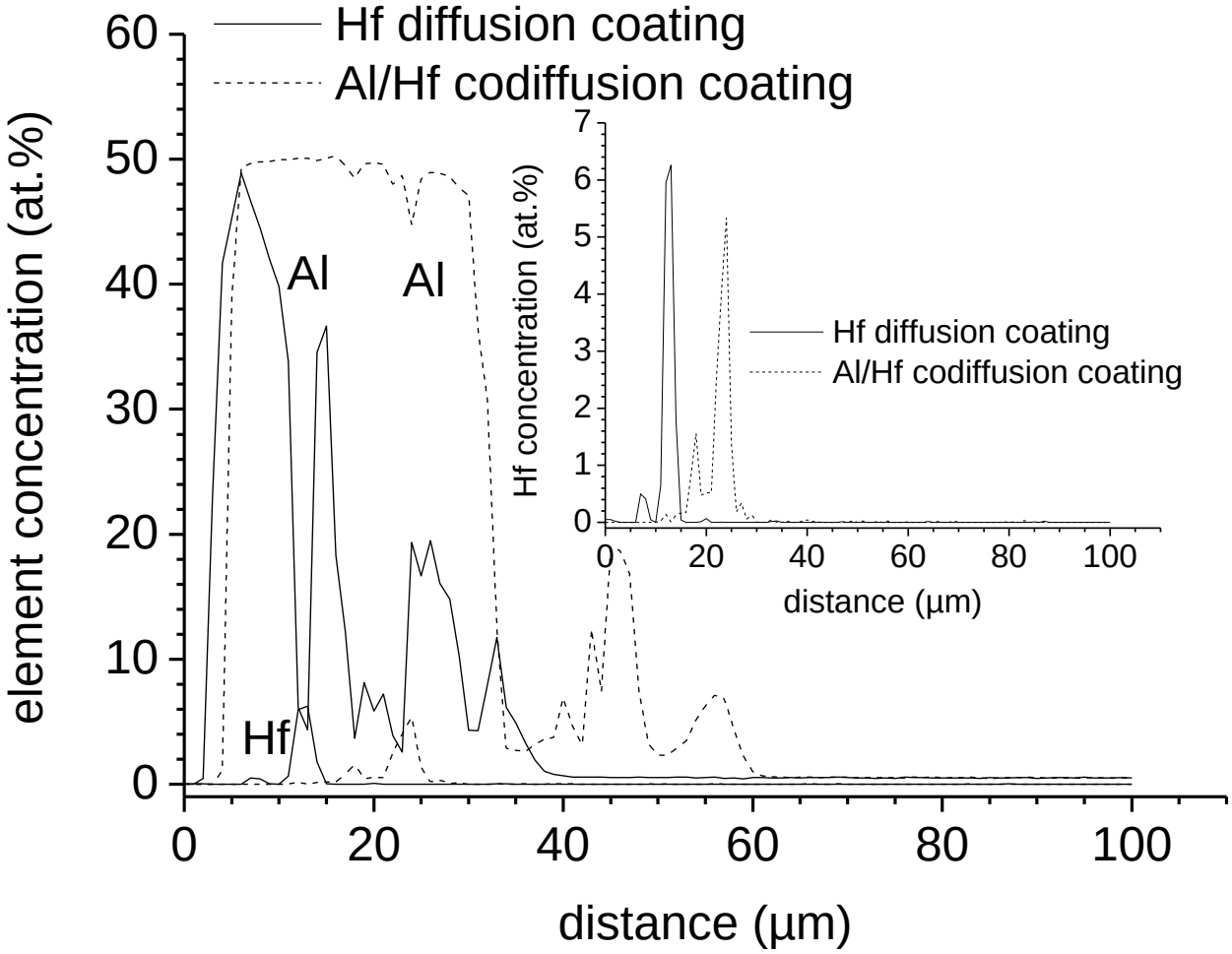


**Figure 49: EPMA (electron probe micro analysis) line scan of the cross section of an Al and Al/Hf coated Alloy 800 steel (*T* = 1000°C, *t* = 4h).**

As shown already for the Si-modified coating, the ratios of the experimentally produced Al coating thicknesses on Alloy 800 for Al, Al/Hf and Hf pack powder mixtures were compared with those, using the calculated partial pressures and determined diffusion coefficients. It can be seen that the calculated and experimentally determined thicknesses fit very well (Table 6). This means that the Hf co-deposition effect on the thermodynamics and the kinetics of the Al pack process and their quantitative values have been determined and successfully applied on the coating design concept in this work.

**Table 6: Comparison of values for the Al, Al/Hf and Hf coating process and their coating thickness ratios (calculated and experimentally developed).**

| | $\Delta a_{Al}$ | $D_{Al}^{FeAl}\left[\frac{m^2}{s}\right]$ | $x_{exp.}$ | $\Delta a$ | $q$ | $\frac{x_{Al/Hf,exp.}}{x_{Hf,exp.}}$ | $\frac{x_{Al,calc.}}{x_{Al/Hf,calc.}}$ |
|---|---|---|---|---|---|---|---|
| Al coating | 0.19 | $14.88 \cdot 10^{-14}$ | 102.5 | 0.18-0.072 | 0,48973 | | |
| | | | | | | - | - |
| Al/Hf coating | 0.17 | $2.54 \cdot 10^{-15}$ | 30.0 | 0.17-0.072 | 0,00797 | | |
| | | | | | | 3.0 | 3.0 |
| Hf coating | 0.03 | $1.54 \cdot 10^{-15}$ | 10.0 | 0.03-0.072 | 0,00483 | | |

The diffusion coefficient $D_{Al}^{FeAl}$, determined for the Al/Hf and Hf packs is significantly smaller than in the case of the Al pack. This is because the Al supply in the Al pack is not guaranteed for the process time of 4 hours, which makes the solid state diffusion step the rate limiting step. Otherwise, in the case of Hf and Al/Hf pack the Al supply from the pack is not kept at the same level for the entire process time, which makes the gas diffusion step the rate limiting step.

The thermodynamic calculations in Figure 14b show that the Al activity within the pack is the same, no matter if $Al_2O_3$ is considered in the calculations or not. However, this is not valid for every type of activator and deposition element, since $Al_2O_3$ is not inert if a reactive element is included in the pack powder mixture.
The Gibbs free energy of formation of $Al_2O_3$, e.g., at 1600 K, normalized to a mole of oxygen atoms, is -388 kJ/mole; for the oxides $HfO_2$, $ZrO_2$, $NbO_2$, $Ta_2O_5$ this characteristic value is -407, -397, -257, and -273 kJ/mole, respectively. For hafnium and zirconium oxides these values are more negative than for $Al_2O_3$. These metals can therefore reduce this oxide to pure aluminium [89]. As a result, metallic Al is available in the pack (from $Al_2O_3$), which forms Al halides and thus provides an Al activity of the pack, which is due to the reaction of Hf with $Al_2O_3$ and the release of Al:

$$3\,Hf\ +\ 2\,Al_2O_3\ \leftrightarrow 3\,HfO_2 + 4\,Al \qquad (27)$$

The thermodynamic calculations in Figure 50 show that aluminium chlorides are also formed in a pack consisting only of Hf, an activator and $Al_2O_3$, which is due to the reaction of Hf with $Al_2O_3$ and the release of Al. This calculation agrees with the Gibbs free energy data in [89].

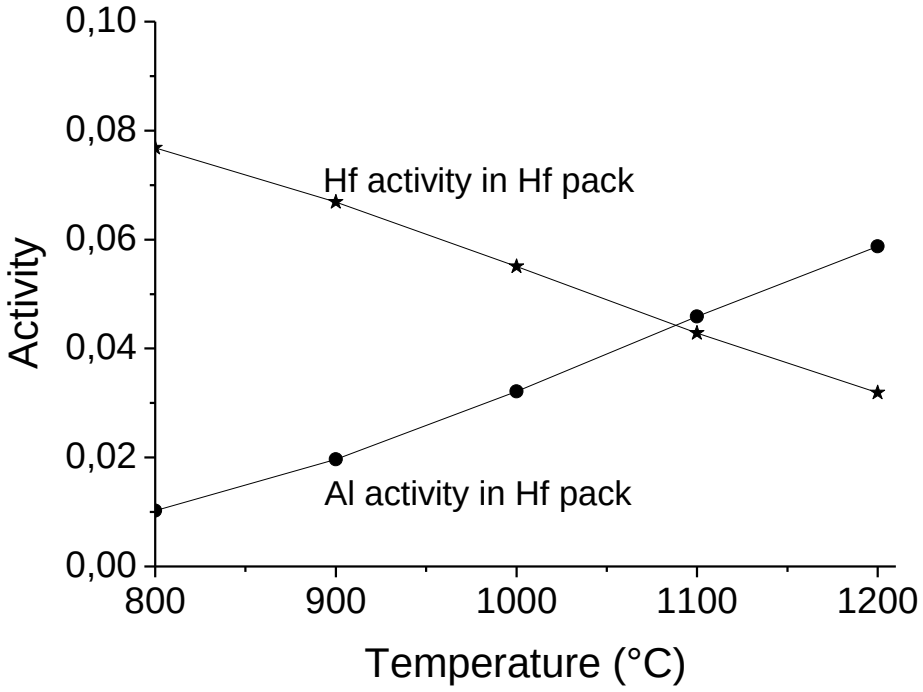


**Figure 50: Calculation of the Hf and Al activities for a Hf pack (3wt.% Hf, 1wt.% $NH_4Cl$, 96wt.% $Al_2O_3$) as a function of temperature.**

## 6.4. Limitations of the Coating Design

### 6.4.1. Calculated Al Activity versus real Al Activity

The overlapping of the calculated Al activities within the pack for a pack mixture of 1 wt.% Al, 1 wt.% $NH_4Cl$, 98 wt.% $Al_2O_3$ and the different intermetallic phases of the Fe-Al system (Figure 28) show that the Al activity within the pack is in the rage of the Al activity within the $FeAl_3$ phase up to 880°C. Since the Al activity within the intermetallic phases increases faster with temperature than the Al activity within the pack, the Al activity of the pack is in the range of the $Fe_2Al_5$ phase above a temperature of 880°C. How could the FeAl phase be formed at these process conditions, whereas the calculations predict the formation of the $Fe_2Al_5$ phase? The formation of the β-phases instead of the $Fe_2Al_5$ and $Ni_2Al_3$ phase is due to the solid state diffusion processes, which takes place during the pack process. As it was mentioned in chapter 6.1.1, the diffusion coefficient of Al in the Fe or Ni aluminide depends also on the other elements of the substrate. This leads to a lower Al diffusion coefficient, the more alloying elements (e.g. the austenite former Ni) are included in the material, which promotes the maintenance of the HA coatings, whereas the Al diffusion coefficient in substrates with less alloying element is high enough to promote the formation of the FeAl phase by a faster interdiffusion to the substrate interior, compared with the Ni-based substrate.

### 6.4.2. Effect of excessive Aluminium Amount

Thermodynamic calculations show that the Al activity in the pack increases with the Al or activator amount, but reaches a limit at a certain amount (Figure 51 and Figure 52). But in fact, a high amount of Al or activator within the pack leads to a longer supply of the substrate with the Al carrying halides, which has an effect on the coating microstructure.

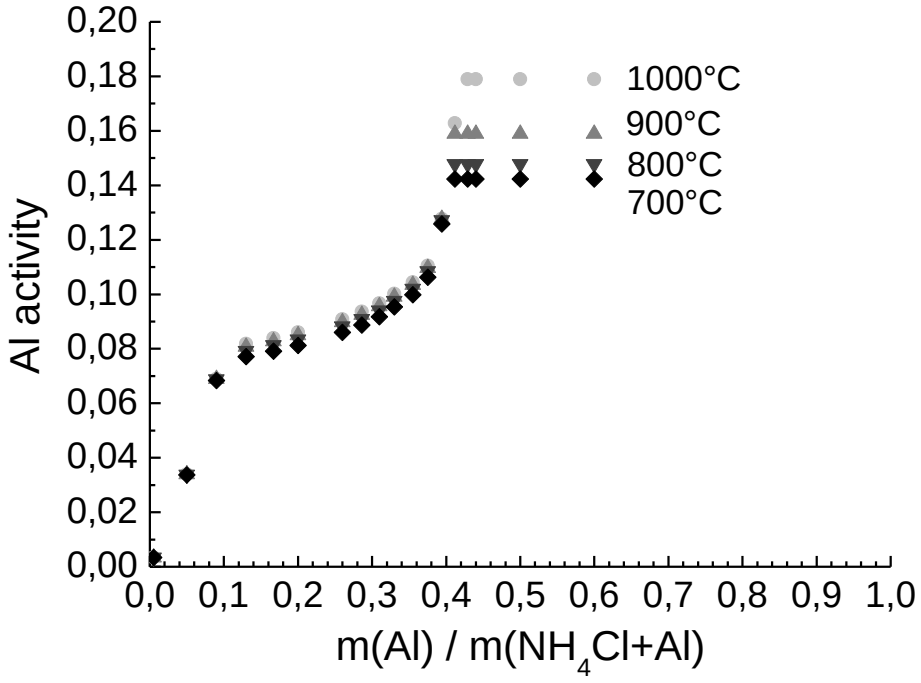


**Figure 51: Plot of the calculated Al activities (total partial pressure of Al chlorides) within the pack (1 wt.% Al, 1 wt.% $NH_4Cl$, 98 wt.% $Al_2O_3$) for several process temperatures versus the mass ratio of Al to $NH_4Cl$.**

The influence of metal content was calculated by Xiang et al. by predicting the effects of Al concentration on the AlCl partial pressure for the aluminising packs activated by 4 wt% $CrCl_3 \cdot 6H_2O$. The results for coating temperatures of 900, 1000 and 1100°C are plotted against the Al concentration in Figure 52. It can be seen that the AlCl partial pressure increased strongly as the Al concentration in the pack was increased from 1 to 2 wt% and then remained constant with further increase of Al concentration in the pack [10].

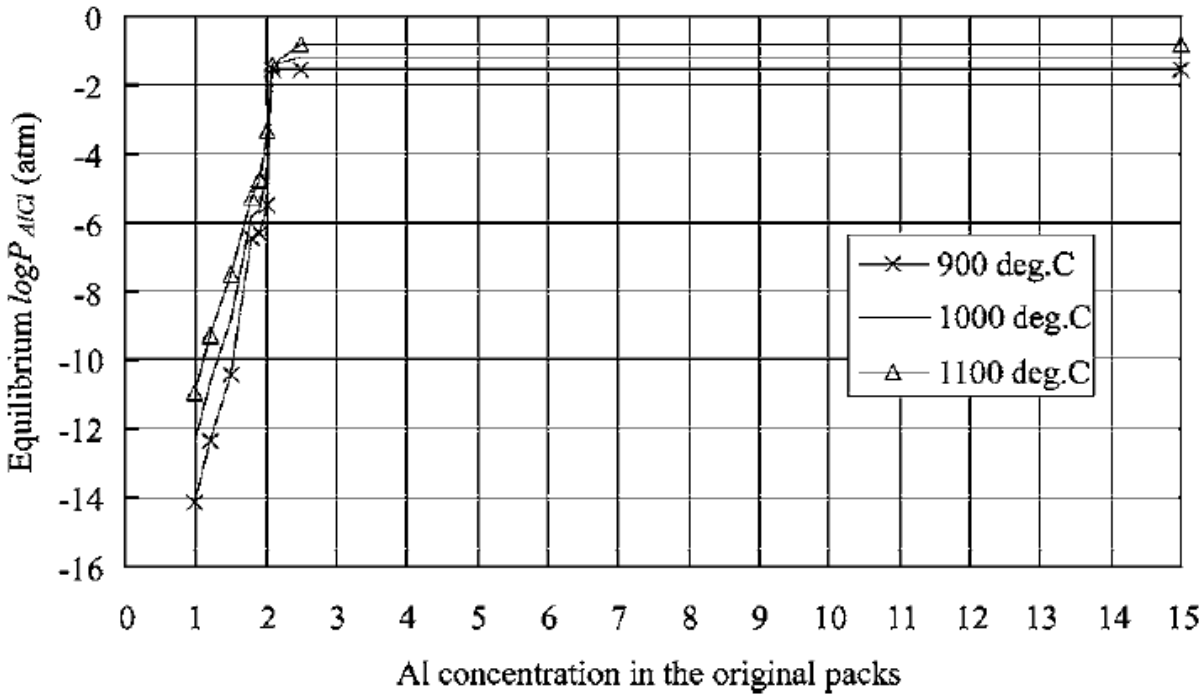


**Figure 52: Dependence of AlCl partial pressure on Al concentration in aluminising packs activated by 4 wt% $CrCl_3 \cdot 6H_2O$ [10].**

Taking kinetic aspects into account, this only applies for a limited time, since Al and the activator are continuously consumed during the pack cementation process, and a higher Al amount would lead to a longer supply with Al. Pack Cementation procedures were carried out with an increasing Al amount for 1 hour and the mass gain $\Delta m/A$ was plotted against the Al amount (Figure 53). The results show that the mass gain increases strongly with the Al amount up to 2 wt.%. Afterwards the increase flattens.

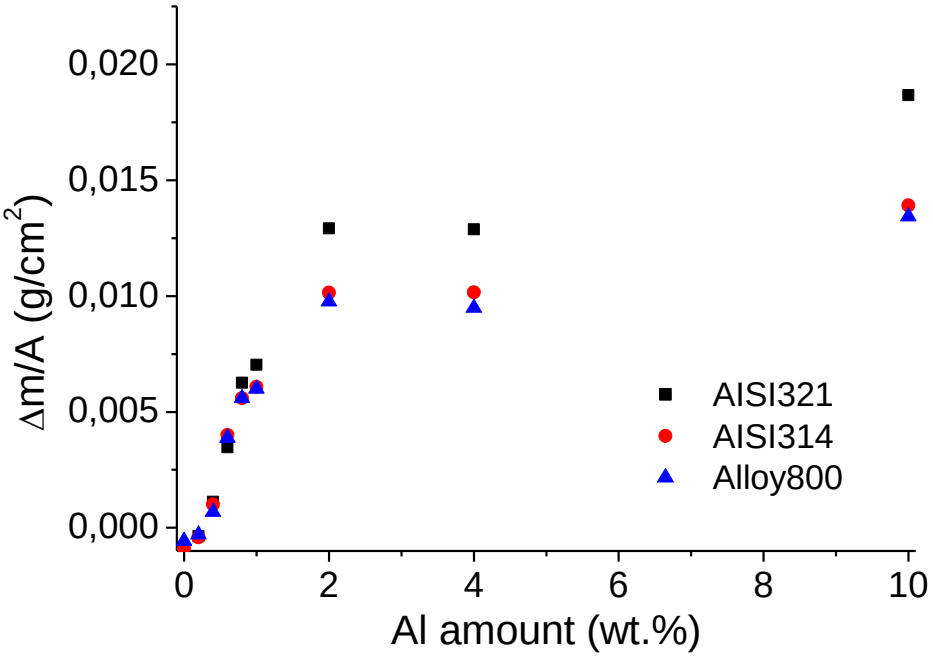


**Figure 53: Mass gain in dependence of the Al amount within the pack (x wt.% Al, 1 wt.% Al, 99-x wt.% $Al_2O_3$) at 1000°C for 1 hour.**

### 6.4.3. Effect of excessive Activator Amount

Thermodynamically, the Al activity in the pack increases for a constant Al amount and an increasing activator amount, but reaches a limit, where the Al activity cannot be increased anymore, due to a saturation of the pack with the chlorides. Experiments have shown that an excessive activator amount within the pack leads to deterioration of the specimen to be coated, since the partial pressure of the halides (HF, HCl, HBr etc.) increases with increasing the activator amount. The halides can attack the specimen (e.g. Fe-based alloy), and form Fe halides, instead of Al halides, as it is shown exemplary for $NH_4Cl$ and an Fe-based alloy:

$$NH_4Cl \rightarrow NH_3 + HCl \tag{28}$$

$$a\,HCl + Fe \rightarrow FeCl_a + {}^{a}/_{2}\,H_2 \tag{29}$$

This detrimental effect was not considered in the coating design. Coating experiments on Alloy 800 with an increasing $NH_4Cl$ and a constant Al amount (x wt.% $NH_4Cl$, 1 wt.% Al, 99-x wt.% $Al_2O_3$) were performed at 1000°C for 4 h in order to observe the influence of the activator amount on the material (Figure 54). The

experiments have shown that 1 wt. % activator is a sufficient amount and that an increase of the Al activity in the pack has to be performed only by increasing the Al amount.

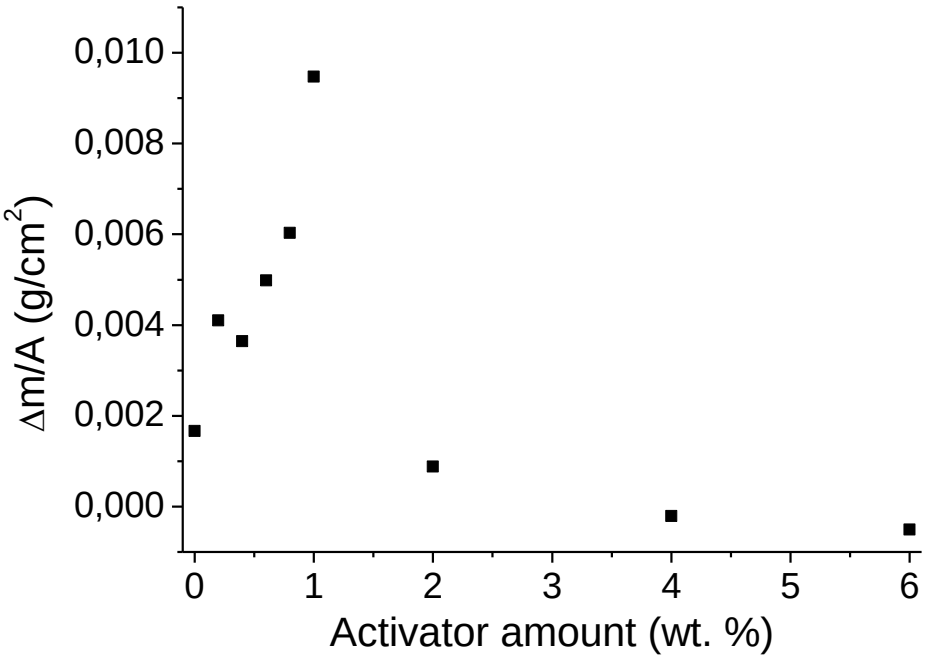


**Figure 54: Mass change of Alloy 800 in dependence of activator amount within the pack (x wt.% $NH_4Cl$, 1 wt.% Al, 99-x wt.% $Al_2O_3$) at 1000°C for 4 h.**

Pack experiments with a pack, which contains only 1 wt.% Al and 99 wt.% $Al_2O_3$ and no activator were performed at 1000°C for 4 hours in order to test if Al is deposited on the substrate only via gas phase diffusion from the bulk to the substrate surface or also by direct contact. The measurements have shown that the mass gain without activator is about 0.001 $gcm^{-2}$ whereas the mass gain with 1 wt.% $NH_4Cl$ is about 0.009 $gcm^{-2}$. Indeed, the difference is very high, but the pack experiment without activator shows that Al deposition only by direct contact of the Al particles with the substrate without an activator is very poor, because the largest part of the powder pack consists of $Al_2O_3$, which surround the Al grains and inhibit a reaction between Al and the substrate elements. Even if the activator amount within the pack is higher and the Al amount is 1 wt.%, a β-FeAl coating is formed rather than a $Fe_2Al_5$, because the high diffusion coefficient of Al at 1000°C leads to a strong Al interdiffusion to the substrate interior, which promotes the formation of LA coatings.

According to Hickl and Heckel the pack cementation process is a two-step aluminizing process, in which initially an Al rich phase is formed (e.g. η-$Fe_2Al_5$ or the δ-$Ni_2Al_3$), and then by continuous interdiffusion of Al into the substrate intermetallic phases with lower Al amount are formed (e.g. β-FeAl or β-NiAl) [70]. They assume that the Al activity within the pack is 1 during the entire pack process, since Al exists in the pack as a pure powder. In this work two pack processes on specimens of AISI 321 were performed with both a HA and a LA pack for 30 minutes at 1000°C. This was done in order to examine, whether the Al activity within the powder pack equals 1 in the entire process, and the formation of the Al poorer intermetallic phases occurs due to Al interdiffusion into the substrate interior, or if the Al activity within the powder pack is controlled by the process parameters and is not equal 1.

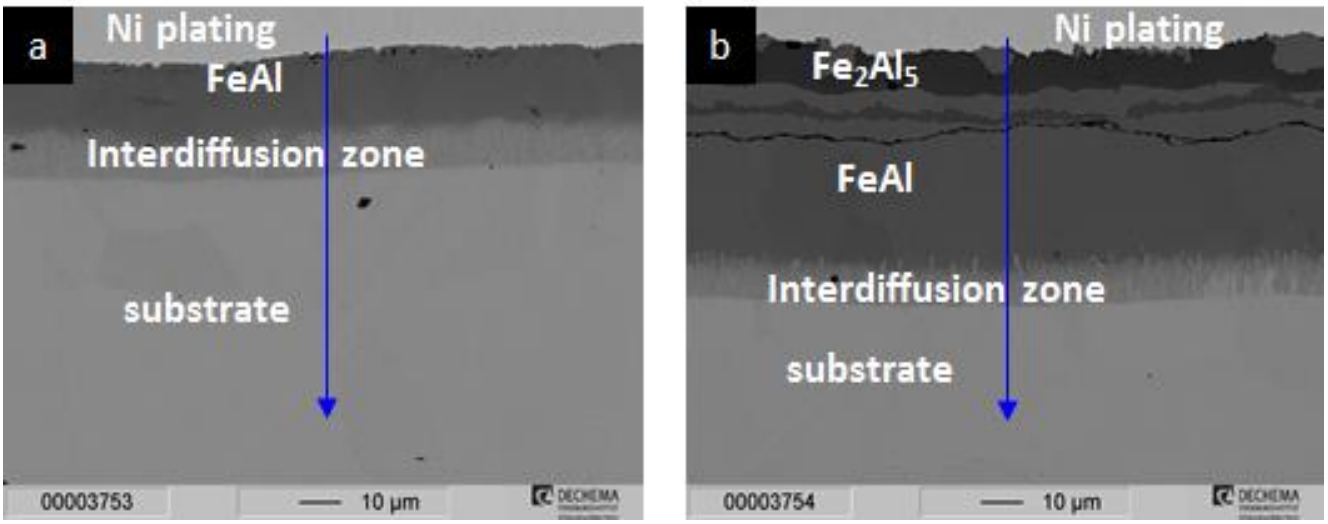


**Figure 55: BSE (backscattered electron) image of the cross section of Al coated AISI 321 at 1000°C for 30 minutes with a pack composition of a) 1 wt.% Al, 1 wt.% $NH_4Cl$, 98 wt.% $Al_2O_3$ and b) 10 wt.% Al, 1 wt.% $NH_4Cl$, 89 wt.% $Al_2O_3$.**

The first case would occur if the Al supply into the substrate by interdiffusion would take place by direct contact, without gaseous diffusion of halides. The second case would mean that the effect of a HA and a LA powder is visible, especially at early stages of the pack process, where the diffusion effect is not large.

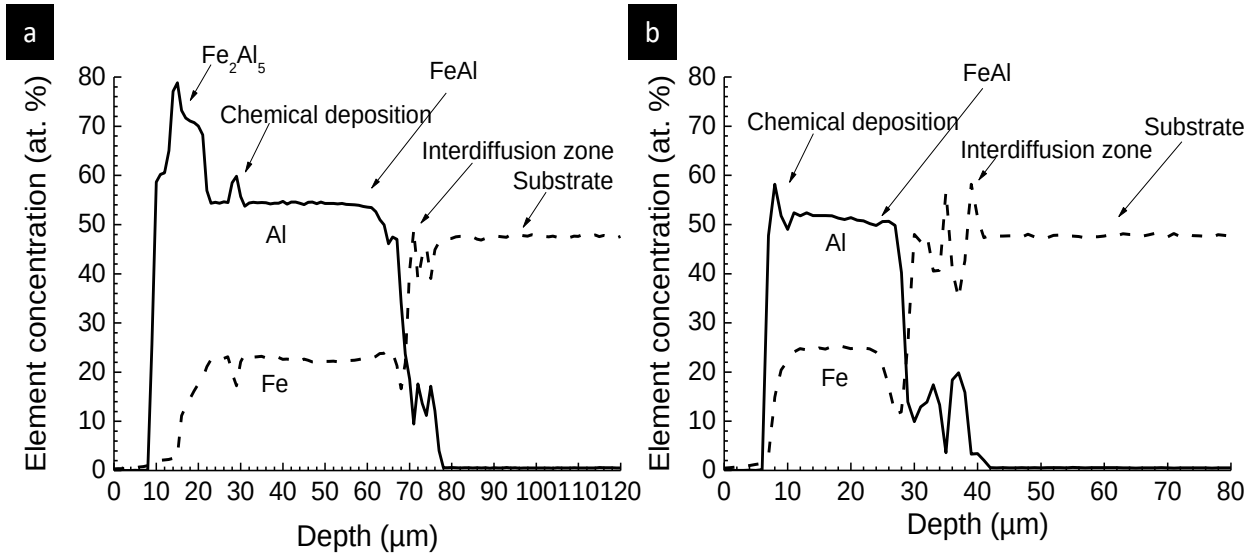


**Figure 56: EPMA (electron probe micro analysis) line scan of the cross section of Al coated AISI 321 at 1000°C for 30 minutes with a pack composition of a) 1 wt.% Al, 1 wt.% $NH_4Cl$, 98 wt.% $Al_2O_3$ and b) 10 wt.% Al, 1 wt.% $NH_4Cl$, 89 wt.% $Al_2O_3$.**

Figure 55 and Figure 56 show the cross section and EPMA line scan of the two coated austenitic AISI 321 steels ($T$ = 1000°C, $t$ = 30min). The first pack consisted of 10 wt.% Al, whereas the other pack consisted of 1 wt.% Al. The $NH_4Cl$ amount was 1 wt. % in both packs. It can be seen in Figure 56 a that the LA coating (developed with 1 wt.% Al and 1wt.% $NH_4Cl$ in the pack) consists only of FeAl (x = 27 µm), whereas the line scan of Figure 56 b shows the two phases $Fe_2Al_5$ and FeAl ($x$ = 65µm, developed with 10 wt.% Al and 1wt.% $NH_4Cl$ in the pack).

## 6.5. Cyclic Oxidation Tests

### 6.5.1. Cyclic oxidation of an Al and Al/Si coated AISI 321

Cyclic oxidation tests of the specimens of an AISI 321 steel with an Al mono-element and an Al/Si co-diffusion coating were performed at 1000°C for 1000 h (250 cycles) in an artificial hydrogen reforming process atmosphere (55% $H_2$, 28% $H_2O$, 8% $CO_2$, 7.5% CO, 1.5% $CH_4$). The higher mass gain curve (Figure 57) of the Al coated AISI 321 material indicates an initially relatively fast oxide scale growth and afterwards the occurrence of spallation of the oxide scale, whereas the mass gain curve of the Al/Si coated AISI 321 steel is smooth and does not indicate the occurrence of spallation.

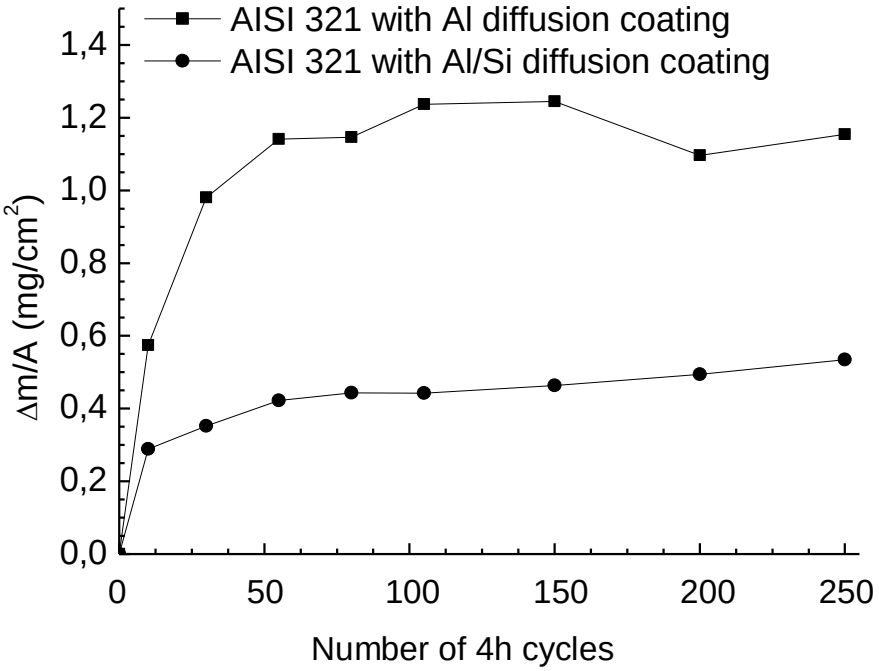


**Figure 57: Mass gain curves of Al and Al/Si coated AISI 321 in a process atmosphere (55% $H_2$, 28% $H_2O$, 8% $CO_2$, 7.5% CO, 1.5% $CH_4$) at 1000°C for 1000 h (250 cycles). The mass gain Δm/A is plotted against the number of cycles.**

Nevertheless, mass gain curves do not give a complete information about the degradation of the materials. Thus, the cross sections of the exposed specimens were analysed. Al coatings with a high Al concentration promote the Al interdiffusion to the interior of the material during exposure (Figure 58).

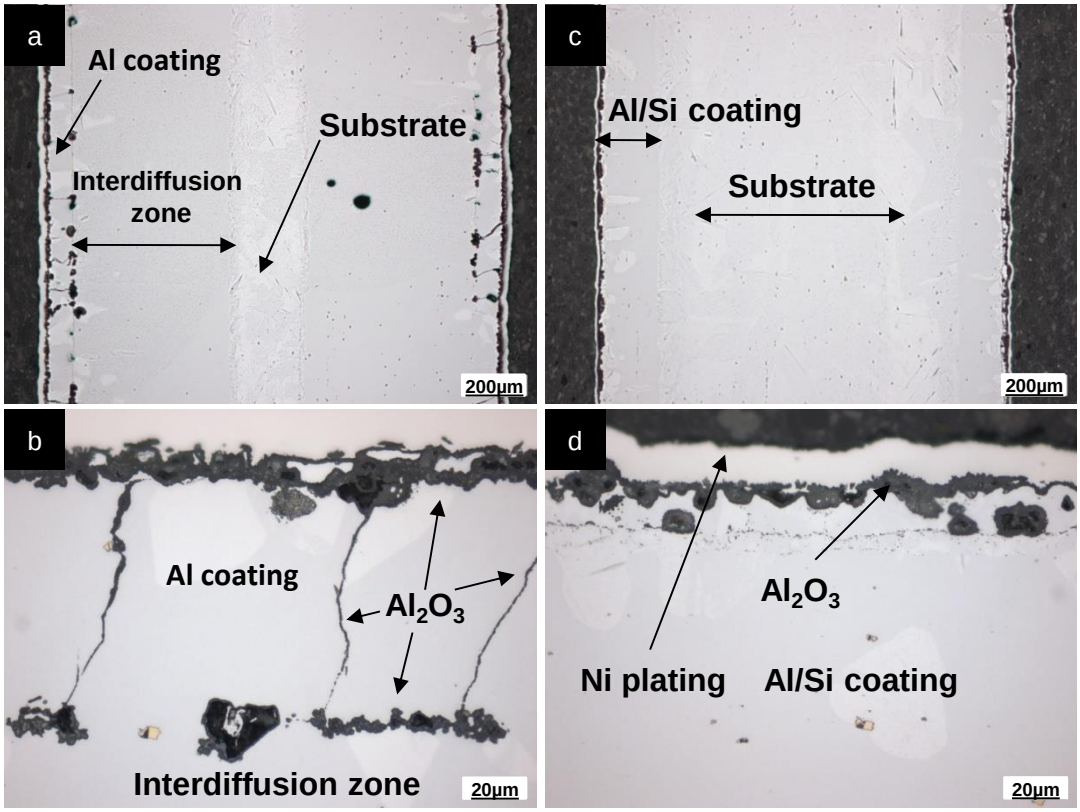


**Figure 58: Cross sections of the a,b) Al coated and c,d) Al/Si coated AISI 321 after exposure in a process atmosphere (55% $H_2$, 28% $H_2O$, 8% $CO_2$, 7.5% CO, 1.5% $CH_4$) at 1000°C for 1000 h (250 cycles). The Ni plating (for maintaining a contrast between embedding and specimen surface), the formed oxide scale, the increased interdiffusion zone and the residual substrate can be seen.**

Furthermore, the cross sections show that the high activity Al coating, which consists of the $Fe_2Al_5$ intermetallic phase, exhibits cracks and that the lower part of the coating is oxidized, apparently, an oxide scale is being developed parallel to the oxide scale of the surface, which can spall when the lower oxide scale is closed, since there will be no more adhesion if the coating and the material are separated by an oxide scale. The inhibition of spallation within the Si enriched Al coating is because of the lower Al activity within the coating due to the Si addition in the pack powder. Al coatings with high Al content are more brittle than Al coatings with a lower Al content and their coefficient of thermal expansion mismatch to the substrate material is higher, which promotes crack formation [90].

### 6.5.2. Cyclic oxidation of Al and Al/Hf coated Alloy 800

Cyclic oxidation tests on specimens of an Alloy 800 steel with an Al and Al/Hf and coating were performed at 1000°C for 140 h (140 cycles) in an artificial combustion atmosphere (3% $O_2$, 52% $N_2$, 32% $H_2O$, 13% $CO_2$). The coatings were manufactured in a pack cementation process at 1000°C for 4 h with a powder mixture of 1wt.% Al, 1wt.% $NH_4Cl$, 98wt.% $Al_2O_3$ for the Al coating and 1wt.% Al, 3wt.% Hf, 1wt.% $NH_4Cl$, 95wt.% $Al_2O_3$ for the Al/Hf coating.

The mass gain measurements in Figure 59 indicate that after 10 h exposure time parts of the oxide scale of the Al coated Alloy 800 seem to spall and afterwards oxide scale self-healing occurred. The mass gain curve of the Al/Hf coated Alloy 800 specimens shows no fluctuations and no spallation which indicates the growth of a continuous oxide scale.

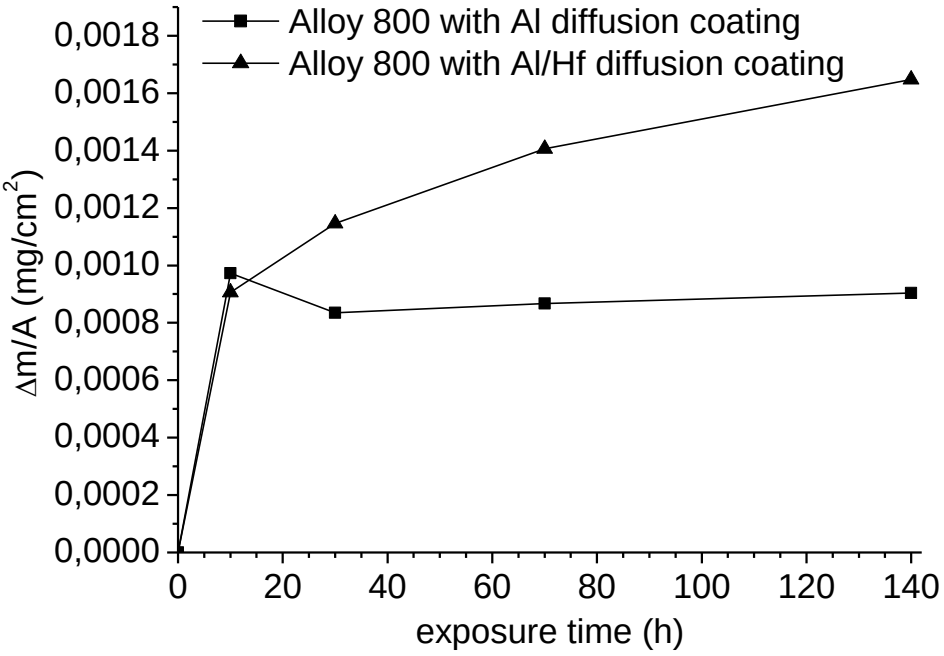


**Figure 59: Mass gain curves of Al and Al/Hf coated Alloy 800 in a combustion atmosphere (3% $O_2$, 52% $N_2$, 32% $H_2O$, 13% $CO_2$) at 1000°C for 140 h (140 cycles).**

While the Al coating (intermetallic β-FeAl phase) exhibits cracks at its upper part and corrosion pits, which are up to 50 µm deep into the coating, the Hf/Al coating (intermetallic β-FeAl phase enriched with Hf) is free of cracks and a dense oxide scale with comparatively small corrosion pits is formed (up to 20 µm) (Figure 60). In the literature, the reactive element addition necessary for the beneficial reactive element

effect is mentioned to be tenths of a percent. The reason is that internal oxidation of reactive elements and incorporation of reactive element oxides in the scale increase the mass gain [49], which is in agreement with the mass gain curves in Figure 59. The Hf amount within the coating was higher than what is recommended in the literature. Nevertheless, the high amount Hf doped Al coating showed enhanced cyclic oxidation resistance. The cross section of the Al/Hf coated Alloy 800 after 140 h (140 cycles) exposure in a combustion atmosphere (3% $O_2$, 52% $N_2$, 32% $H_2O$, 13% $CO_2$) at 1000°C shows no spallation and a lower mass gain than the Al coating without Hf doping.

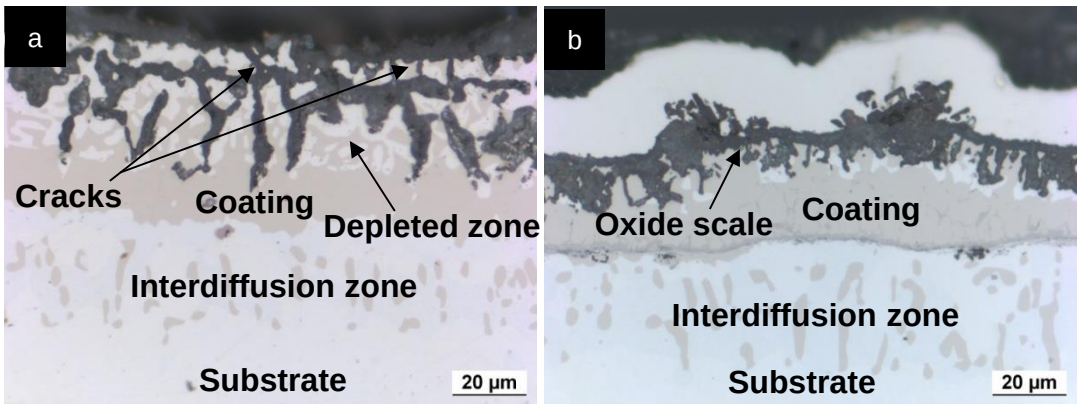


**Figure 60: Cross sections of the a) Al coated and b) Al/Hf coated Alloy 800 after exposure in a combustion atmosphere (3% $O_2$, 52% $N_2$, 32% $H_2O$, 13% $CO_2$) for 140h (140 cycles). The Ni plating (for maintaining a contrast between embedding and specimen surface), the formed oxide scale, an Al depleted zone, the residual coating, the interdiffusion zone and the substrate can be seen.**

# 7. Conclusions

This work showed that it is possible to design Al diffusion coatings by a quantitative consideration of the pack cementation process. Since pack cementation is a process with many variables as the process parameters (process time, process temperature, and powder mixture and powder amount), the substrate, the deposition element and the coating characteristics, the resulting coating properties are very sensitive to a change of each variable.

The coating design is based on assumptions and simplifications, which could be proven by considerations and which do not lead to a large deviation between prediction and experimental result. One of the most important assumptions is that during the pack process the solid state diffusion is the rate limiting step, as long as the Al supply in the powder mixture is maintained. The validity of this assumption is assured for a coating time of 4 hours, as it was mostly performed. The most important simplification is the linearization of the Al activity difference between the intermetallic phases and the substrate, which made an analytical solution of Fick's first law possible. Nevertheless, the Al coating design exhibits limitations. Ultra-short coating process times lead to a mismatch between predicted and formed coating thickness, since at short process times the heating process (e.g. from 150 to 1000°C with 5°C/min) also causes coating formation, which is not negligible. An insufficient Al amount in the powder mixture or ultra-long coating process times turn the pack process from a solid state to a gaseous diffusion rate limited process. The loss of Al carrying halides during the pack process due to the decomposition of the $NH_4Cl$ activator or the Al escape lead to less Al deposition than calculated via FactSage®. Furthermore, an excessive activator amount degrades the substrate to be coated by hydrogen halide attack on the material. Finally, the great advantage of this coating design is that the entire thermodynamic and kinetic information needed for the coating application on a material can be achieved by means

of the thermodynamic calculation program FactSage® or by means of “calibration” experiments, which makes this coating design autarkic. The equations and principles of the coating design can also be used to describe processes beyond the coating process of materials, e.g. where interdiffusion between a coating and substrate occurs due to element concentration gradients, such as the determination of the development of a certain diffusion profile during high temperature exposure.

# 8. Summary

Components, which consist of metallic materials and operate at high temperatures, can degrade due to high temperature corrosion attack. The most frequently occurring phenomenon is oxidation. When metallic materials are exposed to an oxidizing atmosphere, it is desired that elements, which are called protective oxide forming elements, diffuse from the material interior to the material surface and form a dense and slow-growing oxide scale, which acts as a diffusion barrier and decelerates further oxidation. Since for several reasons most high temperature alloys contain only a limited amount of protective oxide forming elements, coatings are applied with higher amount of these elements. The concept of the diffusion coatings is to enrich the substrate surface with one or more protective oxide forming elements (e.g. Al). Aluminization of Fe- and Ni-based alloys leads to Al diffusion coatings, which can consist of one phase or several stacked phases, depending on the Al activity within the intermetallic phase, according to the Fe-Al and Ni-Al phase diagrams. In this work, the aim was to develop a predictive design procedure for the manufacturing of pack cementation Al coatings on austenitic steels and Ni-based alloys. The pack cementation process is a CVD (chemical vapour deposition) process, where the substrate to be coated is embedded in a powder mixture, consisting of the deposition element (e.g. Al), an activator (e.g. $NH_4Cl$) and a filler (e.g. $Al_2O_3$) and is heated in a tube furnace for several hours in an Ar/5%$H_2$ inert atmosphere. The coating design is based on thermodynamic and kinetic considerations of the pack cementation process. Thermodynamic considerations were conducted by calculations with the thermodynamic software FactSage®, to determine the Al activity (total partial pressure of Al carrying halides) within the pack powder as a function of process temperature and powder composition. Furthermore, the determination of the full range of the binary phase diagram of the Fe-Al and Ni-Al systems and the Al activities of these systems were calculated as a function of

temperature and mole fraction. Kinetic values, as the diffusion coefficient, which affect the resulting coating thickness, have been determined via a limited amount of experiments for each alloy system, followed by Matano analysis. It was shown that based on the model considerations and the collection of the thermodynamic and kinetics data for a material/deposition element couple, the coating design approach developed enables a quantitative prediction and adjustment of the resulting coating properties (intermetallic phases and coating thickness) for a wide range of process parameters. Coating experiments on austenitic steels (AISI 321, AISI 314 and Alloy 800) and a Ni-based alloy (Alloy 601) have shown that low pack process temperatures (up to 900°C) promote the formation of HA coatings. This observation is in agreement with the thermodynamic calculations, but also kinetic considerations show that a high process temperature promotes the interdiffusion of Al from the coating to the interior of the material during the coating process, which promotes the formation of LA coatings. The coating design postulates that it is possible to determine the entire kinetic values (the pre-factor $D_0$, the activation energy $E_A$ and the constant $q$) for a deposition element/substrate couple by means of three "calibration" pack experiments at three different temperatures. The determined diffusion coefficients for the coating procedure on AISI 321, AISI 314, Alloy 800 and Alloy 601 at 800, 900 and 1000°C showed good agreement with literature values. The collection of the entire thermodynamic and kinetic information made it possible to predict the coating microstructure for these four materials and to compare the predicted and experimentally formed coating properties, which showed good agreement. On the other side, the coating design contains limitations. For example, an extensive activator amount in the pack, which would theoretically cause a higher Al activity in the pack, leads to an attack of the substrate by the hydrogen halides. The co-deposition of another element to the main deposition element Al reduces the Al activity within the pack, since the activator is consumed by both deposition elements. Experiments have shown that Si and Hf can be co-deposited to an Al coating. The coating thickness is reduced in comparison to a mono-element Al coating, which is not only caused by the Al activity reduction due to co-deposition. Diffusion coefficient determinations of Al and the co-deposition elements (Si and Hf) have shown that also the diffusion coefficient of Al was reduced, because the co-deposition element occupies Al lattice sites. Cyclic oxidation experiments in an oxidizing and reducing atmosphere at 1000°C have shown that Si co-deposited Al coatings enhance the high temperature corrosion

resistance, since the Al activity within this two-element coating is lower in comparison with the mono-element Al coating. Thus, the Al interdiffusion to the interior substrate and the coating brittleness is reduced. Also, Hf co-deposited Al coatings have shown an enhancement compared to the mono-element Al coating in a way that oxide scale thickness is lower, which indicates a slower oxide scale growth rate. The design concept has successfully been applied to a combustion chamber in a reformer system and is available for further use in coating technology.

# References

[1] http://www.corrosion.org/wco_media/nowisthetime.pdf. [Online]

[2] M. Schütze, Corrosion and Environmental Degradation, Material Science and Technology Series Volume I (1999), Wiley-VCH.

[3] D.P. Whittle, Oxidation of Metals 4 (1972), pp. 171-179.

[4] R. Bürgel, Handbuch Hochtemperatur-Werkstofftechnik, 2006, Vieweg, Wiesbaden.

[5] D.R. Gaskell, Introduction to the Thermodynamics of Materials, Third Edition, 1995, Taylor & Francis.

[6] B. Rammer, T. Weber, M. Schütze, Corrosion Engineering, Science and Technology 44 (2009), pp. 227-233.

[7] R.V. Hillery, Coatings for High-Temperature Structural Materials: Trends and Opportunities,1996, National Academy of Sciences, Washington D.C.

[8] Z.D. Xiang, P.K. Datta, Materials Science and Technology 19 (2003), pp. 935-942.

[9] T.L. Hu, H.L. Huang, D. Gan, T.Y. Lee, Surface and Coatings Technology 201 (2006), pp. 3502-3509.

[10] Z.D. Xiang, J.S. Burnell-Gray, P.K. Satta, Journal of Material Science 36 (2001), pp. 5673-5682.

[11] T. Van Aller, Treatment of Metals, U.S. Patent No. 1,155,974.

[12] R.P. Seelig and R.J. Steuber, High Temperatures - High Pressures 10 (1978), pp. 207-213.

[13] G.W. Goward and L.W. Cannon, Transactions of the ASME 110 (1988), pp. 150-154.

[14] R. Sivakumar, Metallurgical Transactions 7 (1976), pp. 1073-1079.

[15] G.W. Goward, Journal of Metals 22 (1970), pp. 31-39.

[16] T. Weber, Dissertation: Korrosionsschutzschichten für Apparatewerkstoffe unter sulfidierenden Bedingungen bei hohen Temperaturen, 2004, Shaker, RWTH Aachen.

[17] R. Bianco, M.A. Harper, R.A. Rapp, Journal of Metals 43 (1991), pp. 68-73.

[18] L. Levin, A. Ginzburg, L. Klinger, T. Werber, A. Katsman, P. Schaaf, Surface and Coatings Technology 106 (1998), pp. 209-213.

[19] V. Rohr, Dissertation: Development De Revetements Pour Les Aciers D'echangeurs Thermiques Et Amelioration De Leur Resistance A LA Corrosion En Environnement Simulant Les Fumees De Combustion De Charbon, 2005, Toulouse.

[20] N. Voudouris, Ch. Christoglou, G.N. Angelopoulos, Surface and Coatings Technology 141 (2001), pp. 275-282.

[21] Final Conference COST Action 535 Thermodynamics of Alloyed Aluminides (THALU), 4th Discussion Meeting on the Development of Innovative Iron Aluminum Alloys, 21 – 24 October 2007, Interlaken, Switzerland.

[22] A. Kostov, B. Friedrich and D. Živković, Journal of Mining and Metallurgy 44 B (2008), pp. 49-61.

[23] M. Eggersmann and H. Mehrer, Philosophical Magazine A80 (2000), pp. 1219-1244.

[24] Y.S. Touloukian, Thermophysical Properties of Matter, Plenum Publishing Corporation New York, 1975.

[25] V.N. Yeremenko, Y.V. Natanzon, V.I. Dybkov, Journal of Material Science 16 (1981), pp. 1748-1756.

[26] M. Johnson, D.E. Mikkola, P.A. March, R.N. Wright, Wear 140 (1990), pp. 279-289.

[27] C.G. McKamey, J.H. Devan, P.F. Tortorelli, V.K. Sikka, Journal of Materials Research 6 (1991), pp. 1779-1805.

[28] J.R. Knibloe, R.N. Wright, C.L. Trybus, V.K. Sikka, Journal of Materials Science, pp. 2040-2044.

[29] R.G. Baligidad, A. Radhakrishna, Material Science and Engineering A287 (2000), pp. 17-24.

[30] N.S. Stoloff, Material Science and Engineering A258 (1998), pp. 1-14.

[31] S. Kobayashi, T. Yakou, Materials Science and Engineering A338 (2002), pp. 44-53.

[32] K. Ganesh Kumar, Sivarao, T.J. Anand, International Journal of Engineering & Technology 11 (2011), pp. 208-215.

[33] M. Schütze and H.J. Grabke, Oxidation of Intermetallics, 1998, Wiley-VCH, Weinheim, Germany.

[34] M. Göken, H. Vehoff, P. Neumann, Scripta Metallurgica et Materialia 33 (1995), pp. 1187-1192.

[35] Z.D. Xiang, S.R. Rose, P.K. Datta, Materials Chemistry and Physics 80 (2003), pp. 482-489.

[36] Z.D. Xiang, P.K. Datta, Acta Materialia 54 (2006), pp. 4453-4463.

[37] Z.D. Xiang, P.K. Datta, Materials Science and Engineering 356 (2003), pp.136-144.

[38] R. Bianco, R.A. Rapp, Journal of The Electrochemical Society 140 (1993), pp. 1181-1190.

[39] W.D. Costa, B. Gleeson, D.J. Young, Journal of The Electrochemical Society 141 (1994), pp. 1464-1471.

[40] J. Grüters, M.C. Galetz, Intermetallics 60 (2015), pp. 19-27.

[41] R. Bianco, M.A. Harper, R.A. Rapp, The Journal of the Minerals, Metals and Materials Society 43 (1991), pp. 20-25.

[42] M. Zandrahimi, J. Vatandoost, H. Ebrahimifar, Oxidation of Metals 76 (2011), pp. 347-358.

[43] X. Montero, M. C. Galetz, M. Schütze, Surface & Coatings Technology 236 (2013), pp. 465-475.

[44] M.C. Galetz, habilitation treatise, 2014, University of Bayreuth.

[45] W.J. Quadakkers and M. Schütze, Novel Approaches to improving high temperature corrosion resistance, 2008, Woodhead Publishing.

[46] E. Fitzer, H.J. Mäurer, W. Nowak, J. Schlichting, Thin Solid Films 64 (1979), pp. 305-319.

[47] P.Y. Hou, J. Stringer, Materials Science and Engineering 202 (1995), pp. 1-10.

[48] L.B. Pfeil, U.K. Patent no. 459848 (1937).

[49] B.A. Pint, Progress in Understanding the Reactive Element Effect Since the Whittle and Stringer Literature Review, Proc. John Stringer Symposium on High Temperature Corrosion 2003, ASM International, Materials Park, OH, pp. 9-19.

[50] I. Gab, V. Zhuravlev, D. Kurkova, T. Stetsyuk, Y. Naidich, Powder Metallurgy and Metal Ceramics (36), 1997.

[51] Y. Zhang, B.A. Pint, G.W. Garner, K.M. Cooley, J.A. Haynes, Surface and Coating Technology 35 (2004), pp. 188-189.

[52] A. Agüero, R. Muelas, M. Gutiérrez, R. Van Vulpen, S. Osgerby und J.P. Banks, Surface and Coating Technology 201 (2007), pp.

[53] V. Rohr, M. Schütze, Material Science Forum 401 (2004), pp. 461-464.

[54] B.A. Pint, Y. Zhang, P.F. Tortorelli, J.A. Haynes, I.G. Wright, Mater High Temperature 18 (2001), pp. 185-192.

[55] D. Risanti, J. Deges, L. Falat, S. Kobayashi, J. Konrad, M. Palm, B. Potr, A. Schneidr, C. Stallybrass, F. Stein, Intermetallics 13 (2005), pp. 1337-1342.

[56] ThyssenKrupp VDM, Werkstoffdatenblatt Nr. 4103, 2005.

[57] ThyssenKrupp VDM, Werkstoffdatenblatt Nr. 4129, 2003.

[58] E. Essuman, G. H. Meier, J. Zurek, M. Hänsel, W. J. Quadakkers, Oxidation of Metals 69 (2008), pp. 143-162.

[59] E. J. Opila, D. L. Myers, N. S. Jacobson, I. M. B. Nielsen, D. F. Johnson, J. K. Olminsky, M. D. Allendorf, Journal of Physical Chemistry A 111 (2007), pp. 1971-1980.

[60] H. Asteman, J.-E. Svensson, L.-G. Johansson, Oxidation of Metals 57 (2002), pp. 193-216.

[61] J. Margalit, G. Kimmel and S. Niedzwiedz, Journal of the Institute of Metals 98 (1970), pp. 126-133.

[62] J.K. Redden, Transactions of the TMS-AIME 242 (1968), pp. 1695-1705.

[63] M.J. Fleetwood, Journal of the Institute of Metals 98 (1970), pp. 1-12.

[64] M.M.P. Janssen and G.D. Rieck, Transactions of the TMS of the AIME 239 (1967), pp. 1372-1385.

[65] M.M.P. Janssen, Metallurgical and Materials Transactions 4 (1973), pp. 1623-1633.

[66] G.W. Goward, D. H. Boone and C. S. Giggins, Transactions of the ASM 60 (1967), pp. 228-233.

[67] D.H. Boone and G. W. Goward, Oxidation of Metals 3 (1970), pp. 476-484.

[68] R.M. Caves and S. R. Levine, Journal of the Electrochemical Society 121 (1974), pp. 1051-1064.

[69] S. Shankar and L.L. Seigle, Metallurgical Transactions 9A (1978), pp. 1467-1476.

[70] A.J. Hickl and R.W. Heckel, Metallurgical Transactions 6A (1975), pp. 431-440.

[71] J.T. John, G.B. Kale, S.R. Bharadwaj, R.S. Srinivasa, P.K. De, Thin Solid Films 466 (2004), pp. 331-338.

[72] B. Nciri, L. Vandenbulke, Surface Technology 24 (1985), pp. 365-381.

[73] B.K. Gupta, A.K. Sarkhel, L.L. Seigle, Thin Solid Films 39 (1976), pp. 313-320.

[74] N.V. Bangaru and R.C. Krutenat, Journal of Vacuum Science and Technology B (1984), pp. 806-815.

[75] C.W. Bale, E. Bélisle, P. Chartrand, S.A. Decterov, G. Eriksson, K. Hack, I.-H. Jung, Y.-B. Kang, J. Melançon, A.D. Pelton, C. Robelin and S. Petersen, Calphad 2008.

[76] T. S. Weber, V. Rohr, M. Schütze, Conference Proceeding, 210th ECS Meeting, High Temperature Corrosion and Materials Chemistry 6, 2006, pp 59-72.

[77] R.A. Rapp, S.C. Kung, Oxidation of Metals 32 (1989), pp. 89-109.

[78] R. Bianco, R.A. Rapp, Metallurgical and Ceramic Protective Coatings, 1996, Chapman & Hall, London, pp. 236-260.

[79] N.S. Jacobson and G.M. Mehrotra, Metallurgical Transactions 24B (1993), pp. 481-486.

[80] P. Desai, J. Phys. Chem. Ref. Data 16 (1987), pp. 109-124.

[81] L. Bencze, D.D. Raj, D. Kath, W.A. Oates, L. Singheiser, K. Hilpert, Metallurgical and Materials Transactions 35B (2004), pp. 867-876.

[82] A. Steiner and K.L. Komarek, Transactions of the Metallurgical Society of Aime 230 (1964), pp. 786-790.

[83] C. Matano, Japanese Journal of Applied Physics 8 (1933), pp. 109-113.

[84] L. Boltzmann, Wiedemanns Annalen der Physik 53 (1894), pp. 959-964.

[85] R. Nakamura, K. Takasawa, Y. Yamazaki, Y. Iijima, Intermetallics 10 (2002), pp. 195-204.

[86] M. Salamon, D. Fuks, H. Mehrer, Defect and Diffusion Forum Vols. 237-240 (2005), pp. 444-449.

[87] M. Eggersmann, H. Mehrer, Philosophical Magazine A, Vol. 80, No. 5 (2000), pp. 1219-1244.

[88] R. Sivakumar, E. Janardhana Rao, Oxidation of Metals, Vol. 17, Nos 5/6. (1982), pp. 391-405.

[89] I.I. Gab, V.S. Zhuravlev, D.I. Kurkova, T.V. Stetsyuk, Yu.V. Naidich, Contact interaction of oxidic materials with high melting metals in high temperature solid-phase pressure welding, Powder Metallurgy and Metal Ceramics (36) 1997, pp. 416-419.

[90] Y. Zhang, B.A. Pint, K.M. Cooley, J.A. Haynes, Surface & Coatings Technology 202 (2008), pp. 3839-3849.